Soft X-ray Spectroscopy of Light Elements in Energy Storage Materials

Bin Wu,[1,2] Bao Wang,[3] Tristan Petit[1,]*

1*Young Investigator Group Nanoscale Solid-Liquid Interfaces, Helmholtz-Zentrum Berlin für Materialien und Energie GmbH, Albert-Einstein-Straße 15, 12489 Berlin, Germany*

2 *Institute of Physics, Humboldt University Berlin, Newton-Straße 15, 12489 Berlin, Germany*

3 *State Key Laboratory of Biochemical Engineering, Institute of Process Engineering, Chinese Academy of Sciences, 100190 Beijing, China*

*email: tristan.petit@helmholtz-berlin.de

Abstract

The increasing demand for electrochemical energy storage devices continuously promotes the development of new electrode materials and electrolytes. As a result, understanding their structural and electronic properties affecting electrochemical performance becomes crucial. The role of light elements, which are found in anode and cathode materials, in electrolytes and hence in the solid-electrolyte interphases, requires a special attention. Soft X-ray spectroscopies are particularly relevant to probe selectively light elements in complex environment. Here, the recent advances in the characterization of light elements in energy storage materials by soft X-ray spectroscopy and microscopy techniques are reviewed. After introducing the main X-ray spectroscopic methods and their application to *ex situ/in situ/operando* characterization of electrochemical processes, the role of light elements in the electrode for supercapacitors and Li/Na-ion storage applications is described. The characterization of electrolytes and related ion solvation is then briefly reviewed before describing how the formation and evolution of solid-electrolyte interphases can be monitored with these methods. Finally, major challenges and future opportunities for soft X-rays spectroscopy in the context of electrochemical energy storage are highlighted.

1. Introduction

Efficient electrochemical energy storage (EES) systems are urgently needed to face global challenges of energy shortage in the 21st century.[1–5] Thus, a brand-new era of low-cost, high-performance, and environmentally-friendly energy materials is coming.[6–9] Improving the efficiency of materials in energy storage and conversion has become an intractable challenge for energy scientists.[10] To this aim, new analytical methods are constantly being developed to enable real-time probing of electronic and chemical structures in a real working environment that can bring critical new knowledge for improving their material properties. [10–12] Such techniques are imperative to achieve a comprehensive understanding of chemical states, electronic structures as well as physical and chemical reactions in the interfacial area for energy materials systems. [1,13–15]

With the development of third and fourth-generations of synchrotron facilities, X-ray characterization techniques have become very attractive for *in situ/operando* characterization of the electronic and geometric structures of energy storage materials.[16–18] The development of scattering and diffraction techniques,[19–25] spectroscopy [18,26–28] and microscopy [29–32] for the characterization of energy storage materials have been recently reviewed. The structure of crystalline electrodes and particle size and shape of the electrode materials can be obtained by X-ray Diffraction (XRD) and Small Angle X-ray Scattering (SAXS), respectively. [33] Observing local morphological change is also a key factor to investigate the electrochemical performances of materials which is best performed using microscopy and tomography techniques.[12] Besides structural and morphological insights, chemical information about interfacial processes and redox activity of EES materials requires spectroscopic techniques. A wide variety of X-ray spectroscopy and microscopy with various sample environment and bulk/surface sensitivity are currently being applied to solve main research questions related to EES.

X-ray spectroscopy techniques are highly sensitive to the chemical bonding of elements in energy materials systems thanks to their element-specificity and high sensitivity to the chemical environment. [34–36] X-ray spectroscopy techniques are mainly constituted of X-ray photoelectron spectroscopy (XPS), X-ray absorption spectroscopy (XAS), X-ray emission spectroscopy (XES) and resonant inelastic X-ray scattering (RIXS), which are probing the different electronic states of the atoms contained in the investigated sample. They can be applied *ex situ*, *in situ,* or *operando* to provide new insights into the mechanism of

electrochemical processes in EES. Coupled with X-ray microscopy enabling sub-50 nm spatial resolution, nanoscale imaging of individual battery electrode materials has recently been achieved. [12,37,38] Several recent reviews the characterization of energy storage materials by X-ray spectroscopy and microscopy techniques are available but are mostly focused on the characterization of transition metals.[12,13,28,39–43] The high sensitivity of X-ray spectroscopies to the metal oxidation state at both the K- and L-edges make them particularly relevant for this topic. In addition, light elements, especially carbon, nitrogen, oxygen and fluorine, can also be probed by X-ray spectroscopies, which has not been reviewed so far in the field of energy storage materials to our knowledge. We therefore intend to fill this gap with the current review. X-ray spectroscopy has been applied for decades for the characterization of organic materials for life science,[44–46] catalysis,[47–49] environmental science [50–52] and geology. [53–55] We forward the reader to these reviews for more details on these field of research and concentrate on energy storage materials in the following.

Light elements are essential constituents of the main components of energy storage systems which are summarized in Figure 1.[56–62] Carbon-based electrodes, often doped with nitrogen, are the majority for supercapacitors or anode for Li-ion batteries (LIBs) and Na-ion batteries (NIBs).[63] For metal-based electrodes, a polymeric binder is required to ensure good conductivity between the particles and decrease large volume change of particles during electrochemical cycling.[64] The oxide layer on these particles is also of high relevance as it governs interactions with the electrolyte. Probing the oxygen bonding environment, especially after binding with Li^+ or Na^+, is highly complementary to the characterization of the metal oxidation state. [65,66]
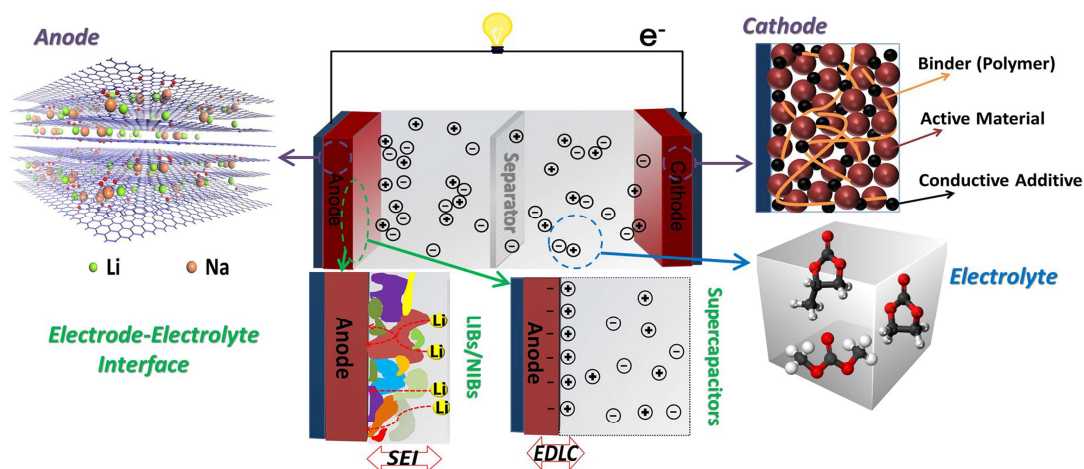
Figure 1 Main components of an electrochemical energy storage device containing light elements that can be investigated by soft X-ray spectroscopies.

Secondly, the in-depth characterization of the electrolytes would be very highly desired. Aqueous and organic electrolytes, as well as ionic liquids that are attracting increasing interest for energy storage, are mostly constituted of light elements. Understanding their hydrogen bonding environment, the solvation of charge carriers, being either protons, Li- or Na-ions, or anion-cation interactions in liquid phase are of high relevance. [67–71]

Finally, the analysis of the Solid-Electrolyte Interphase (SEI) should not be overlooked. The formation and composition of the SEI as a result of the evolution of products and the degradation of the electrolyte at the electrode surface requires intense research efforts. The SEI has been previously investigated via a series of *in situ/ex situ* methods including Fourier-transform infrared spectroscopy (FTIR),[72,73], scanning ion conductance microscopy (SICM) [74,75] and scanning electron microscopy (SEM).[76] However, high element- and interfacial-sensitivity to light elements make X-ray spectroscopies powerful tools to monitor the electronic structure of SEI composition. [77–79]

In this review, we will first briefly introduce the soft X-ray spectroscopy and microscopy techniques that have been used for the characterization of light elements in EES systems. Methodologies to achieve *in situ/operando* characterization of energy storage systems will be briefly discussed. Then, representative studies focusing on the soft X-ray spectroscopy characterization of the electrodes, electrolytes and SEI will be presented. We do not intend to provide a fully exhaustive coverage of previous litterature in the field but rather concentrate on recent examples demonstrating various possibilities offered by these techniques. Finally,

an outlook of future development required to achieve major progress in this emerging field of research is provided.

2 X-ray Spectroscopy of Light Elements

2.1 Soft X-ray Photons

Light elements, namely carbon, nitrogen, oxygen and fluorine, have between 6 and 9 electrons. Two electrons are located in the first electronic shell (core electrons) and the others are involved in chemical bonding (valence electrons). The K-edge energies corresponding to the energy required to excite core electrons into the first unoccupied electronic states ranges for these elements between 280 and 700 eV (Figure 2a).[80] The definition of X-ray "hardness" intrinsically originates from the fact that the soft, tender and hard X-ray photons penetrate shallow, thin and thick matters, respectively depending on their photon energy. Soft X-rays have a photon energy range of several tens of electron volts (eVs) to about 1 keV whereas tender X-rays are ranging between1 keV and 5 keV. Hard X-rays are then covering an energy range from 5 keV up to tens of keV. In addition to light element K-edges, transition metal L-edges as well as Li and Na K-edge, which are particularly relevant for energy storage materials, can also be analyzed by soft X-ray photons. Note that few soft X-ray beamlines are currently enabling resonant excitation at the Li K-edge at 55 eV.[81,82] On the other hand, the Li 1s core level can be easily characterized by XPS because it does not necessarily require resonant excitation. Soft X-ray photons are usually generated by synchrotron light sources but table-top soft X-ray light sources are also emerging.[83]
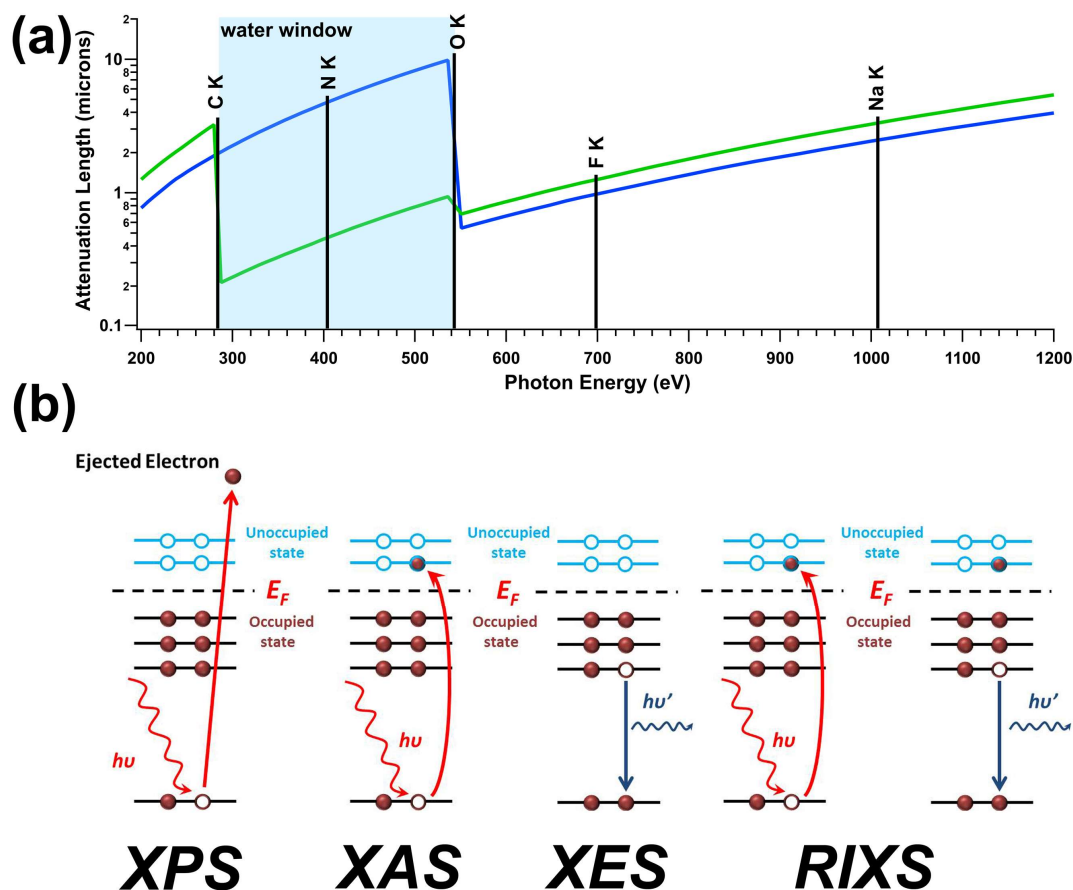
Figure 2 (a) Energies of X-ray absorption K-edges of light elements (black lines). X-ray attenuation length in water (blue) and polycarbonate (green) in the soft X-ray range obtained from the CXRO database. The so-called water window is highlighted in light blue, (b) Schematic diagrams of XPS, XAS, XES and RIXS spectroscopies.

So far, most of the studies on energy storage materials are related to *ex situ* spectroscopic studies in vacuum. Indeed, the use of soft X-rays imposes several experimental constraints that complicates the use of classical battery and supercapacitor architecture. Especially, soft-X-ray spectroscopy requires an (ultrahigh) vacuum environment due to the short attenuation length of X-ray photons in air. This makes experiments with liquids having low vapor pressure (aqueous and organic electrolytes) particularly complicated. In addition, aqueous and organic electrolytes absorb soft X-ray over a few microns as shown in Figure 2a, which will also have consequences for measurements in a real EES system. The direct analysis of the core electrons or of the decay process of valence electrons to fill the core hole led to a range

of different spectroscopy methods, especially XPS, XAS, XES and RIXS.[84] Their basic principles are depicted in Figure 2b and are briefly introduced in this section.

2.2 X-ray Photoelectron Spectroscopy

As a typical photon-in/electron-out spectroscopy, XPS resulting from the photoelectric effect is one of the most developed surface-sensitive X-ray spectroscopy techniques. When the energy of an incident photon is sufficient to excite electrons from a particular electronic shell above the vacuum level, the sample is ionized and corresponding electrons are emitted out.[85,86] By analyzing the kinetic energy of emitted electrons, the binding energy of the probed core levels is obtained. XPS provides quantitative information such as the absolute binding energy, which can be affected by band bending or change of surface chemistry. Relative elemental content in the surface layers can also be extracted from the different core level intensities.

The use of synchrotron light source for XPS brings an increased energy resolution but also a high brilliance enabling measurements in liquid or gaseous atmosphere with reasonable signal-to-noise ratio using ambient pressure XPS (AP-XPS). In addition, the incident photon energies can be selected to enable depth profiling because the electron mean free path depends on the electron kinetic energy.[87,88] Site-selectivity is also achieved by tunable X-rays using resonant photoemission spectroscopy (RPES), which is particularly useful to decipher electronic contribution from dilute species in solution.[89] RPES has not been applied to energy storage materials yet to our knowledge.

2.3 X-ray Absorption Spectroscopy

XAS probes unoccupied partial electronic states as shown in Figure 2b. Specifically, an incident X-ray photon excites a core electron to an unoccupied state above the Fermi level. The recombination of an electron from occupied state levels into the core hole leads to the emission of fluorescent X-rays or the release of an Auger the electrons.[84] The collection of XAS signals can be realized via the following main detection modes:

- Transmission: This mode is based on the measurement of the transmitted X-ray intensity through the sample as compared to the incident photon intensity as for other classical absorption spectroscopies. [90] In transmission mode, increasing

concentration and uniformity of samples are necessary to increase the difference for high-quality data which is corresponding to Beer's law. [91,92]

- Electron yield (EY): Electron yield is particularly adapted to light elements as electronic recombination constitutes >99% of the decay processes.[18,93] The main detections are the total electron yield (TEY), in which drain current is measured, or Auger electron yield (AEY) in which only Auger electrons are detected. AEY and TEY are very surface sensitive due to the short escape length of electron, with probing depths of a few nanometers.[92]

- Fluorescence yield (FY): The fluorescence mode detects the X-rays emitted from the decay process of valence electron into the core hole. [90,91] In Total Fluorescence Yield (TFY), all emitted photons are detected while in Partial Fluorescence Yield (PFY), only X-ray photon from a particular energy level are analyzed. FY mode is relatively bulk sensitive with a probing depth of hundreds of nanometers.

Generally, EY and FY modes are mostly used for XAS in the soft X-ray range of energy materials because of the short penetration depth of incident X-rays. Preparing <100-nm thin and homogeneous electrodes required for X-ray transmission in this energy range is difficult. In addition, EY-XAS and FY-XAS can be collected simultaneously, providing a comparison between surface and bulk electronic states of the samples.

2.4 X-ray Emission Spectroscopy and Resonant Inelastic X-ray Scattering

XES is probing the partially occupied electronic states of the excited atom. The excitation of a core electron to an unoccupied electronic state by an incident X-ray photon is first achieved, similar as in the XAS process. [94] The energy of emitted X-ray photon during the decay process of valence electrons into the core hole is analyzed. When the excitation energy is well above the absorption edge, non-resonant XES is measured. Only X-ray photons emitted from the decay from a definite absorption edge are analyzed. It provides hence information on the partially occupied electronic states in the valence band. Combining XES and XAS can be used to estimate the electronic bandgaps of different elements in energy materials. [35,95]

RIXS occurs by a similar decay process as XES, except that unoccupied electronic states are resonantly excited. In that case, both elastic and inelastic scattering processes occur. In RIXS, the energy loss resulting from inelastic scattering processes is analyzed as a function of the

excitation energy.[94] It offers deeper information about the electronic structure of the probed materials compared to XES and has recently been extensively applied to characterize redox reactions in batteries.[96] It has to be noted that XES and RIXS rely on radiative decay processes which are quite inefficient for light elements and therefore require a high photon flux and relatively long measurements time in comparison to other X-ray spectroscopy methods for light elements. On the other hand, it does not require the sample to be conductive and benefit from a longer probing depth than electron out methods, which is more adapted to *in situ* measurements.

2.5 Scanning Transmission X-ray Microscopy

X-ray microscopes with non-destructive, highly-resolved (tens of nanometers) detection are powerful tools for the visualization of electrochemical processes and chemical mapping in energy storage materials. [56,97,98] Transmission X-ray microscopy (TXM) and Scanning Transmission X-ray Microscopy (STXM) are using X-ray contrast for imaging with a nano-focused synchrotron X-ray light source.[41] When the soft X-ray energy is scanned in the energy scale, transmission XAS with high spatial resolution are recorded. For TXM, a strong incoherent X-ray beam is focused on the material via a condenser lens. Subsequently, the X-rays refracted and transmitted across the material are collected by objective lens in order to form the second refraction. Finally, the final x-ray image originated from secondly-refracted X-rays are obtained on the area detector, which is a real space intensity image [99].

On the other hand, STXM is based on a small X-ray beam, focused using one condenser lens, which is scanned over the sample. The characterized material is scanned horizontally and vertically with the X-ray beam and the intensity of the transmitted x-ray is recorded on the detector. [100] STXM has therefore a slower speed of data acquisition than TXM but is well-suited for in-situ imaging of energy storage material. STXM has a more flexible view field and induces less radiation damage to the material under test. In addition, the high spatial resolution (<30 nm) promotes the rapid development of STXM application for in situ/operando imaging of individual battery particles. [101] Finally, the EY and FY detection modes previously presented for XAS are also available on STXM, even if they have not been extensively been applied to energy storage materials so far. [102,103] New developments in the field of ptychography recently achieved <10 nm resolution in battery materials.[104,105][105]

2.6 X-ray Photoemission Electron Microscopy

X-ray photoemission electron microscopy (XPEEM) is a photon-in/electron-out imaging technique. [106] The XPEEM images are obtained by the analysis of photoelectrons and secondary electrons emitted upon core-level excitations with inherently two- dimensional resolution in space. [107] Generally, there are two types of XPEEM, one is to use a tunable X-ray source, such as a synchrotron, and the other is to use an energy filter. [106,108] In the former mode, XPEEM pictures are measured while scanning the excitation photon energies over a specific energy range, enabling the recording of XAS with high spatial resolution. Chemical contrast based on different X-ray absorption cross-section before and after an absorption edge can be used to map elemental composition, even without a tunable light source if appropriate filters are used. All in all, the XPEEM method has a potentially great advantage for directly observing dynamic chemical or physical behaviors at surfaces, including adsorption, diffusion, and surface reactions. New developments of XPEEM in the field of electrochemistry and the characterization of energy storage materials demonstrate that this technique is very promising for these applications [109–111].

2.7 In Situ/Operando Cells

Ex situ measurements are performed under vacuum and can either be applied to as-synthesized materials or *post mortem*, *i.e.* after dismounting a cell that has been cycled externally. This approach has lead to significant insights into the mechanisms of energy storage processes. Nevertheless, the sample preparation after cell dismounting may damage sensitive surface layers, for example during rinsing or unadventurous exposure to air. Dynamics and real-time study of the change in the electronic structure for material under a real work environment cannot be achieved by *ex situ* studies. [14,88,112] Furthermore, many questions such as SEI formation and stability can only be investigated *in situ* or *operando*.

In situ characterization of energy storage materials usually refers to measurements performed in a relevant environment, typically an electrode exposed to an electrolyte at open or a fixed potential, while *operando* characterization refers to measurements on a real EES system under normal operation. In the context of soft X-ray spectroscopy, *operando* measurements rather refer to experiments performed during cycling in an electrochemical cell simulating as close as possible a real system. As mentioned earlier, the use of soft X-ray imposes physical constraints to the design of *in situ/operando* cells.

Different *in situ/operando* cell designs enabling X-ray characterization during electrochemical reactions were proposed so far,[113–118] and some of them are shown in Figure 3. For ionic liquids or solid electrolytes, the system can be directly exposed to the vacuum (Figure 3a). Else, the main paradigm to solve the challenge of vacuum environment is to seal the liquid samples in a cell that isolate the electrolyte from the vacuum chamber. Photon-in/photon-out spectroscopies can be applied through thin membranes, usually made out of silicon nitride or carbide, which are relatively transparent in the soft X-ray range.[119] For photon-in/electron-out spectroscopies, the shorter inelastic mean free path of electrons implies that ultrathin membranes such as graphene single or bilayers have to be used.[120–122] The cell can either be closed or used in a flow configuration. The working electrode is generally deposited on the X-ray transparent membrane while counter and reference electrodes are placed further away in the cell. Electrochemical cells based on fluorescence/electron detection (Figure 3b) and transmission cells using two membranes have been proposed (Figure 3c). For STXM, geometrical constraints for the X-ray optics make the cell design more complicated but such systems have also been recently demonstrated for visualizing working battery electrodes under the charging/discharging conditions.[114] Flow cell approaches allow *operando* experiments with various solvent, concentrations, pHs and temperatures. [35,112,119]

One of the first *in situ* electrochemical XAS studies was applied to the study of corrosion of copper in $NaHCO_3$ aqueous solutions. [123] Meanwhile, soft X-rays *in situ* cells have been widely utilized for studying (electro)catalytic reactions, semiconductor solar cells and energy storage mechanisms. [17,34,49,88,124–126] For the study of real EES system via soft X-ray spectroscopy, several additional challenges are encountered. For instance, low stability of SEI for battery, change of surface chemistry upon air exposure/vacuum as well as change and consumption of electrolyte.
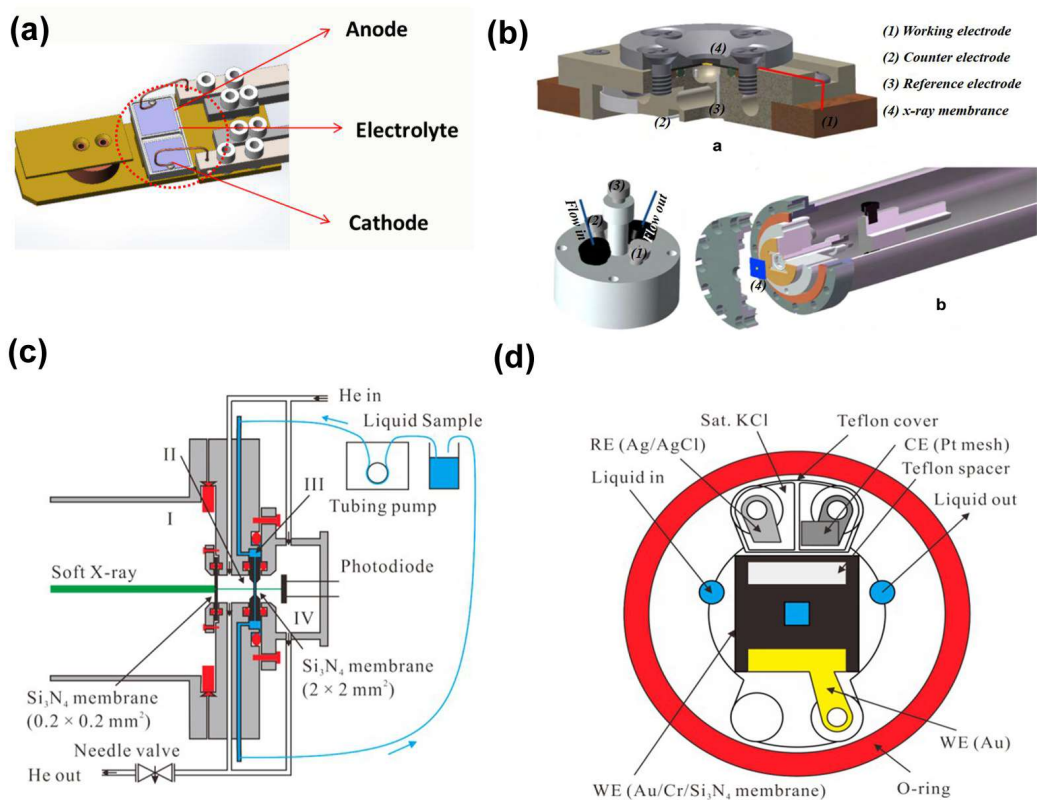
Figure 3 In situ cells for soft X-ray spectroscopies. (a) In situ cell for battery cycling and *in situ* XPS characterization (reproduced with permission from [117], copyright 2017, American Chemical Society), (b) In situ electrochemical static (top) and flow (bottom) liquid cells for FY-XAS/XES (reproduced with permission from [118], copyright 2018, World Scientific Publishing Co Pte Ltd), (c-d) In situ 3-electrodes electrochemical cell for XAS in transmission mode (reproduced with permission from [116], copyright 2013, American Chemical Society).

Liquid microjet has also arisen as an excellent technique to probe liquid samples or dispersed nanoparticles using XPS and XAS by offering a true liquid/vacuum interface.[127–130] Liquid microjet allows refreshing of the interface at a constant rate and therefore remains contamination-free. [131] Obviously this technique cannot be applied to a battery system but it can be used to characterize the electrolyte electronic structure and ion coordination in an electrolyte. [132–136]

3.1 Electrodes

3.1 Supercapacitors

3.1.1   Carbon-based Supercapacitors

Carbon-based supercapacitors with outstanding power density, high discharge/charge rates and high stability are an essential class of EES devices.[137–141] The electrical charges in supercapacitors are either stored by ion electrostatic adsorption on the surface of the electrode material for electrochemical double layer capacitors (EDLCs) [136[138] or involve faradaic processes, in which case the term pseudocapacitor is used.[142] Soft X-ray spectroscopies, especially XPS and XAS, are well adapted to characterize pseudocapacitive reactions leading to surface modification of carbon-based electrodes.

In general, redox actives states involved in pseudocapacitive charging at the carbon surface are associated with oxygen-terminated functional groups. For example, Bagge-Hansen *et al* investigated 3D nanographene (3D-NG) electrode during electrochemical biasing in 1 M NaCl aqueous electrolyte using *in situ* XAS at the C K-edge (Figure 4a).[143] Interestingly, two resonances attributed to C-OH σ* transition (287.3 eV) and C-C σ* transition (291 eV) appeared under positive potential. The first contribution is due to a surface hydroxylation during charging, demonstrating that a pseudocapacitive charging process occurs. At the same time, structural modification of the graphene plane suggests internal electronic reorganization in the electrode originating from strong interfacial interactions with the electrolyte. Both pseudocapacitive and capacitive processes are thus occurring on this type of electrode. Similar conclusions were obtained on reduced graphene oxide (RGO) electrodes. [144] Based on *ex situ* XAS at the C and O K-edges measured at different potentials, Chang *et al* found that C=O groups are reversibly formed and removed from the edge sites of RGO and quinone groups were identified as an active redox site for pseudocapacitance. Similarly, on biomass-derived supercapacitors, the contribution of C=O groups to pseudocapacitive charging was evidenced by a significant decrease of its contribution in XAS at the O K-edge after 10000 cycles.[145]
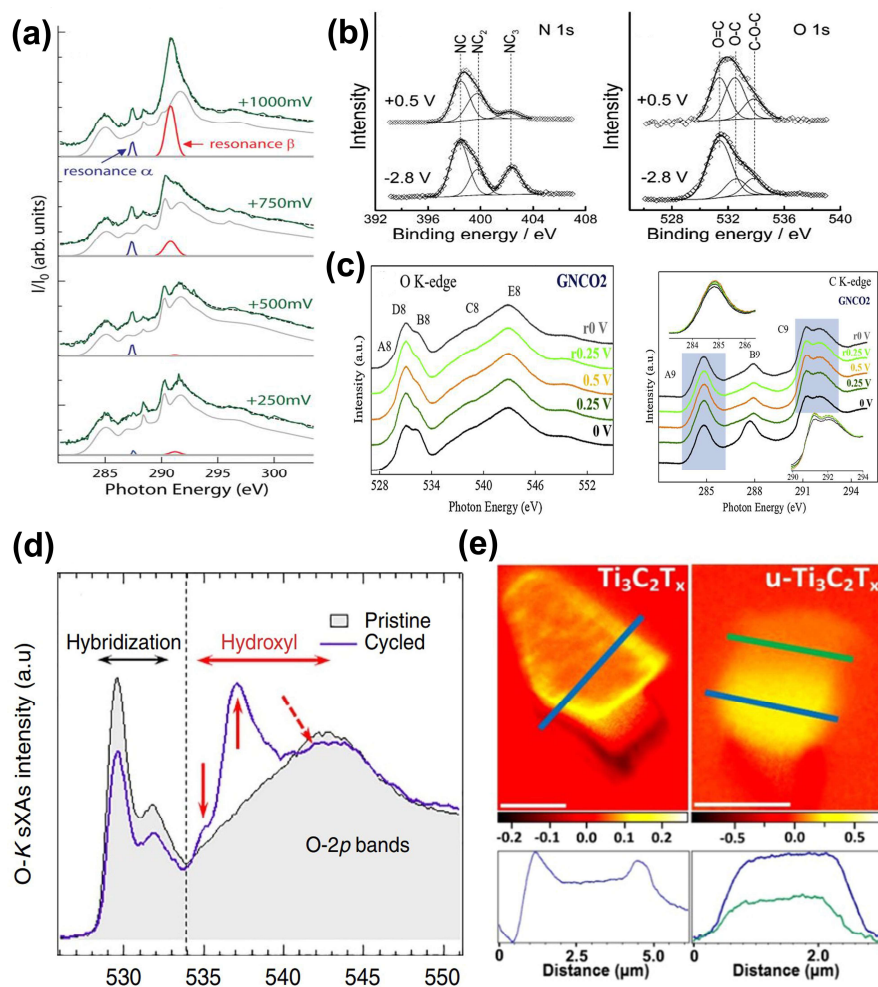
Figure 4 (a) *Operando* C K-edge XAS for a 3D-NG capacitor electrode in 1 M NaCl (aq) under constant biases between +250 and +1000 mV (green). Fitting components showing bias-dependent intensity are highlighted in blue and red (reproduced with permission from [143], copyright 2015, Wiley-VCH Verlag GmbH & Co. KGaA, Weinheim), (b) N1s (left) and O1s (right) *ex situ* XPS of HGNS electrode polarized at -2.8 V to +0.5 V (reproduced with permission from [147], copyright 2015, Wiley-VCH Verlag GmbH & Co. KGaA, Weinheim), (c) *Ex situ* O and C K-edges XAS spectra of GNCO$_2$ during the charge/discharge process (reproduced with permission from [148], copyright 2019, Elsevier), (d) O K-edge XAS of pristine and cycled (two CV cycles between 1.7 and 0.8 V) Mn$_5$O$_8$ electrodes. (reproduced with permission from [151], copyright 2016, Springer Nature), and (e) Oxygen content distribution over individual MXene flakes obtained from XPEEM micrographs at the O K-edge. The

corresponding line profiles across the flake are shown underneath (reproduced with permission from [153], copyright 2020, American Chemical Society).

A pseudocapacitive behavior was also reported in ionic liquid electrolyte on carboxylate-modified hollow carbon nanospheres (HCN) characterized *post mortem* XPS.[146] A significant increase of the hydroxyl contribution to the XPS O 1s spectra was observed after the first discharged on both positive and negative electrodes, implying that the protonation of carbonyl groups contribute to the pseudocapacitive behavior of HCN electrodes in ionic liquid. The adsorption of ionic liquid molecules was investigated in more details on holey graphene nanosheets (HGNS) by Yang *et al* (Figure 4b).[147] In a BMP–DCA ionic liquid electrolyte, they found a higher BMP^+ concentration (NC and NC_2 contribution in XPS N1s) on the electrode surface at negative potential, while DCA^- (NC_3 contribution in XPS N1s) appears as the main component at positive potential. Meanwhile, the C=O signature decreases while the C-O signature increases at positive potential at the XPS O1s, implying the contribution of reversible redox transitions on oxygen functional groups to the pseudocapacitive storage.

Nitrogen-containing groups can also be involved in redox processes. Wang *et al* investigated hierarchical nitrogen-doped porous carbon (HPC-N) with *ex situ* XPS at N 1s after electrochemical cycling.[58] After the reduction process, the peaks attribute to pyridone/pyrrolic nitrogen atoms and oxidized pyridine nitrogen atoms decrease while pyridinic and quaternary nitrogen contributions increase. After oxidation, the opposite is observed, accompanied by the appearance of protonated pyridinic nitrogen. These results demonstrate that nitrogen-containing functional groups may be involved in the following surface redox reactions: 1) the double-electron-transfer between pyridone and pyridine; 2) single-electron-transfer between pyridine and oxidized pyridine.

Finally, metal-organic complexes may also be considered for increasing pseudocapacitance. Chang *et al* investigated $NiCo_2O_4$/graphene quantum dots (GQDs) hybrid supercapacitors by *ex situ* XAS at the C and O K-edges at different states of the charging process (Figure 4c).[148] Redox-active sites on the $NiCo_2O_4$/GQDs are related to the formation of C-O-Ni bonds between $NiCo_2O_4$ and GQDs. As a result, $NiCo_2O_4$/GQDs hybrid have more active Ni sites than that in $NiCo_2O_4$, benefiting from metal-to-ligand charge transfer at the interface between $NiCo_2O_4$ and GQDs, which has a positive impact on electrochemical performance.

3.1.2 Transition Metal Oxide and MXene-based Supercapacitors

The rich redox chemistry of transition metal oxides is of high interest for supercapacitors based on pseudocapacitance.[149] Soft X-ray spectroscopy techniques, especially XAS, are perfectly adapted to probe the transition metal oxidation state at the metal L-edge. In addition, they are also well fitted for probing the oxygen bonding environment.[150] An example with Mn_5O_8 electrodes is shown in Figure 4d.[151] Oxygen atoms involved either in the hybridization between the Mn 3d and O 2p states (below 534 eV) or from interaction with water molecules (peaks at 535 and 537 eV) can be resolved as they are energetically separated on XAS at the O K-edge.[151] In this study, Mn_5O_8 electrodes were cycled in an aqueous Na-containing electrolyte and after cycling, two characteristic features of liquid water remain on the dried sample, interpreted as the adsorption of a highly ordered hydroxyl phase at the Mn_5O_8 surface. It is suggested that such an interface may extend the potential window stability of the electrode in aqueous environment.

Beyond metal oxides, a new class of 2D transition metal carbides and nitrides, so-called MXenes, are gaining increasing interest for pseudocapacitive storage as they combine the rich surface chemistry of metal oxides while having a conductive carbide core enabling a high structural stability and a rapid transfer of charge carriers transferred at the electrochemical interface.[152] Their layered structure also offer a large redox active surface area. We have recently shown using XAS at the Ti L-edge and O K-edge that intercalation of molecules or cations can modify the oxidation of MXene surface.[153,154] Especially, using XPEEM at the O K-edge, the oxygen bonding configuration was mapped over individual MXene particles.[153,155] The edges of MXene particles appear predominantly oxidized on pristine MXene while after interaction of urea or cations, a more homogeneous surface oxidation is visible (Figure 4e). Such a higher surface oxidation was proposed as one of the reasons that could increase the pseudocapacitance of electrodes prepared with pre-intercalated MXene materials.

3.2 Anode in Li- and Na-ion Batteries

3.2.1 Li-ion Intercalation in Carbon-based Anodes

The negative electrode for LIBs is often mainly based on carbon derivatives. [156–160] Graphite anode attracted most of the attention because of its low cost and long durability. Understanding de/lithiation processes in graphite anode, especially in the form of LiC_6, LiC_{12},

LiC$_{18}$, and LiC$_{24}$ [161–163] became hence an important field of research. [164–166] These compounds are highly unstable with oxygen and monitoring fine changes in their chemical structure during de/lithiation processes requires a high sensitivity to carbon chemical environment, for which soft X-ray spectroscopies applied in vacuum are particularly adapted.

As an example, the electronic structure of LiC$_6$ was investigated by Zhang *et al* using XAS and RIXS at C K-edge (Figure 5a).[167] On the XAS of LiC$_6$, the σ* states shifts to lower energy compared to highly oriented pyrolitic graphite, while no shift is observed for the π* states. This is attributed to the transfer of Li 2s electrons into the carbon π* states upon full lithiation of graphite. This process is observe both at the surface, probed by TEY, and in the bulk, probed by TFY, but the photon polarization has a strong impact on the signal intensity as it depends on the graphite basal plane orientation. A similar charge transfer was previously reported after Li$^+$ intercalation underneath a graphene layer investigated by XPS.[168] Zhang *et al* found that the deposition of Li on the graphene surface induced an upshift of the C 1s peak, which was recovered after annealing of the Li/graphene/Cu sample at 300 ºC due to the Li atoms intercalation into the interface of graphene/Cu. The electronic structure of lithiated natural graphite was further studied by Lapteva et al. [169] using *in situ* XPS and XES. They found that lithium vapor thermal deposition results in the formation of a lithiated graphite surface layer with new chemical bonds between the carbon and lithium atoms with the appearance of an sp^2- hybridized carbon component. From the comparison between experimental and theoretical C Kα XES of lithiated graphite, lithium atoms are suggested to be located mostly on the edges of graphite crystallites rather than on the basal planes.

For carbon-based electrodes, doping by heteroatom is an effective way to improve their electrochemical performance.[170–174] In particular, nitrogen is considered as an ideal doping element for carbon material because of its similarity of atomic size and abundant reserves in the form of nitrogen-containing molecules. [171,175–177] On graphene films, a higher accumulation of lithium atoms whas observed on N-doped graphene as monitored by XPS and XAS. [178] From the shift of the XPS C1s and N1s, the charge density donated by lithium is found rather localized near the (substitutional) nitrogen defects. The type of nitrogen atoms involved in Li-ion storage on N-doped porous graphitic materials has been further investigated by Lapteva *et al* using *in situ* XAS at the N K-edge.[179] Comparing XAS with theoretical calculation, they concluded that Li mostly bond to pyridinic and hydrogenated at the edges and defects of the surface graphitic layers while graphitic nitrogen

remains unchanged. On the other hand, Hu *et al* [180] reported that pyrrolic nitrogen is the most likely adsorption site for Li$^+$ atoms on N-doped graphene while pyridinic sites remains barely unchanged after Li insertion. Finally, Xi *et al* [181] observed that graphitic nitrogen is capable of storing more lithium ions compared to other N species in N- and N, S-doped graphene based on changes of the *ex situ* XPS N 1s at charged and discharged states after 100 cycles. These studies illustrate that Li bonding in N-doped carbon is a complex problem and most likely strongly depends on the structure of the carbon anode.
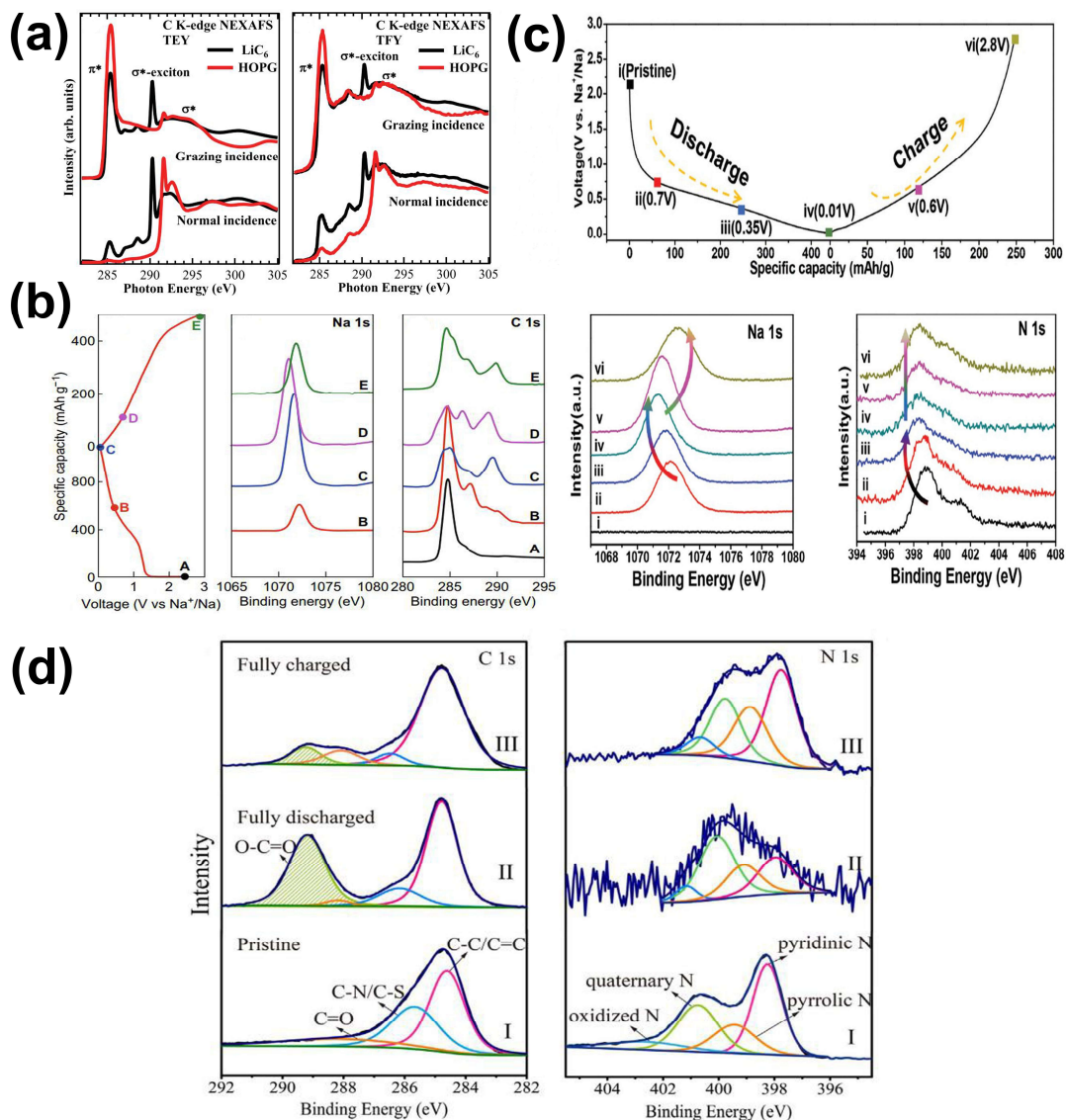

Figure 5 (a) Polarization-dependent C K-edge XAS of LiC6 and HOPG in TEY (left) and TFY (right) modes. (reproduced with permission from [167], copyright 2017, AIP Publishing), (b) *Ex situ* XPS Na 1s and C 1s of S-doped porous carbon in different

charge/discharge states during the initial cycle (reproduced with permission from [183], copyright 2019, Springer Nature), (c) voltage profile (top) of N-doped anode and *ex situ* XPS at the Na 1s and N 1s the different discharge/charge states in the first cycle (bottom) (reproduced with permission from [184], copyright 2018, Wiley-VCH Verlag GmbH & Co. KGaA, Weinheim), (d) XPS C 1s and N 1s of the N, S-doped graphene nanosheets electrode at the pristine (I), fully discharged (II), and fully charged (III) states (reproduced with permission from [186], copyright 2018, Elsevier).

3.2.2 Na-ion Storage in Carbon-based Anode

In recent years, high capacity, low ion storage potential, and good cycling stability were reported for carbon-based NIBs anode electrodes. [171,172] Based on *ex-situ* XPS, Li *et al* proposed that Na^+ adsorption and chemisorption on the carbon surface, leading to a chemical shift of the N1s, are observed in different electrochemical regimes. [182] Such a chemical shift of the Na 1s along a decrease of the C-C bond signature in the C1s at different cycling stage is shown on Figure 5b for S-doped carbon electrodes. [183] The reversibility of the Na-ion storage is confirmed by the Na 1s shifting back to the initial position and the C-C signature increasing again after full charging. Note the appearance of a strong peak at 289.6 eV in the C1s spectra, which is most likely associated to the adsorption of carbonates in the SEI layer as discussed in the last section.

As previously discussed for LIBs, N-doping can improve the electrochemical performance of carbon electrodes. The adsorption of Na^+ ions in electrodes with various N configurations was monitored by Liu *et al* by *ex situ* XPS.[184] Reversible shifts of the Na 1s peak were also observed during a full cycle but at the N1s, an irreversible sodiation of pyridinic and pyrrolic nitrogen sites is observed, while other nitrogen sites can (partly) recover their initial states (Figure 5c). Meanwhile, they concluded that the charge is transferred from Na to the N-dopants to form Na-protonated N structures in the carbon materials.[185] Co-doping of N and S was also investigated by Ma *et al* on graphene nanosheets (Figure 5d).[186] They observed changes of the pyridinic and pyrrolic N signatures upon discharging/charging in terms of both peak intensity and position in N 1s spectra. In particular, the electrochemical interaction of sodium with the active sites near pyridinic N is found more active, which was also supported by a previous similar report that pyridinic N favored the transfer of Na^+ and electrons.[187]

3.2.3 Li/Na-ion Intercalation in MXene

MXenes have been mostly used for pseudocapacitors so far but they also have a high potential for electrochemical Li/Na-ion storage applications.[188–190] Bak *et al* used *ex situ* soft XAS at C and O K-edges to investigate the Na-ion intercalation and charge storage mechanism in vanadium carbide MXene (V_2C).[191] They confirmed that Na^+ intercalation/deintercalation states in the V_2C electrode are highly related to the reversible formation/decomposition of fingerprint feature CO_3^{2-} species upon sodiation/desodiation. In particular, compared to the TFY-XAS spectra, the change of C and O K-edge spectra in surface-sensitive TEY mode is prominent, suggesting that carbonate species are mainly due to surface reaction between the Na^+-intercalated V_2C and the carbonate-based electrolyte solvents. Similar conclusions were obtained from Li^+ intercalation in Sn^{4+} modified V_2C MXene.[192] Wang *et al* considered that this carbonate adsorption could be related to the electrochemical reaction between oxygen on V_2C layers and the electrolyte. They also confirmed the formation of V-O-Sn bonding in O K-edge spectra which contributes to the outstanding rate and cyclic stability of the electrode.

3.3 Cathodes in Li- and Na-ion Batteries

3.3.1 Carbon-based Li/Na-Oxygen Batteries

Lithium/sodium-oxygen (Li/Na-O_2) batteries could offer outstanding gravimetric energy density compared to traditional LIBs/NIBs. [193,194] However, electrochemical stability of the electrolyte solvent and oxygen reduction products with the existence of lithium salts further limit their practical application because of poor electrochemical work efficiency and cycling life of Li/Na-O_2 batteries. [195,196] The reaction products from Li-O_2 batteries during electrochemical cycling was investigated by Gallant *et al* [197] by *ex situ* XAS (Figure 6a). Fingerprints of carbonates at both the C and O K-edges are observed, showing the formation of Li_2CO_3-like species at the interface between oxygen electrode and discharge products Li_2O_2. The oxidation kinetics was slowed down during Li-O_2 cycling as a result of the growth of these Li_2CO_3-like species. The cathodic discharge products of ether-based Li-O_2 batteries were identified by Olivares-Marín *et al* [198] by mapping the distribution of oxygen species using TXM (Figure 6b). A large number of small particles and aggregates of carbonates, resulting from degradation of ether electrolyte, were formed on the electrode surface of lithium peroxide particles. Meanwhile, in the core of the particle, toroidal-shaped lithium peroxide particles phase dominate. The formation of these characteristic particles can be

related to the availability of large superoxide amounts in the solution phase. By changing to TFSI-based ionic liquid electrolytes, they observed that Li_2O_2 and LiO_2 are the primary products in similar proportions compared to ether-based electrolytes.[98] However, the formation of carbonates was almost negligible, suggesting a higher stability of ionic liquid electrolytes. Additionally, LiOH is clearly observed in the ionic liquid electrolytes, which is preferentially associated with peroxide.
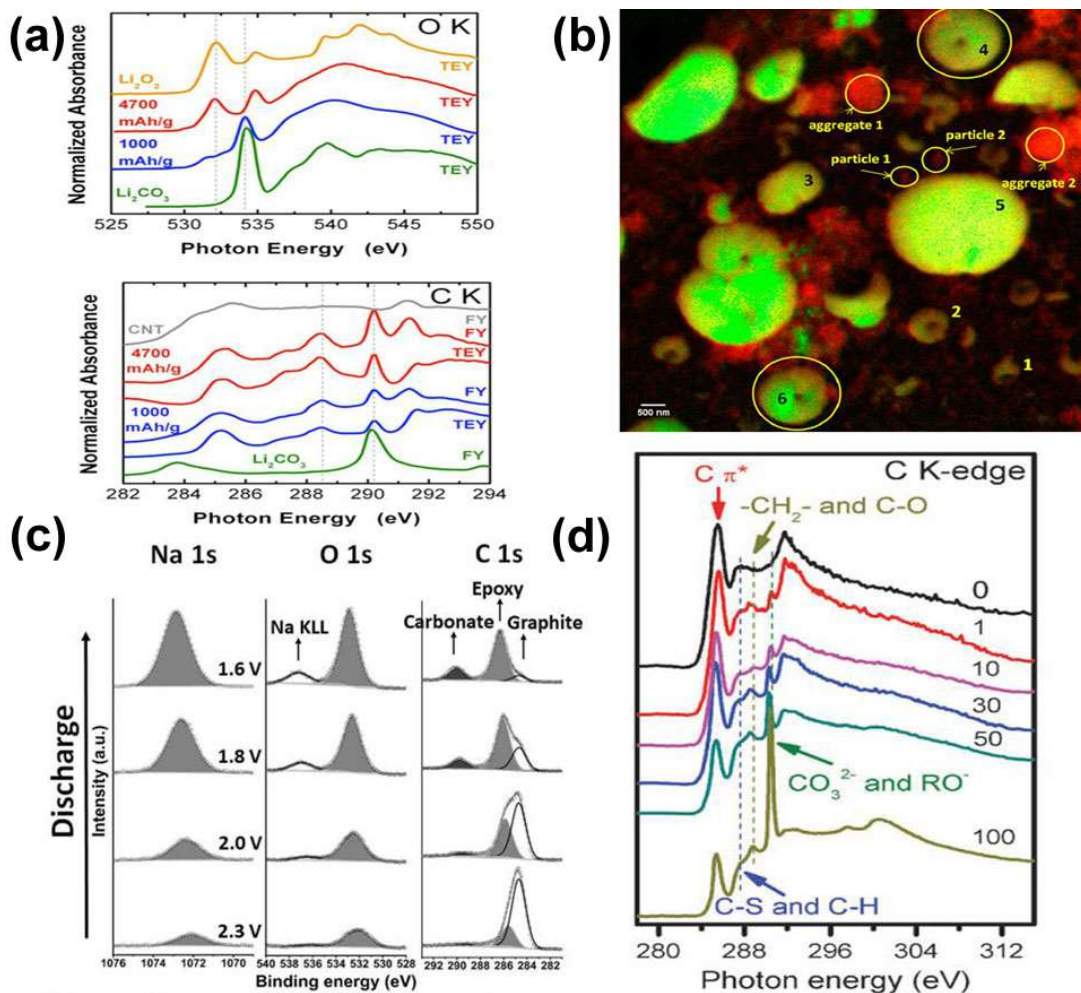

Figure 6 (a) XAS at the O K-edge (TEY) and C K-edge (TEY/TFY) of electrodes discharged to 1000 mAh/gC and 4700 mAh/gC on the first discharge with reference spectra (reproduced with permission from [197], copyright 2012, American Chemical Society) (b) TXM images of a carbon-based cathode after fully discharge at 100 mA per total gram of carbon in Li-O_2 batteries, which contain the result of overlapping three-color maps with intensities proportional to the amounts of Li superoxide (cyan), Li peroxide (green), and carbonate (red)

(reproduced with permission from [198], copyright 2015, American Chemical Society) (c) Operando XPS of Na 1s, O 1s, and C 1s on the cathode of Na–O2 batteries during discharge process (reproduced with permission from [66], copyright 2018, Springer Nature) and (d) XAS at the C K-edge of the S–GO cathode materials at different discharge–charge cycles (reproduced with permission from [207], copyright 2014, The Royal Society of Chemistry).

The formation of the main discharge product, sodium carbonate (Na_2CO_3) in Na–O_2 batteries at different stages of the first discharge process was monitored by Mao *et al* employing *operando* XPS (Figure 6c).[66] The formation of Na_2CO_3 on the cathode during the discharge cycle was evidenced from the clear change of characterized peaks in C1s and O 1s spectra at discharged states. Moreover, the formation of Na_2CO_3 is proved as the main discharge product of the Na–O_2 cell resulting from the instability of the graphite electrode, particularly when exposed to sodium oxides and sodium radicals, which is a potential cause of capacity fading of the Na–O_2 batteries. The evolution of the chemical compositions of the discharge products in oxygen electrode during charging in Na-O_2 batteries was verified by Sun *et al* by means of *ex situ* XAS at O and N K-edges.[65] The formation of intermediate phases like Na_2O_2 and Na_2CO_3 during the charging process results in high overpotentials and at the end collapse of carbon electrode.

3.3.2 Carbon-based Lithium-Sulfur Batteries

Lithium-sulfur (Li-S) batteries is another promising choice for rechargeable battery chemistries due to its low cost, high theoretical specific energy and high energy density. [199,200] However, the practical application of Li–S batteries has been limited because of the insulating property of S, high solubility and shuttle phenomena of polysulfides that trigger low coulombic efficiency and poor cycle life.[199,201] To solve these problems, S-doped carbon materials were considered to increase the active-sulfur utilization, cycle stability and high-rate capability of sulfur cathodes. [202–205] The actual roles of carbon material in Li–S systems was probed using XAS. [57,203,206]

The evolution of Li in S-doped graphene oxide (Li/S-GO) cathode materials after the dis/charge process was studied by Feng *et al* [207] employing *ex situ* XAS at C and O K-edges (Figure 6d). Peaks for the C 1s transition to CO_3^{2-} and R-O σ* states, constituting a spectroscopic signature of lithium carboxylate and possibly lithium alkoxide, were observed to increase over 100 cycles. The strong interaction between Li atoms and carboxyl is further

confirmed by the clear change of characteristic peak for the O 1s transition to carboxyl π^* state. The reacted lithium compounds are therefore mainly deposited on the cathode surface, leading to the formation of a lithium compound blocking layer at the electrolyte/electrode interface, which contributes to capacity fading.

Further understanding of the effects of N-doping in Li-S battery was investigated by Zhu *et al* using *ex situ* XAS at C and N K-edges.[57] A significant change in oxygen coordination structure was observed with different amounts of sulfur loading, whereas the nitrogen chemical environment remains unchanged. In that case, sulfur does not directly interact with carbon through nitrogen bonding for the sulfur immobilization. Inversely, the surface oxygen functional groups became more reactive because of the presence of nitrogen, which can provide excellent adsorption sites to host more S to fix on the carbon cathode. [204] The sulfur bonding on oxygen functional group, promoted by N-doping, was confirmed on mesoporous carbon electrodes. [208] In addition, N-doping may enhance the binding of lithium polysulfide on graphene sheets.[209] Qui *et al* observed the appearance of a new peak at the fully discharged state after 200 cycles in *ex situ* XAS at the N K-edge, attributed to N...Li_2S_x interactions and which could improve their electrochemical performance.

3.3.3 Oxygen Redox State in Li-ion Batteries Oxide Electrodes

Oxygen redox reactions related to the lithium insertion/desertion process of Li-rich cathodes are essential to the performance and stability of high-energy batteries. However, the fundamental understanding of oxygen-anionic redox reactions (O^{2-}/O_2^{n-}) is still at an initial stage and its reversibility remains an issue.[210,211] The structure and stability of the layered oxides at high voltages are associated with oxygen-related reactions for charge compensation. [212] Recent studies reported the reversible anionic redox activity of oxygen on Li-rich cathodes.[213,214] In general, two different oxygen types are involved in oxygen-anionic redox: (i) the O_2 and CO_2 release and related surface reactions and (ii) the lattice oxygen of the oxide. [215,216] The quantitative detection of the lattice oxygen, strongly evolving during charge compensation mechanisms, is particularly challenging. The high sensitivity of soft X-ray spectroscopy to the chemical states of oxygen species is thus well-adapted to monitor the oxygen-anionic redox processes in LIBs. [93,217]

The chemical state of lattice oxygen and of decomposition products can be characterized by XPS at the O1s. [218–220] Nevertheless, the high sensitivity of XAS to hybridization

between metal 3d and O 2p provides more insights into the contributions of oxygen ions into electrochemical processes and charge compensation mechanisms in Li-rich electrodes. [150,221–223] The pre-edge peak intensity is often used to estimate charge compensation of oxygen in the metal oxide lattice. [223,224] TEY and TFY detection modes enable simultaneous characterization of the surface and bulk components of the metal oxide.[222] The charge compensation mechanism during two lithium extraction/insertion between Li_2FeSiO_4 and $FeSiO_4$ was for example investigated by Masese $et\ al.$[225] The Fe-3d band contributes dominantly for the first lithium extraction process from Li_2FeSiO_4 to $LiFeSiO_4$. During the second lithium extraction process from $LiFeSiO_4$ to $FeSiO_4$, a large amount of the ligand holes in the O 2p states make compensation for the valence change instead of further oxidation of Fe^{3+}. This reversible anion redox processes ($O^{2-} \rightarrow O_2^{2-}$) could explain the high capacity achieved in Li_2FeSiO_4. For $LiMnNiCoO_2$ electrodes, Redel $et\ al$ found that the charge compensation during lithium extraction from the interlayer spaces is first provided by partial oxidation of transition metals.[226] At high voltage, the lithium ions are also extracted from the transition metal layers and the charge is compensated by extracting electrons from the O 2p level in the hybridized metal 3d and O 2p orbitals.

Further understanding of redox reaction products can be provided using RIXS at the O K-edge.[227] As an example, comparison of anionic oxygen activity in two different lithium-rich layered oxides was studied by Xu $et\ al.$[228] A fluorescence feature associated with anionic oxygen redox species was observed at 523.7 eV emission energy at 531 eV excitation energy on RIXS maps for $Li_{1.2}Ni_{0.2}Mn_{0.6}O_2$, that is absent in $Li_{1.2}Ni_{0.2}Ru_{0.6}O_2$. It implied that the ruthenium atoms rather than the oxygen are the electrochemically active sites in $Li_{1.2}Ni_{0.2}Ru_{0.6}O_2$. The nature of this fluorescence contribution led to very active research in the field.[210,214,229–232] A similar feature at 523.7 eV emission energy on RIXS maps was observed on other cathode materials as shown in Figure 7a.[215] The comparison of its energy-dependent broadening and related evolution of the elastic line with O_2, CO_2 and Li_2O_2 molecules led to the conclusion that this oxygen signature is not coming from a well-defined molecular state. On the other hand, House $et\ al$ recently evidenced the trapping of molecular O_2 in $NaLiMnO_2$ compounds during the first charge by high-resolution RIXS.[230] In high-resolution RIXS, molecular vibrations of the O_2 molecules are resolved as a peak progression related to its different vibrational states as shown in Figure 7b. In addition, the formation of localized holes on O^{2-} in ribbon-ordered structures is evidenced on the XAS at the O K-edge.

Operando XAS at O K-edge using an electrochemical flow cell can provide further information on the oxide redox process in Li-rich oxide electrode. Yamamoto *et al* demonstrated that enhancement of the covalent or ionic character in cathode materials are necessary conditions to stabilize anion redox.[233] For high covalency with transition-metal such as Ru, the formation of peroxide species is possible (Figure 7c). On the other hand, weak covalency cannot stabilize holes, leading to irreversible oxygen loss. These recent works highlight the relevance of in-depth investigation of oxygen bonding and these techniques will certainly contribute to the improvement of layered oxide materials as energy storage materials.
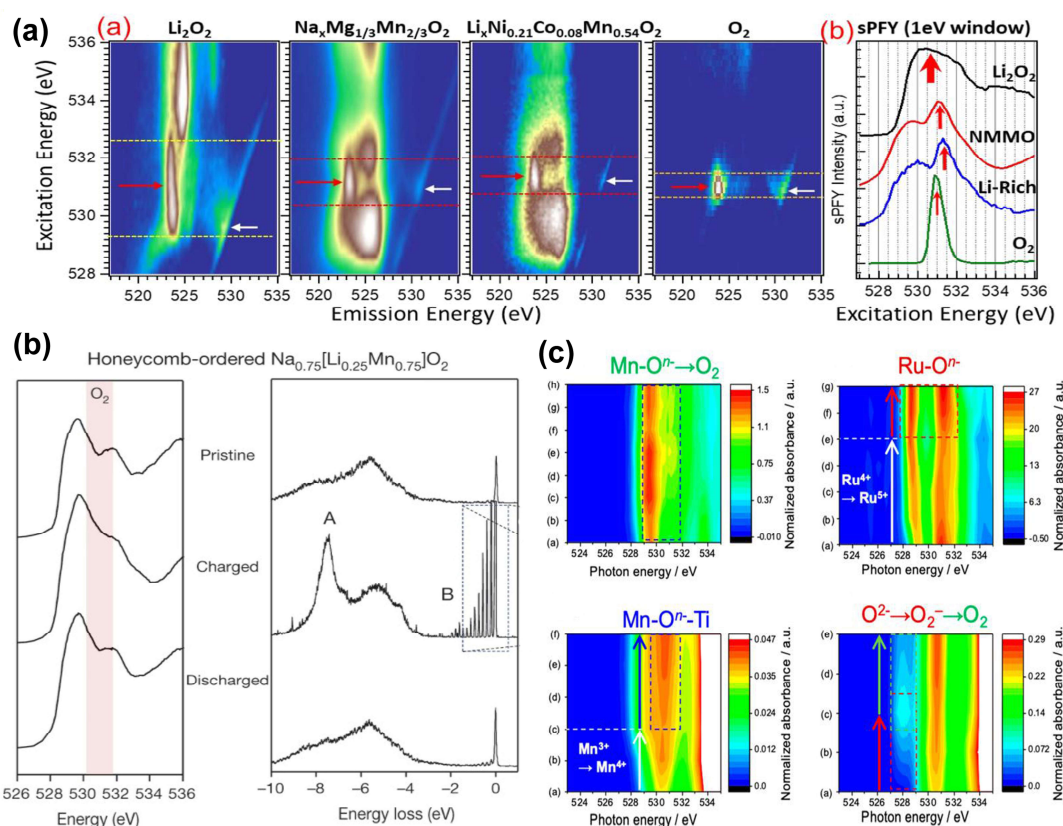

Figure 7 (a) Direct comparison of full mRIXS profile of oxidized oxygen states in four systems: Li_2O_2, charged $Na_{2/3}Mg_{1/3}Mn_{2/3}O_2$, charged $Li_{1.17}Ni_{0.21}Co_{0.08}Mn_{0.54}O_2$, and O_2 along with PFY-XAS of the four systems extracted from mRIXS maps by integrating the intensity within 0.5 eV of 523.7 eV emission energy (reproduced with permission from [215], copyright 2020, American Chemical Society), (b) XAS at the O K-edge and high-resolution RIXS spectra collected at an excitation energy of 531 eV for $Na_{0.75}[Li_{0.25}Mn_{0.75}]O_2$

(reproduced with permission from [230], copyright 2020, Springer Nature), and (c) Operando XAS at the O K-edge of $Li_{1.33}Mn_{0.67}O_2$, $Li_{1.33}Ru_{0.67}O_2$, $Li_{1.2}Ti_{0.4}Mn_{0.4}O_2$ and $Li_{1.2}Ti_{0.4}Fe_{0.4}O_2$ obtained at different charge states (reproduced with permission from [233], copyright 2019, American Chemical Society).

3.4 Polymer-based Binder

The large volume change of high-capacity materials during electrochemical work, which is harmful to the performance of battery systems, could be reduced by modifying the polymeric binders.[234] The chemical structure of binders was then also the topic of soft X-ray spectroscopic investigations. Carbonyl groups were found to lower the LUMO level by using XAS at C K-edge, which can improve the binder performance.[235] More precisely, the lithium binding energy in the carbonyl-containing binder is higher than for binder without carbonyl group. As a result, the lithium ions interact with the binder before lithiation of the Si anode in this case, which does not happen for a classical binder. The stability of the lithiated electrode is then significantly increased. In the same vein, the addition of fluorine-containing groups was also found to lower the LUMO states of the polymer-based binder of about 0.7 eV compared to an F-free polymer from XAS at the C K-edge.[236]

The binder can also have an impact on the SEI formation and stabilization. Different types of binders have been investigated by Nguyen *et al* using *ex situ* XPS at C 1s and F 1s.[237] They reported that carboxylic acid functional groups of poly(acrylic acid) (PAA) binder are reactive toward the electrolyte, resulting in the decomposition of $LiPF_6$ and dissolution of SiO_x during the electrode wetting process. PAA and sodium carboxymethyl cellulose (CMC) binders, on the other hand, form a protective layer on Si during the first cycle which can effectively suppress the decomposition of carbonate solvents. For polyvinylidene difluoride (PVDF) binder, a continuous reduction of carbonate solvents was found during cycling, leading to the generation of a thicker SEI layer. The formation of a surface film made of organic/inorganic mixtures induced by electrolyte decomposition was also reported after cycling with a fluorinated polyimide binder and characterized by XPS. [238] Particularly, the formation of C-F functional groups, improving the contact between binder and electrode upon cycling, was evidenced by XPS at the C1s and F1s. Such a film protects the cathode surface and suppresses metal dissolution and cathode degradation. Moreover, the formation of LiF was observed

upon charge on the low-voltage LiFePO$_4$-Li$_4$Ti$_5$O$_{12}$ full cell by Leanza et al due to the reaction between PVDF binder and lithium. [239] LiF was found to migrate towards the Li$_4$Ti$_5$O$_{12}$ anode and precipitate on the surface rather than deposited on the LiFePO$_4$ cathode, as proved by XPS at the F 1s, XAS at F K-edge, and XPEEM imaging, suggesting the PVDF was electrochemically unstable at relatively low potentials.

4 Electrolyte

4.1 *Aqueous Electrolyte*

The development of microjet technology enabled the rapid development of soft X-ray spectroscopy of water and aqueous solutions. The high sensitivity of X-ray spectroscopies, in particular XAS, to the water local hydrogen-bonding network opened new perspectives on solvation and solid-water interfaces as reviewed previously.[240,241] Here only a few representative examples of aqueous electrolytes that are relevant for EES are summarized.

Acidic aqueous electrolytes are often used for redox pseudocapacitive energy storage. XAS at the O K edge of water is constituted of a pre-, main- and post-edge around 535, 538 and 540 eV, respectively, which are sensitive to different hydrogen bonding configurations.[242] At a high concentration of hydrochloric acid, a significant decrease of the pre-edge and an increase at the post-edge observed on XAS at the O K-edge were interpreted as an increase of protonated water ordering from H$_5$O$_2^+$ into H$_3$O$^+$ with the concentration.[243] Niskanen *et al*, observed by X-ray Raman Scattering the complete disappearance of the pre-edge in highly concentrated sulfuric acid solutions as shown in Figure 8a.[244] Supported by molecular dynamics simulations, they attributed the changes to an increase of the number of donated hydrogen bonds per water oxygen for high acidic concentration. TEY-XAS at the platinum-water interface in diluted sulfuric acid have shown, on the other hand, that this pre-edge is predominant under applied positive potential.[245] This was attributed to the accumulation of sulfate ions at the solid-liquid interface, which electronic signature also contributes at similar excitation energy.
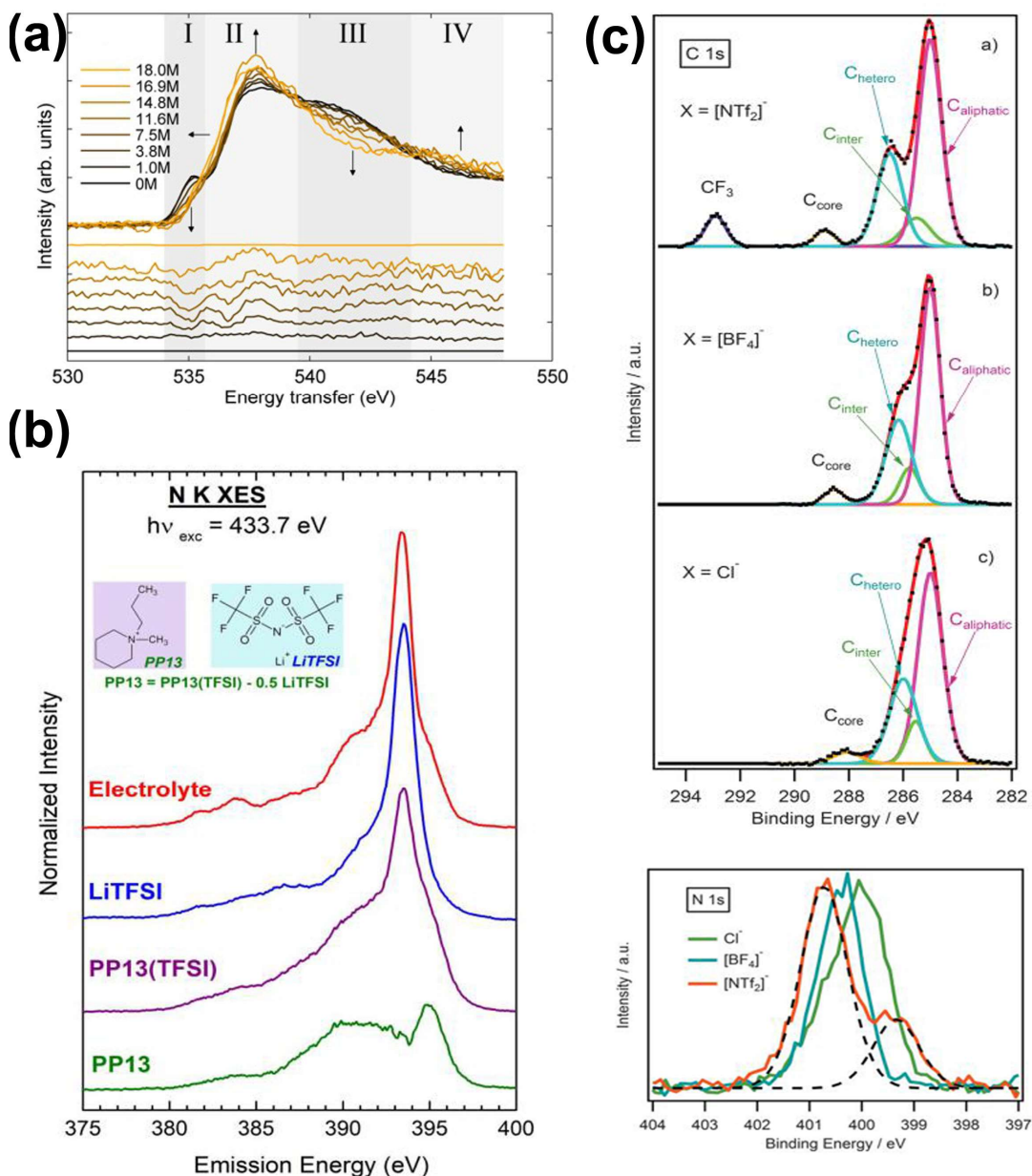
Figure 8 (a) Non-resonant inelastic X-ray Raman scattering at the O K-edge of $H_2SO_4(aq)$ for different concentrations (reproduced with permission from [244], copyright 2015, American Chemical Society), (b) XES at the N K-edge of the electrolyte, Li(TFSI), PP_{13}(TFSI) and PP_{13} (reproduced with permission from [69], copyright 2019, American Chemical Society) and (c) XPS C 1s and N1s XPS of $[NTf_2]^-$, $[BF_4]^-$ and $[Cl]^-$ anions (reproduced with permission from [270], copyright 2015, The Royal Society of Chemistry).

Alkaline solutions were also extensively studied by X-ray spectroscopies. Especially, the hydroxide ion was found to have a well-defined signature at 532.5 eV in XAS[246] and 536

eV in XPS,[247] which facilitates its characterization compared to protons in water.[248] The use of RPES enabled the probing of transient hydrogen bonding between hydroxide and neighboring water molecules directly in aqueous solution.[247] Recently, the accumulation of hydroxide ions at the TiO_2 nanoparticle surface was evidenced by in situ XAS and XPS.[249] These studies illustrate that XAS and XPS would be highly valuable to investigate proton or hydroxyde accumulation in the electric double layer of supercapacitors.

The solvation of ions has also been probed by XAS. For different monovalent cations, similar changes of the XAS signature are observed, showing that they mostly disturb their first solvation shell irrespective of the cation.[250] This was later confirmed using X-ray Raman Scattering on highly concentrated LiCl solutions as saturation was only observed for very high concentration (11m). [251] Above this concentration, the hydrogen bonding network of water do not change anymore. Divalent cations are found to have a more profound impact of the water structure, attributed to a charge transfer between the cations and nearby water molecules. [250] A deeper understanding of the ion solvation structure can be obtained using RIXS, which was applied in various chloride and bromide salts.[252–254] RIXS is particularly interesting as cations and anions are affecting different regions of the RIXS spectra.[254] Notably, the ultrafast dissociation of water molecules was found to be reduced upon increasing the salt concentration as a result of a strong change of the water hydrogen bonding. [253] That may possibly explain the reduced reactivity of water in water-in-salt electrolytes, leading to a higher operational voltage window.

4.2 Organic Electrolyte

Organic electrolytes are generally used for LIBs/NIBs due to their high ionic conductivity, low viscosity, good wettability and large electrochemical window. [255–257] In recent years, several organic electrolytes and mixture of them were probed by XAS.[258] As an example, Smith *et al* studied propylene carbonate (PC) electrolyte using XAS at the O K-edge.[259] They identified a concentration-dependent blue shift from transitions related to carbonyl groups upon addition of $LiBF_4$ in PC. By combination with theoretical calculation, they suggested that it results from strong coordination between PC molecules and Li^+ ions. Hydrogen bonding interaction between oxygen-containing functional groups and polar organic solvents can be monitored at the XAS at the O K edge as shown on acetic acid molecules by Horikawa *et al.*[260] In hexane, they observed a resonance peak shift, resulting

from a strong hydrogen bonding between acetic acid molecules, forming cyclic dimers, similar to the behavior of cluster molecules in vacuum. Meanwhile, the concentration-dependent peak differences in XAS for acetonitrile solutions suggests a weakening of hydrogen bonding between the acetic acid molecules. Moreover, Li^+ solvation in carbonate-based electrolytes was also investigated by El Kazzi *et al* [261] using near ambient pressure XPS. The changes in the binding energies of the Cl 2p and Li 1s core levels between the EC: DMC and the DMSO were interpreted in terms of different Li^+ solvation structures. XPS measurements on battery electrolyte are also possible by stabilizing a drop of electrolyte at its vapor pressure as demonstrated on 1 M LiTFSI in propylene carbonate (PC).[262] The accumulation of ionic species was observed at the electrolyte surface while the bulk electrolyte is up to the expected composition.

Binary solutions mixing acetonitrile and methanol were also investigated by Nagasaka *et al* using XAS at C, N and O K-edges.[263,264] In methanol−water binary solutions, concentration dependence of the hydrophobic interaction at the methyl group in the C and O K-edge XAS spectra is observed. Three different local structures and steric configurations based on the different proportions of methanol and water in binary solutions are identified. Microscopic inhomogeneities are evidenced in acetonitrile−water binary solutions. Similarly, they proved that three different local structures between acetonitrile and water play a significant role in microscopical inhomogeneity in the C, N and O K-edge XAS.

4.3 Ionic Liquid-based Electrolyte

Ionic liquids are considered as tunable solvents which are increasingly used as electrolyte for EES systems due to their good solubility, high conductivity, stability and hydrophobicity. [265–267] Ionic liquids are non-flammable and thermally stable in electrochemical reactions, which would increase the safety of the battery systems. [266] Understanding the interaction between the cation and the anion is important for the design of ionic liquids for specific functions in electrolyte, particularly on the study of degradation product of ionic liquids-based electrolyte. [268] Due to their high vapor pressure, they can be easily characterized in vacuum, which makes their characterization with soft X-ray spectroscopies easier than aqueous or organic electrolytes.[269]

Probing the valence electronic states of ionic liquids with XES may provide new insights into the stability of the molecules composing the electrolyte. In this regard, Léon *et al* investigated

the solvent PP_{13}(TFSI), the salt LiTFSI, and the PP_{13} cation with *in situ* XES at the N K-edge, also at different applied potentials (Figure 8b).[69] The chemical environment of the nitrogen atoms is significantly modified during the first discharge/charge cycle, suggesting a decomposition of the salt suggesting that it is highly unstable during the electrochemical process. Meanwhile, the ionic liquid solvent remains mostly as an ion pair, although some decomposition into PP_{13} cations and TFSI anions possibly exist.

Cation-anion interactions in ionic liquids can also be probed by XPS. Santos *et al* studied charge distribution in nitrogenous cations of guanidinium-based ionic liquids by XPS (Figure 8c).[270] They found a large difference between measured binding energies for the N 1s of cations compared to other families of ionic liquids according to the binding energy in order: $[NTf_2]^->[BF_4]^->Cl^-$ in N 1s and C 1s. These results suggested a weak bond between the guanidinium cation and the anion through the delocalization of the positive charge around the three nitrogen centers as opposed to one for pyrrolidinium cation. The chemical shift of the XPS N 1s was also monitored to probe the effect of the N3-substituted alkyl chain on the electronic environment of 1,3-dialkyl imidazolium-based ionic liquids.[267] The electronic environment of the cationic nitrogen can be affected by changing from methyl to butyl groups. The binding energy shift of the N1s is stronger in the presence of less basic anions and inversely proportional to the basicity of the anion. The increase of the N3-substituted alkyl chain length can also influence the charge-transfer effect from the anion to the cation. Men *et al* also investigated the impact of methylation on the electronic environment of pyridinium cations in picolinium-based ionic liquids. [271] They observed a significant increase in electron density on the cationic nitrogen because of the electron-donating effect of the methyl group. The methylation position also affects the electronic environment of the cationic nitrogen and the trend of binding energy is in agreement with the cation acidity in N 1s spectra. Based on that, with the increase of the inductive effect of cations, the cation-anion interactions become weaker through charge transfer from the anion to the cation.

4.4 Solid-State Electrolyte

Solid-state lithium-ion battery has attracted great attention due to its high safety and increased energy density. [272] Compared to conventional lithium-ion batteries with highly flammable organic liquid electrolytes or polymer electrolytes, solid electrolytes not only have high thermal stability but also have much better electrochemical stability and are compatible with

higher potential cathode materials to increase energy density. [272–274] Additionally, since no liquid electrolyte is used in solid-state lithium-ion battery, packaging for batteries can be much simplified so that dead weight in battery packaging can be largely reduced, further resulting in increased energy density as well. [272,273] In recent years, Li_2S–P_2S_5 (LPS) solid electrolyte possessing higher conductivity with exceeding 5 mS/cm has been demonstrated. [275,276] Importantly, the chemical and electronic properties of electrolyte–electrode interfaces in LPS-based batteries is easier to probe by soft X-ray spectroscopies than liquid electrolyte as they do not evaporate in vacuum.

For example, Wu *et al* [277] investigated LPS solid electrolytes oxidation process at the interface with $LiCoO_2$ by using operando XPS. The formation of oxidized solid electrolytes byproducts was observed at both S 2p and P 2p spectra upon charge, while no further changes in the spectra at 3.6 V for over 60 h were observed, indicating the end of the oxidation process. During delithiation, the formation of solid electrolytes byproducts passivates the electrode surface against further significant oxidation. Mirolo *et al* [278] probed similar redox reactions during de-/lithiation of SnO_2 electrode cycled in LPS by operando XPS and in situ XAS. Beyond de/lithiation of the SnO2 electrode, side reaction related to the reduction of the LPS solid electrolyte at the interface with the active materials or conductive carbon was reported. They also observed the formation of Li_2O on the surface of SnO_2, rather than carbonate species, caused by the residual trace oxygen and/or water present in the ultrahigh-vacuum environment. On $Li_4Ti_5O_{12}$ electrodes, no carbonate species were found either after LPS reduction but the formation of Li_2S and Li-P functionalities (Li_xP) was reported instead of Li_2O. [279] Similar observations were reported on Li metal electrodes. Wood *et al* [280] evidenced a significant SEI formation and evolution at the LPS surface by the appearance of new chemical states in both the S 2p and P 2p XPS from the original LPS functional groups (such as: Li-S-P, P-S-P, and P=S) to Li_2S and Li_xP after 0.5 h of charging by operando XPS. The transformation between Li_xP and Li_3P and reaction between Li-P and Li_2O leading to the formation of Li_2O_2 and Li_3PO_4 were evidenced by comparing the different XPS core levels at dis/charging states. In general, solid electrolytes are particularly promising for operando X-ray spectroscopic studies inside vacuum chambers and conclusions obtained with these electrolytes may possibly be extended to liquid electrolytes as decomposition reactions may behave similarly.

5   Solid-Electrolyte Interphase

The analysis of the morphology, composition, and electrochemical behavior of SEI has been a major field of research over the last 30 years.[14,281–287] SEI layers are usually formed as a result of electrochemical instability of the electrolyte during the initial cycles. While *in situ* characterization would be preferable due to the high instability of SEI layers, it remains experimentally challenging for soft X-ray spectroscopies. As a result, most of the studies reported in this section are based on *ex-situ* investigations. Nevertheless, *in situ/operando* characterization techniques sensitive to electrode/electrolyte interface are emerging [14] and some examples involving the characterization of light elements will be mentioned.

5.1 Solid-Electrolyte Interphase in LIBs

The formation and dissolution of SEI were mostly studied for LIBs so far. The usual main components of SEI layers are lithium carbonate and fluoride compounds which are clearly observed by XAS.[288,289] For example, Qiao *et al* compared the XAS signature at C K-edge, O K-edge and F K-edge of SEI formed on Sn electrodes in 1 M $LiPF_6$, EC: DEC (1:2 w:w) electrolyte to different references (Figure 9a).[288] They found that SEI on Sn (100) mainly contains porous Li_2CO_3 species with clear fingerprints of carbonates (CO_3^{2-}), namely the transitions from C1s and O1s to the π^*(C=O) orbital at 290.2 eV at the C K-edge and 533.7 eV at the O K-edge. On Sn (001), on the other hand, the SEI is principally constituted of LiF and organic molecules, with a small amount of carbonate and electrolyte. This result proves that the reactive (001) surface facilitates the decomposition of $LiPF_6$ to form a LiF layer, whereas the decomposition of carbonate-based electrolyte preferentially occurs on (100) surface. Moreover, based on XAS at the C and F K-edges, the LiF is found to passivate Sn (001) after one cycle while the porous carbonate layer does not affect the activity of (100) surface, which leads to drastically different electrochemical behavior and morphology of the two SEIs. An inhomogeneous distribution of the decomposition compounds within the SEIs can also be concluded based on the significant differences between TEY (surface) and TFY (bulk) measurements.
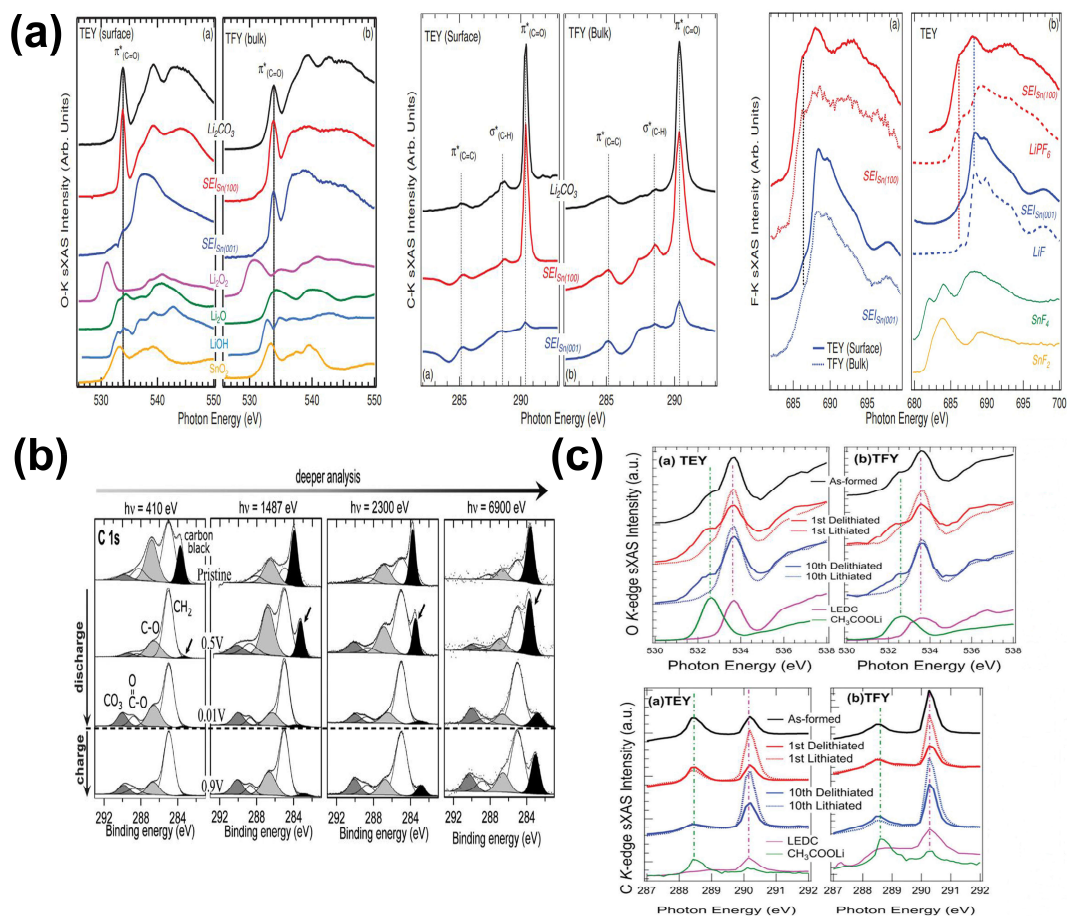
Figure 9 (a) XAS at the C, O and F K-edges of the SEI layers formed on Sn (100) and (001) single crystal electrodes along with reference spectra (reproduced with permission from [288], copyright 2014, Wiley-VCH Verlag GmbH & Co. KGaA, Weinheim), (b) *Ex situ* XPS C 1s of the Si/C/CMC composite electrodes upon the first discharge/charge cycle (reproduced with permission from [290], copyright 2012, American Chemical Society) and (c) XAS at the C K-edge in TEY and TFY modes of the as-formed SEI (black), and the SEIs at delithiated (solid lines) and lithiated (dotted lines) states at the 1st (red) and 10th (blue) cycles (reproduced with permission from [291], copyright 2018, The Royal Society of Chemistry).

Rezvani *et al* [82] also benefited from the different probing depths of XAS detection modes to investigate the evolution of SEI layer surface structure of $ZnFe_2O_4$-C anode during the first cycle and after 20 cycles. A passivation layer mostly constituted of Li_2O was found to be formed in the vicinity of the electrode. At the SEI surface (~5-7 nm), probed by TEY-XAS and XPS, a partially reversible layer of alkyl lithium carbonates, being partly replaced by Li_2CO_3 during delithiation when reaching higher Li storage levels was found. These results

34

demonstrate that the SEI layer acts as a Li reservoir which can contribute to extra-capacity of the electrodes. With synchrotron-based XPS, the probing depth can be tuned by varying the excitation energy. Philippe *et al* used this strategy to probe *ex situ* the SEI formation in Si anode at the first dis/charge cycle with excitation energies ranging between 230 eV and 6990 eV.[290] A typical example for the carbon C1s level is shown on Figure 9b, for which the signal intensity of the carbon black signature enables an estimation of the SEI thickness. They found that at the very beginning of discharge (0.5 V vs Li^+/Li), lithium has not reacted with silicon but a thin SEI layer has already formed. Upon discharge, the thickness of SEI increases, and lithiums start to react with Si nanoparticles to form Li_2O and Li_xSiO_y compounds. After full charge (0.9 V vs Li^+/Li), lithium atoms have been almost fully extracted out, accompanied by a decrease of the thickness of the SEI and disappearance of Li_2O.

The XAS signature of carbonates was later used by Zhuo *et al* to investigate the evolution of the SEI on Cu electrode at different cycling stages in 1 M $LiClO_4$, EC: DEC electrolyte (Figure 9c).[291] The carbonate species in the SEI layer demonstrate redox reversibility and decompose during the delithiation (oxidation) process, resulting in a significant shrinking of the SEI thickness. Additionally, the carbonates also evolve during each lithiation cycle and become more inert upon cycling according to intensity change on the fingerprint peak at the C K-edge during electrochemical cycling, suggesting SEI growth may be an oscillating and highly dynamic process with a breathing growth.

XPEEM is a powerful tool to characterize SEI layer and the complex electrode-electrolyte interface reactions in LIBs as demonstrated by the work of El Kazzi's group. They investigated the surface modification of $Li_4Ti_5O_{12}$ (LTO)[111] and $LiNiCoMnO_2$ (HE-NCM) or $LiFePO_4$ (LFPO) compounds [110] during cycling by *post mortem* XPEEM analysis. The different batteries elements (conductive additives, active material and binder) were identified based on their XAS signature at the C and F K-edges and imaged with < 50 nm spatial resolution as shown in Figure 10a. At different charge/discharge states, no obvious changes in XAS spectra of both carbon and active material could be observed while a significant change of the LTO signature was observed during cycling. In particular, the reduction of the electrolyte at the surface of LTO is evidenced by the disappearance of C=O and carbonate resonances in the C K-edge XAS after the discharge process, leading to electrolyte consumption. Using *post mortem* XPEEM, the electrolyte decomposition byproducts was only

detected on the LTO particles, while no carbonate signal is present in the carbon areas as shown in Figure 10b.[109] On NCM particles, no byproducts from electrolyte decomposition were found. Interestingly, agglomerates of transition metals coming from the surface of HE-NCM are also found on the LTO anode surface, illustrating degradation of the HE-NCM surface during delithiation.[110]
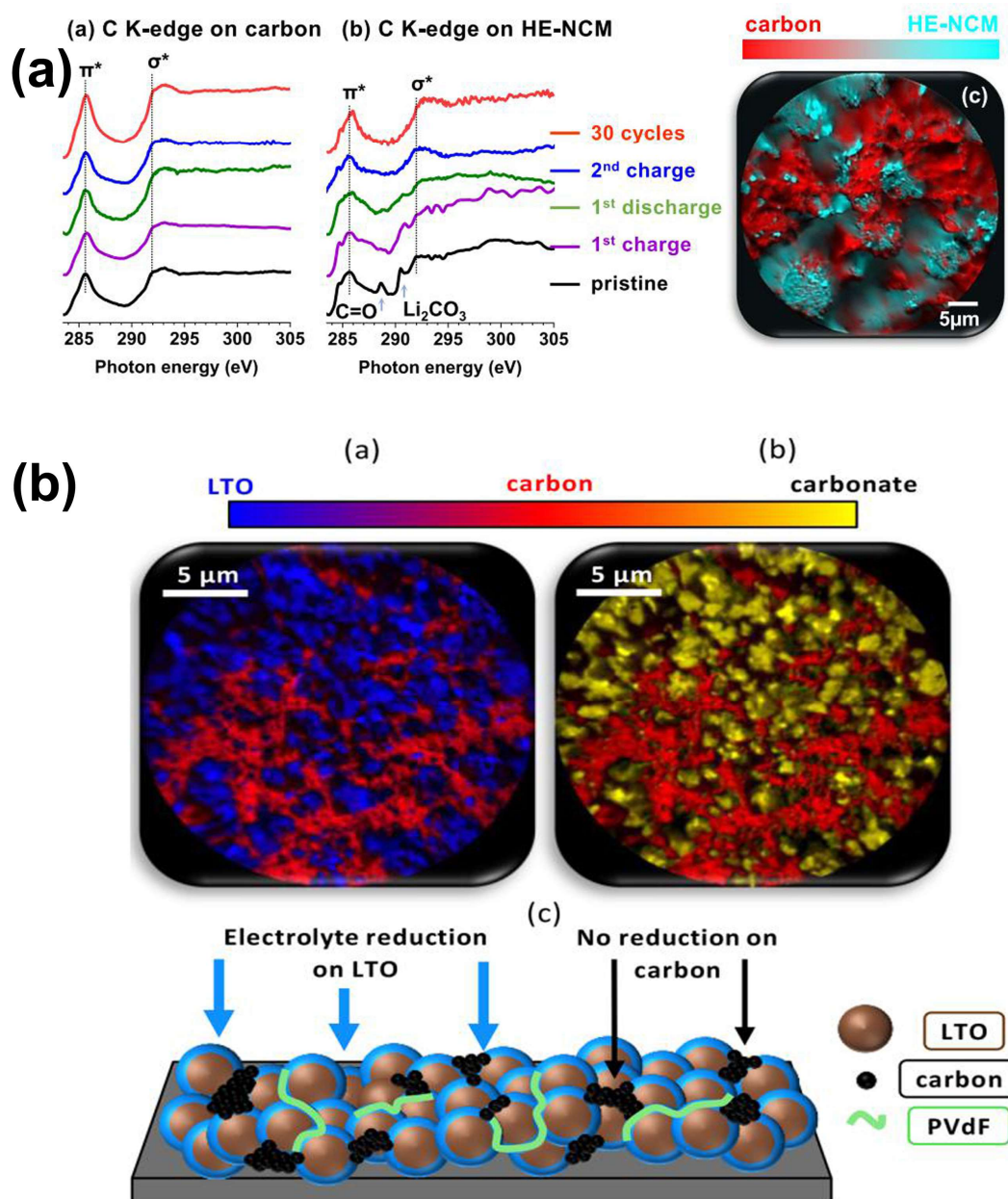

Figure 10 (a) Local C K-edge carried out on carbon and HE-NCM particles performed on

pristine and cycled cathode at different stages of charge and discharge and elemental contrast XPEEM image of HE-NCM electrode after 30 cycles at discharged state (reproduced with permission from [110], copyright 2019, American Chemical Society). (b) Elemental map of a lithiated LTO electrode (top) and the proposed mechanism leading to the electrolyte decomposing only on the LTO particles (bottom) (reproduced with permission from [109], copyright 2020, American Chemical Society).

Varying the electrolyte has naturally a tremendous impact on the structure of the SEI, which was extensively studied using *ex situ* XPS on various electrodes. The SEI layer formed by the reductive decomposition of an electrolyte based on ethylene carbonate (EC) mainly consists of alkyl carbonates, while the SEI layer formed by electrolyte based on fluoroethylene carbonate (FEC) is primarily composed of LiF along with a tiny amount of Li_2CO_3 upon cycling.[292] On magnetite-based electrodes, the higher concentration of LiF in the SEI formed in FEC-based electrolyte led to better electrochemical performance as opposed to EC-based electrolyte by limiting the growth of the SEI layer.[293]

Ionic liquid-based electrolytes are increasingly used to avoid irreversible decomposition in the electrochemical reaction compared to the traditional organic electrolytes. The structure of the SEI formed in such electrolytes is then simpler than organic electrolytes. In general, FSI- and TFSI-based electrolytes are mostly used for LIBs. Using a high FSI salt/solvent ratio, Ren *et al* demonstrated that solvent decomposition may indeed be suppressed.[294] Using *ex situ* XPS and sputtering for probing the SEI with different depth, they found no signal of Li carbides at the C1s for high LiFSI concentration as opposed to dilute condition. Meanwhile, an enrichment of Li_xN species is detected at the N1s, which highly benefits reducing the resistance of the SEI layer due to its highest Li^+ ionic conductivity among all the SEI components. In other XPS studies, the SEI formed during initial cycling was found to mostly result from decomposition products of the TFSI anion and related cation.[70,266,295–297] For example on silicon-copper anode, the detection of CO_x and CF_x features in C1s and F 1s XPS spectra, respectively, associated with a strong increase in oxygen signal confirms that an SEI effectively passivates the electrode surface during initial cycling in LiTFSI-containing electrolyte. [295] Similar results were observed on silicon oxide anode-based on another TFSI derivative.[70]

In graphitized carbon anode, Sugimoto *et al* observed a reversible Li intercalation in FSI⁻-based RTIL with EMI⁺ cation, while such intercalation is completely irreversible without FSI⁻.[266] Meanwhile, the surface-layer components on the graphitized electrodes cycled in the ionic liquid electrolytes with and without FSI⁻, characterized by *ex situ* XPS, are found to be chemically similar. Depth profiling was performed by etching progressively the surface in the XPS chamber. The anode surface inorganic layer from RTILs with and without FSI⁻ was found thinner than that produced from a typical organic solvent electrolyte. The decomposition of FSI⁻ anion on Li metal anode cycled in phosphonium/LiFSI RTIL electrolytes was also demonstrated by Girard *et al* based on *ex situ* XPS.[296] They found that the chemical nature of the SEI formed on the Li metal surface is highly dependent on the Li salt concentration and a concentrated electrolyte was found to promote the formation of a thicker and more uniform SEI with larger amounts of reduced species from the FSI⁻ anion.

5.2 Solid-Electrolyte Interphase in Li-S batteries

Li-S batteries are expected to have a quite different SEI due to the presence of polysulfide compounds. Nandasiri *et al* developed an *in situ* XPS to investigate the SEI layer evolution on Li anode in [bmpyr]⁺[TFSI]⁻ electrolyte Li-S batteries (Figure 11a).[117] An increase in Li-F and C-F species with a decrease in CF_3 is reported, implying the decomposition of TFSI⁻ anion in the proximity of the Li-anode. Besides that, the formation of Li_2S due to polysulfide reduction processes is also observed. The evolution of both Li_2S and Li-F species with cycling brings about the precipitation of an inorganic multiphase layer as the primary SEI component. Upon cycling, the rapid increase of polysulfide species proves a continuous fouling process on the Li anode. Thus based on different dynamic composition of SEI layer, they deducted that the SEI layer evolution has different stages: the formation of a primary composite mixture phase involving stable lithium compounds (Li_2S, LiF, Li_2O) and formation of a secondary matrix type phase due to cross interaction between reaction products and electrolyte components.[298] Electrolyte decomposition with LiFSI and LiTFSI in Li-S batteries were further investigated by Kim *et al* by monitoring the F 1s using *ex situ* XPS.[299] A greater extent of electrolyte decomposition is observed with LiFSI compared with LiTFSI as deduced from the LiF amount in the F 1s XPS spectra. Meanwhile, the highest LiF and lowest S–F compositions can be observed on cathodes suggesting that salt decomposition may form a protective layer on the cathodes.
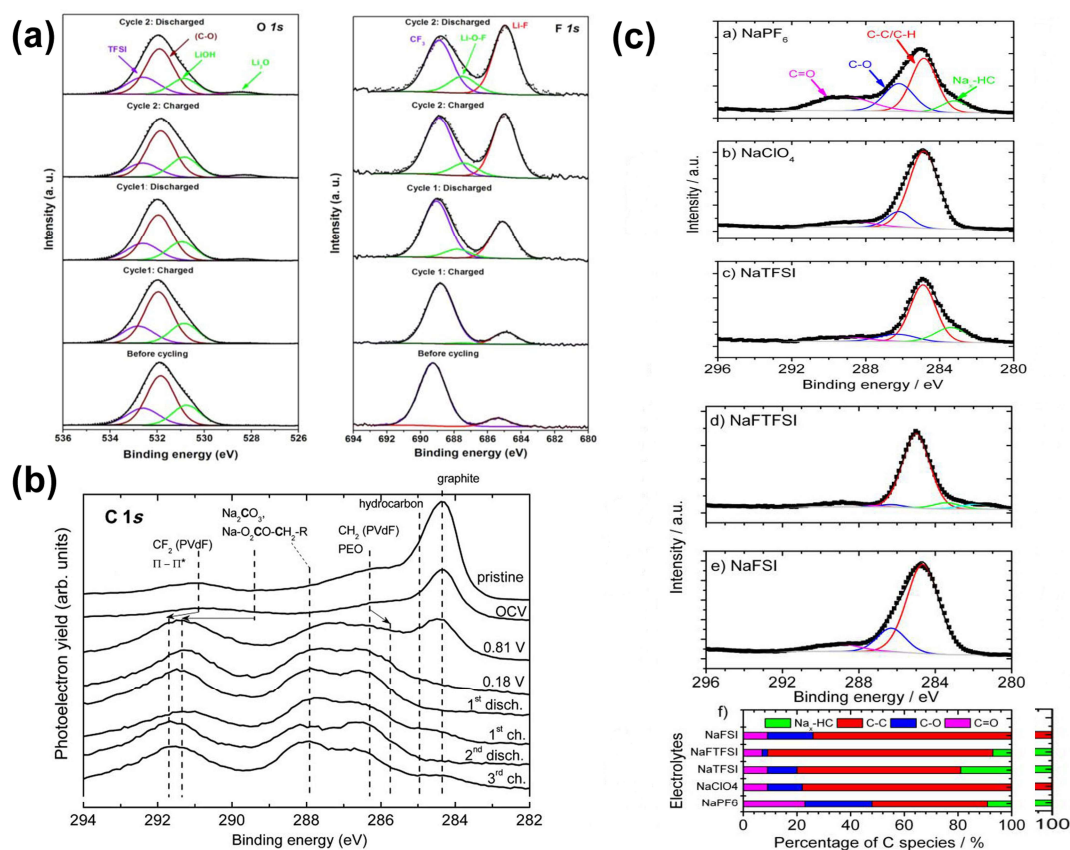
Figure 11 (a) XPS O 1s and F 1s of the Li-electrolyte interfacial region at different charge/discharge stages during 2 cycles (reproduced with permission from [117], copyright 2017, American Chemical Society), (b) XPS C 1s for electrodes before cycling and at different stages of the charge/discharge curve (reproduced with permission from [302], copyright 2015, American Chemical Society) and (c) XPS C 1s of carbon electrodes sodiated in 1M X salts dissolved in EC/DEC (1/1, wt.) electrolytes and percentage of the different carbon species in the outermost SEI layer formed on carbon electrodes sodiated in the above electrolyte formulations. X corresponds to a) NaPF6, b) NaClO4, c) NaTFSI, d) NaFTFSI, and e) NaFSI (reproduced with permission from [303], copyright 2019, Elsevier).

The formation and surface of an electrochemically controlled SEI layer by accurate pretreatment current density on Li anode in the electrolyte of 1,3-dioxolane (DOL) as the solvent and $LiNO_3$ as the additive was investigated by Wang *et al* using *ex situ* XPS.[300] They confirmed that this SEI layer mainly contains LiN_xO_y compound produced from the reaction between the Li anodes and additive $LiNO_3$ and a sulfone structure from the LiTFSI salt. Furthermore, reactions between the LiTFSI salt and the additive $LiNO_3$ were found to

form a complex inorganic/organic mixture with little electropolymerization of DOL because of the almost disappeared O-C-O peak in C 1s spectra. This observation supported the fast breakdown of the LiTFSI salt at a high current density due to an increase of the LiF peak intensity in the F 1s spectra after pretreating for 50 cycles. Thus they thought adequate pretreatment current density is quite important to produce a uniform SEI.

5.3 Solid-Electrolyte Interphase in NIBs

There are relatively fewer studies on SEI in NIBs, although their structure might differ significantly from SEI on LIBs. To illustrate this point, Philippe *et al* compared the chemical composition of SEI on Fe_2O_3 anode between LIBs and NIBs model systems employing *ex situ* XPS.[301] The SEI coverage is more obvious and the presence of homogeneous distribution in inorganic species in the NIBs, compared to the organic/inorganic layered structure observed for the LIB. Meanwhile, the SEI formation gradually occurs during the first discharge in both Li- and Na-system, however, for Na^+, a predeposit layer is formed directly by simple contact of the electrode/electrolyte. Additionally, the thickness of SEI layer in Na^+ system is thicker than that in Li^+ counterpart. The SEI layer of NIBs has more carbonates and alkyl carbonates, as well as more CO-rich species, while more species containing hydrocarbon chains can be observed in Li system according to the results in C 1s and O 1s spectra after cycling.

Another example could be based on the composition of the SEI was applied to $Na_2Ti_3O_7$ anode for NIBs.[302] The surface SEI layer is composed of a thin layer of chemisorbed oxygen, alkyl carbonates and poly(ethylene oxide) over a solid layer of sodium carbonates, NaF and NaCl with a thickness of around 5 nm. NaCl is formed by the decomposition of the electrolyte salt and the NaF result from the PVdF dehydrochlorination reactions during electrode preparation as shown in Figure 11b. Meanwhile, they observed this SEI layer is unstable upon electrochemical cycling.

Eshetu *et al* investigated the impact of the electrolyte salt anion on SEI formation in NIBs using *ex situ* XPS at C 1s and F 1s (Figure 11c).[303] They confirmed that the SEI building species formed on hard carbon anode by solvent reduction upon sodiation are found to decrease with the various salts in the order: $NaPF_6 > NaClO_4 \approx NaTFSI > NaFTFSI > NaFSI$. The SEI layer using Na-based electrolytes has more homogeneous and richer organic species than that in the SEI on lithiated anode. This results mainly from the higher solubility of the

inorganic Na salts and the Na-alkoxide intermediates, compared to the analogous Li compounds.

6 Conclusion and Outlook

While soft X-ray spectroscopy and microscopy have been used for decades to investigate organic materials, its application to the characterization of light elements in EES systems remains relatively novel. Light elements are particularly relevant because carbon, nitrogen, oxygen and/or fluorine are found in all critical parts of batteries and supercapacitors. They should therefore be characterized in complement to transition metals for which soft X-ray spectroscopy are also very well-suited. Surface reactions involved in pseudocapacitive processes and Li-/Na-ion intercalation mechanisms were already investigated in many different electrode materials. XAS and RIXS at the O K-edge are currently contributing to significant progress in the understanding of redox processes in Li oxide materials. X-ray spectroscopies have also been applied to probe the solvation of protons, hydroxyde and halide cations, classically used in supercapacitors. The characterization of organic electrolytes and ionic liquids used in battery would probably still requires further studies. Finally, new insights into the composition and formation of SEI layers have been achieved over the last few years thanks to these techniques.

While the previous studies presented here suggest an active field of research, *in situ/operando* X-ray characterization of light elements in EES systems remains experimentally challenging. Further development in X-ray spectroscopy and microscopy techniques are certainly required to expand the understanding of electrochemical processes relevant for EES. Especially, the following points would be particularly critical to our opinion:

- The development of new detection schemes for X-ray-induced decay processes in liquid would facilitate the *in situ* characterization of light elements by X-ray spectroscopy. Indeed, XAS in liquid cells is so far mostly based on fluorescence detection, while more than 99% of the decay channel is related to non-radiative processes for light elements.[304] However, the short mean free path of electrons makes very challenging the detection of electron yield in liquid phase. The use of graphene membranes enables the investigation of electrochemical processes using XPS but is limited to reactions occurring a few nanometers away from the graphene layer and cannot easily be applied to thin-film electrodes. The use of tender X-rays

excitation is a possible solution to increase the electron escape but resonant excitation of light elements would not be possible anymore.[88] A promising alternative is the detection of electrons emitted close to an electrified surface using a lock-in detection scheme. XAS recorded using this approach has been recently applied to the characterization of interfacial water molecules under applied potential.[245,305] The use of ionic yield to measure X-ray-induced current in liquid was also recently applied to aqueous electrolytes and carbon nanoparticles in water.[306–308] While a better understanding of electron and ionic yield decay processes in liquid is definitely required, these strategies may enable more efficient probing of light elements at the solid-liquid interface in electrochemical systems.

- X-ray induced photochemistry may also contribute to comprehension of chemical reaction in a reductive environment. Previous work performed on *in situ* TEM showed that radiolytic species generated by the electron beam under the microscope could be used to simulate reductive environment occurring in real EES systems.[309] The formation of an SEI layer as a result of radiolysis was recently investigated by XPS.[310] Using soft X-ray photons would enable element-specific excitation to control the type of reductive species. For example, in an aqueous environment, carbon and nitrogen atoms could be selectively excited without ionizing the water molecules since C and N K-edges lies below the O K-edge (Figure 2a). As such, local soft X-ray-induced chemical reactions could be triggered and radical species leading to the SEI formation may be more easily identified. The use of X-ray-induced photochemistry recently demonstrated that the reduction of LiTFSI molecules on a solid surface exposed to X-rays leads to the formation of a lithium fluoride interphase only at high LiTFSI concentration.[311] In the same direction, ultrafast dissociation of molecules can be effectively monitored by RIXS and RPES. The stability of oxygen species in layered oxide electrodes was recently found to depend on X-ray irradiation.[312] Selective excitation of a definite molecule in complex electrolytes, such as water in water-in-salt electrolytes, may provide information on the local electronic interaction and ion-pairing with nearby molecules.

- Last but not least, recent development in *operando* STXM have led to the observation of primary battery particles in an electrochemical cell at metal L-edges with sub-30 nm spatial resolution.[114] Achieving a similar nanoscale imaging at the K-edge of

light elements directly in liquid may provide important spectroscopic insights on electrochemical reactions on carbon electrodes and on the formation of SEI layers for LIBs systems. While successful XPEEM experiments have been mentioned earlier, the bulk sensitivity of STXM may facilitate *operando* characterization in aqueous and organic electrolytes. *In situ* STXM already enabled the identification of reaction product from gas-phase catalysis such as Fischer-Tropsch synthesis on individual catalyst particles.[97,313,314] If similar experiments were performed in an electrochemical cell, theIf similar experiments were performed in an electrochemical cell, the possibility to image both the active phase and the organic reactant phase of the catalyst with nanometer spatial resolution could be transposed to the context of electrochemical energy storage.

We anticipate that the application of X-ray spectroscopy and microscopy techniques to energy storage materials will be rapidly expanding in the coming years. These state-of-the-art techniques, accelerated by recent development in synchrotron facilities, are getting more accessible to users and will facilitate the understanding of new battery chemistry in the future. In particular, they may promote a deeper understanding not only for conventional Li/Na-ion batteries but also for novel K-, Mg-, Al-ion batteries and non-metal cation batteries (such as hydrogen ion and ammonium ion batteries) as well as anion batteries (such as chloride and bromide batteries) in the future.

7   Acknowledgment

References

[1]   C.L. Dong, L. Vayssieres, In Situ/Operando X-ray Spectroscopies for Advanced Investigation of Energy Materials, Chem. Eur. J. 24 (2018) 18356–18373. https://doi.org/10.1002/chem.201803936.

[2]   N.S. Lewis, Research opportunities to advance solar energy utilization, Science. 351 (2016) 353-361. https://doi.org/10.1126/science.aad1920.

[3]   J. Pang, R.G. Mendes, A. Bachmatiuk, L. Zhao, H.Q. Ta, T. Gemming, H. Liu, Z. Liu, M.H. Rummeli, Applications of 2D MXenes in energy conversion and storage systems, Chem. Soc. Rev. 48 (2019) 72–133. https://doi.org/10.1039/C8CS00324F.

[4]   A.K. Shukla, T. Prem Kumar, Nanostructured electrode materials for electrochemical energy storage and conversion, WIREs Energy and Environment. 2 (2013) 14–30. https://doi.org/10.1002/wene.48.

[5]   X. Liu, T.C. Weng, Synchrotron-based x-ray absorption spectroscopy for energy materials, MRS Bulletin. 41 (2016) 466–472. https://doi.org/10.1557/mrs.2016.113.

[6]   W.H. Doh, V. Papaefthimiou, S. Zafeiratos, Applications of Synchrotron-Based X-Ray Photoelectron Spectroscopy in the Characterization of Nanomaterials, In: Kumar C.S.S.R. (eds) Surface Science Tools for Nanomaterials Characterization. Springer, Berlin, Heidelberg (2015) 317–366. https://doi.org/10.1007/978-3-662-44551-8_9.

[7]   W. Xu, Z. Xie, X. Cui, K. Zhao, L. Zhang, L. Mai, Y. Wang, Direct growth of an economic green energy storage material: a monocrystalline jarosite-KFe3(SO4)2(OH)6-nanoplates@rGO hybrid as a superior lithium-ion battery cathode, J. Mater. Chem. A. 4 (2016) 3735–3742. https://doi.org/10.1039/C5TA10622B.

[8]   Y. Zhang, Z. Chen, H. Qiu, W. Yang, Z. Zhao, J. Zhao, G. Cui, Pursuit of reversible Zn electrochemistry: a time-honored challenge towards low-cost and green energy storage, NPG Asia Materials. 12 (2020) 4-27. https://doi.org/10.1038/s41427-019-0167-1.

[9]   X. Liu, D. Wang, G. Liu, V. Srinivasan, Z. Liu, Z. Hussain, W. Yang, Distinct charge dynamics in battery electrodes revealed by in situ and operando soft X-ray spectroscopy, Nature Communications. 4 (2013) 2568. https://doi.org/10.1038/ncomms3568.

[10]   J. Drnec, A. Rack, Use of the advanced X-ray sources to accelerate the development of batteries and fuel cells for mobile applications ., EVS32 Symposium. (2019) 1–7.

[11]   M. Hu, Z. Yao, X. Wang, Characterization techniques for graphene-based materials in catalysis, AIMS Materials Science. 4 (2017) 755–788. https://doi.org/10.3934/matersci.2017.3.755.

[12]   M. Wolf, B.M. May, J. Cabana, Visualization of Electrochemical Reactions in Battery Materials with X-ray Microscopy and Mapping, Chem. Mater. 29 (2017) 3347–3362. https://doi.org/10.1021/acs.chemmater.6b05114.

[13]   Q. Li, S. Yan, W. Yang, Interfacial properties in energy storage systems studied by soft x-ray absorption spectroscopy and resonant inelastic x-ray scattering, Journal of Chemical Physics. 152 (2020) 140901-140909. https://doi.org/10.1063/5.0003311.

[14]   Y. Ye, C.H. Wu, L. Zhang, Y.-S. Liu, P.-A. Glans-Suzuki, J. Guo, Using soft x-ray absorption spectroscopy to characterize electrode/electrolyte interfaces in-situ and operando, Journal of Electron Spectroscopy and Related Phenomena. 221 (2017) 2–9. https://doi.org/10.1016/j.elspec.2017.05.002.

[15]   P. Niehoff, S. Passerini, M. Winter, Interface Investigations of a Commercial Lithium Ion Battery Graphite Anode Material by Sputter Depth Profile X-ray Photoelectron Spectroscopy, Langmuir. 29 (2013) 5806–5816. https://doi.org/10.1021/la400764r.

[16]   I. Manke, H. Markötter, C. Tötzke, N. Kardjilov, R. Grothausmann, M. Dawson, C. Hartnig, S. Haas, D. Thomas, A. Hoell, C. Genzel, J. Banhart, Investigation of Energy-Relevant Materials with Synchrotron X-Rays and Neutrons, Advanced Engineering Materials. 13 (2011) 712–729. https://doi.org/10.1002/adem.201000284.

[17]   X. Liu, W. Yang, Z. Liu, Recent progress on synchrotron-based in-situ soft X-ray spectroscopy for energy materials, Advanced Materials. 26 (2014) 7710–7729. https://doi.org/10.1002/adma.201304676.

[18]   F. Lin, Y. Liu, X. Yu, L. Cheng, A. Singer, O.G. Shpyrko, H.L. Xin, N. Tamura, C. Tian, T.C. Weng, X.Q. Yang, Y.S. Meng, D. Nordlund, W. Yang, M.M. Doeff, Synchrotron X-ray Analytical Techniques for Studying Materials Electrochemistry in Rechargeable Batteries, Chemical Reviews. 117 (2017) 13123–13186. https://doi.org/10.1021/acs.chemrev.7b00007.

[19]   C. Prehal, C. Koczwara, N. Jäckel, A. Schreiber, M. Burian, H. Amenitsch, M.A. Hartmann, V. Presser, O. Paris, Quantification of ion confinement and desolvation in nanoporous carbon supercapacitors with modelling and in situ X-ray scattering, Nature Energy. 2 (2017) 16215-16222. https://doi.org/10.1038/nenergy.2016.215.

[20]   D. Saurel, J. Segalini, M. Jauregui, A. Pendashteh, B. Daffos, P. Simon, M. Casas-Cabanas, A SAXS outlook on disordered carbonaceous materials for electrochemical energy storage, Energy Storage Materials. 21 (2019) 162–173. https://doi.org/10.1016/j.ensm.2019.05.007.

[21]   T. Li, C. Lim, Y. Cui, X. Zhou, H. Kang, B. Yan, M.L. Meyerson, J.A. Weeks, Q. Liu, F. Guo, R. Kou, Y. Liu, V. De Andrade, F. De Carlo, Y. Ren, C.-J. Sun, C.B. Mullins, L. Chen, Y. Fu, L. Zhu, In situ and operando investigation of the dynamic morphological and phase changes of a selenium-doped germanium electrode during (de)lithiation processes, J. Mater. Chem. A. 8 (2020) 750–759. https://doi.org/10.1039/C9TA09750C.

[22]   H. Kim, J. Hong, G. Yoon, H. Kim, K.-Y. Park, M.-S. Park, W.-S. Yoon, K. Kang, Sodium intercalation chemistry in graphite, Energy Environ. Sci. 8 (2015) 2963–2969. https://doi.org/10.1039/C5EE02051D.

[23]   H. Shao, Y.C. Wu, Z. Lin, P.L. Taberna, P. Simon, Nanoporous carbon for electrochemical capacitive energy storage, Chemical Society Reviews. 49 (2020) 3005–3039. https://doi.org/10.1039/d0cs00059k.

[24]   J. Conder, R. Bouchet, S. Trabesinger, C. Marino, L. Gubler, C. Villevieille, Direct observation of lithium polysulfides in lithium–sulfur batteries using operando X-ray diffraction, Nature Energy. 2 (2017) 17069-17075. https://doi.org/10.1038/nenergy.2017.69.

[25]   S. Schweidler, L. de Biasi, A. Schiele, P. Hartmann, T. Brezesinski, J. Janek, Volume Changes of Graphite Anodes Revisited: A Combined Operando X-ray Diffraction and In Situ Pressure Analysis Study, J. Phys. Chem. C. 122 (2018) 8829–8835. https://doi.org/10.1021/acs.jpcc.8b01873.

[26]   M. Giorgetti, A Review on the Structural Studies of Batteries and Host Materials by X-Ray Absorption Spectroscopy, ISRN Materials Science. 2013 (2013) 938625-938647. https://doi.org/10.1155/2013/938625.

[27]   M. Chen, S.-L. Chou, S.-X. Dou, Understanding Challenges of Cathode Materials for Sodium-Ion Batteries using Synchrotron-Based X-Ray Absorption Spectroscopy, Batteries & Supercaps. 2 (2019) 842–851. https://doi.org/10.1002/batt.201900054.

[28]   G. Aquilanti, M. Giorgetti, R. Dominko, L. Stievano, I. Arčon, N. Novello, L. Olivi, Operandocharacterization of batteries using x-ray absorption spectroscopy: advances at the beamline XAFS at synchrotron Elettra, Journal of Physics D: Applied Physics. 50 (2017) 074001-074012. https://doi.org/10.1088/1361-6463/aa519a.

[29]   W.C. Chueh, F. El Gabaly, J.D. Sugar, N.C. Bartelt, A.H. McDaniel, K.R. Fenton, K.R. Zavadil, T. Tyliszczak, W. Lai, K.F. McCarty, Intercalation Pathway in Many-Particle LiFePO4 Electrode Revealed by Nanoscale State-of-Charge Mapping, Nano Lett. 13 (2013) 866–872. https://doi.org/10.1021/nl3031899.

[30]   Y. Li, F. El Gabaly, T.R. Ferguson, R.B. Smith, N.C. Bartelt, J.D. Sugar, K.R. Fenton, D.A. Cogswell, A.L.D. Kilcoyne, T. Tyliszczak, M.Z. Bazant, W.C. Chueh, Current-induced transition from particle-by-particle to concurrent intercalation in phase-separating battery electrodes, Nature Materials. 13 (2014) 1149–1156. https://doi.org/10.1038/nmat4084.

[31]   J. Nelson, S. Misra, Y. Yang, A. Jackson, Y. Liu, H. Wang, H. Dai, J.C. Andrews, Y. Cui, M.F. Toney, In Operando X-ray Diffraction and Transmission X-ray Microscopy of Lithium Sulfur Batteries, J. Am. Chem. Soc. 134 (2012) 6337–6343. https://doi.org/10.1021/ja2121926.

[32]   C.-N. Lin, W.-C. Chen, Y.-F. Song, C.-C. Wang, L.-D. Tsai, N.-L. Wu, Understanding dynamics of polysulfide dissolution and re-deposition in working lithium–sulfur battery by in-operando transmission X-ray microscopy, Journal of Power Sources. 263 (2014) 98–103. https://doi.org/10.1016/j.jpowsour.2014.04.003.

[33]   D. Liu, Z. Shadike, R. Lin, K. Qian, H. Li, K. Li, S. Wang, Q. Yu, M. Liu, S. Ganapathy, X. Qin, Q.H. Yang, M. Wagemaker, F. Kang, X.Q. Yang, B. Li, Review of Recent Development of In Situ/Operando Characterization Techniques for Lithium Battery Research, Advanced Materials. 31 (2019) 1806620-1806676. https://doi.org/10.1002/adma.201806620.

[34]   S.-M. Bak, Z. Shadike, R. Lin, X. Yu, X.-Q. Yang, In situ/operando synchrotron-based X-ray techniques for lithium-ion battery research, NPG Asia Materials. 10 (2018) 563–580. https://doi.org/10.1038/s41427-018-0056-z.

[35]   W. Yang, Z. Liu, Techniques and Demonstrations of Synchrotron-Based In situ Soft X-ray Spectroscopy for Studying Energy Materials, Synchrotron Radiation in Materials Science. (2018) 511–562. https://doi.org/10.1002/9783527697106.ch13.

[36]   S. Muhammad, H. Kim, W.-S. Yoon, Synchrotron Radiation-Based X-Ray Study on Energy Storage Materials, in: M. Khodaei, L. Petaccia (Eds.), X-Ray Characterization of Nanostructured Energy Materials by Synchrotron Radiation, IntechOpen, Rijeka, 2017. https://doi.org/10.5772/67029.

[37]   J. Wang, Y.K. Chen-Wiegart, J. Wang, In operando tracking phase transformation evolution of lithium iron phosphate with hard X-ray microscopy, Nature Communications. 5 (2014) 4570-4579. https://doi.org/10.1038/ncomms5570.

[38]   Y. Xu, E. Hu, K. Zhang, X. Wang, V. Borzenets, Z. Sun, P. Pianetta, X. Yu, Y. Liu, X.-Q. Yang, H. Li, In situ Visualization of State-of-Charge Heterogeneity within a LiCoO2 Particle that Evolves upon Cycling at Different Rates, ACS Energy Lett. 2 (2017) 1240–1245. https://doi.org/10.1021/acsenergylett.7b00263.

[39]   C.-H. Lin, K. Sun, M. Ge, L.M. Housel, A.H. McCarthy, M.N. Vila, C. Zhao, X. Xiao, W.-K. Lee, K.J. Takeuchi, E.S. Takeuchi, A.C. Marschilok, Y.K. Chen-Wiegart, Systems-level investigation of aqueous batteries for understanding the benefit of water-in-salt electrolyte by synchrotron nanoimaging, Science Advances. 6 (2020) 7129-7140. https://doi.org/10.1126/sciadv.aay7129.

[40]   M. Giorgetti, L. Stievano, X-Ray Absorption Spectroscopy Study of Battery Materials, in: M. Khodaei, L. Petaccia (Eds.), X-Ray Characterization of Nanostructured Energy Materials by Synchrotron Radiation, IntechOpen, Rijeka, 2017. https://doi.org/10.5772/66868.

[41]   J. Nelson Weker, M.F. Toney, Emerging in Situ and Operando Nanoscale X-Ray Imaging Techniques for Energy Storage Materials, Advanced Functional Materials. 25 (2015) 1622–1637. https://doi.org/10.1002/adfm.201403409.

[42]   Y.-S. Liu, X. Feng, P.-A. Glans, J. Guo, In-situ/operando soft x-ray spectroscopy characterization of energy and catalytic materials, Solar Energy Materials and Solar Cells. 208 (2020) 110432-110437. https://doi.org/10.1016/j.solmat.2020.110432.

[43]   W. Huang, A. Marcelli, D. Xia, Application of Synchrotron Radiation Technologies to Electrode Materials for Li- and Na-Ion Batteries, Advanced Energy Materials. 7 (2017) 1700460-1700491. https://doi.org/10.1002/aenm.201700460.

[44]   D. Li, C. Xu, C.M. Yeager, P. Lin, W. Xing, K.A. Schwehr, N. Chen, Z. Arthur, D.I. Kaplan, P.H. Santschi, Molecular Interaction of Aqueous Iodine Species with Humic Acid Studied by I and C K-Edge X-ray Absorption Spectroscopy, Environ. Sci. Technol. 53 (2019) 12416–12424. https://doi.org/10.1021/acs.est.9b03682.

[45]   R.W. Strange, M.C. Feiters, Biological X-ray absorption spectroscopy (BioXAS): a valuable tool for the study of trace elements in the life sciences, Current Opinion in Structural Biology. 18 (2008) 609–616. https://doi.org/10.1016/j.sbi.2008.06.002.

[46]   K. Sauer, J. Yano, V.K. Yachandra, X-ray spectroscopy of the photosynthetic oxygen-evolving complex, Coordination Chemistry Reviews. 252 (2008) 318–335. https://doi.org/10.1016/j.ccr.2007.08.009.

[47]   F. (Feng) Tao, Operando Studies of Catalyst Surfaces during Catalysis and under Reaction Conditions: Ambient Pressure X-Ray Photoelectron Spectroscopy with a Flow-Cell Reactor, ChemCatChem. 4 (2012) 583–590. https://doi.org/10.1002/cctc.201200002.

[48]   L. Nguyen, F.F. Tao, Y. Tang, J. Dou, X.-J. Bao, Understanding Catalyst Surfaces during Catalysis through Near Ambient Pressure X-ray Photoelectron Spectroscopy, Chem. Rev. 119 (2019) 6822–6905. https://doi.org/10.1021/acs.chemrev.8b00114.

[49]   V.M. V, G. Nageswaran, Operando X-Ray Spectroscopic Techniques: A Focus on Hydrogen and Oxygen Evolution Reactions, Frontiers in Chemistry. 8 (2020) 23-34. https://doi.org/10.3389/fchem.2020.00023.

[50]   A. Prange, H. Modrow, X-ray absorption spectroscopy and its application in biological, agricultural and environmental research, Reviews in Environmental Science and Biotechnology. 1 (2002) 259–276. https://doi.org/10.1023/A:1023281303220.

[51]   S.C.B. Myneni, Soft X-ray Spectroscopy and Spectromicroscopy Studies of Organic Molecules in the Environment, Reviews in Mineralogy and Geochemistry. 49 (2002) 485–579. https://doi.org/10.2138/gsrmg.49.1.485.

[52]   J. Lehmann, D. Solomon, J. Brandes, H. Fleckenstein, C. Jacobson, J. Thieme, Synchrotron-Based Near-Edge X-Ray Spectroscopy of Natural Organic Matter in Soils and Sediments, in: Biophysico-Chemical Processes Involving Natural Nonliving Organic Matter in Environmental Systems, John Wiley & Sons, Ltd, 2009: pp. 729–781. https://doi.org/10.1002/9780470494950.ch17.

[53]   S.D. Conradson, Application of X-ray Absorption Fine Structure Spectroscopy to Materials and Environmental Science, Appl. Spectrosc. 52 (1998) 252A–279A. http://as.osa.org/abstract.cfm?URI=as-52-7-252A.

[54]   A.N. Kravtsova, Synchrotron-Based X-Ray Absorption Spectroscopy for the Study of Geological Materials, Journal of Surface Investigation: X-Ray, Synchrotron and Neutron Techniques. 14 (2020) 135–149. https://doi.org/10.1134/S1027451020020111.

[55]   A. Lanzirotti, M.D. Dyar, S. Sutton, M. Newville, E. Head, C. Carey, M. Mccanta, L. Lee, P.L. King, J. Jones, Accurate predictions of microscale oxygen barometry in basaltic glasses using V K-edge X-ray absorption spectroscopy: A multivariate approach, American Mineralogist. 103 (2018) 1282–1297. https://doi.org/10.2138/am-2018-6319.

[56]   J. Zhong, H. Zhang, X. Sun, S.T. Lee, Synchrotron soft X-ray absorption spectroscopy study of carbon and silicon nanostructures for energy applications, Advanced Materials. 26 (2014) 7786–7806. https://doi.org/10.1002/adma.201304507.

[57]   P. Zhu, J. Song, D. Lv, D. Wang, C. Jaye, D.A. Fischer, T. Wu, Y. Chen, Mechanism of Enhanced Carbon Cathode Performance by Nitrogen Doping in Lithium–Sulfur Battery: An X-ray Absorption Spectroscopic Study, J. Phys. Chem. C. 118 (2014) 7765–7771. https://doi.org/10.1021/jp4123634.

[58]   D.W. Wang, F. Li, L.C. Yin, X. Lu, Z.G. Chen, I.R. Gentle, G.Q. Lu, H.M. Cheng, Nitrogen-doped carbon monolith for alkaline supercapacitors and understanding nitrogen-

induced redox transitions, Chem. Eur. J. 2012, 18, 5345 – 5351.
https://doi.org/10.1002/chem.201102806.

[59]   J. Zhang, Z. Xia, L. Dai, Carbon-based electrocatalysts for advanced energy
conversion and storage, Science Advances. 1 (2015) 1500564-1500583.
https://doi.org/10.1126/sciadv.1500564.

[60]   Q. Li, R. Cao, J. Cho, G. Wu, Nanocarbon Electrocatalysts for Oxygen Reduction in
Alkaline Media for Advanced Energy Conversion and Storage, Advanced Energy Materials. 4
(2014) 1301415-1301433. https://doi.org/10.1002/aenm.201301415.

[61]   Q. Wu, L. Yang, X. Wang, Z. Hu, From Carbon-Based Nanotubes to Nanocages for
Advanced Energy Conversion and Storage, Acc. Chem. Res. 50 (2017) 435–444.
https://doi.org/10.1021/acs.accounts.6b00541.

[62]   S. Zhao, D.-W. Wang, R. Amal, L. Dai, Carbon-Based Metal-Free Catalysts for Key
Reactions Involved in Energy Conversion and Storage, Advanced Materials. 31 (2019)
1801526-1801547. https://doi.org/10.1002/adma.201801526.

[63]   Y. Yuan, M. Li, Z. Bai, G. Jiang, B. Liu, T. Wu, Z. Chen, K. Amine, J. Lu, The
Absence and Importance of Operando Techniques for Metal-Free Catalysts, Advanced
Materials. 31 (2019) 1–7. https://doi.org/10.1002/adma.201805609.

[64]   H. Zhao, Z. Wang, P. Lu, M. Jiang, F. Shi, X. Song, Z. Zheng, X. Zhou, Y. Fu, G.
Abdelbast, X. Xiao, Z. Liu, V.S. Battaglia, K. Zaghib, G. Liu, Toward Practical Application of
Functional Conductive Polymer Binder for a High-Energy Lithium-Ion Battery Design, Nano
Lett. 14 (2014) 6704–6710. https://doi.org/10.1021/nl503490h.

[65]   Q. Sun, J. Liu, B. Xiao, B. Wang, M. Banis, H. Yadegari, K.R. Adair, R. Li, X. Sun,
Visualizing the Oxidation Mechanism and Morphological Evolution of the Cubic-Shaped
Superoxide Discharge Product in Na–Air Batteries, Advanced Functional Materials. 29 (2019)
1–9. https://doi.org/10.1002/adfm.201808332.

[66]   B. Mao, Y. Dai, J. Cai, Q. Li, C. Jiang, Y. Li, J. Xie, Z. Liu, Operando Ambient
Pressure X-ray Photoelectron Spectroscopy Studies of Sodium–Oxygen Redox Reactions,
Topics in Catalysis. 61 (2018) 2123–2128. https://doi.org/10.1007/s11244-018-1066-3.

[67]   S. Li, X. Xu, X. Shi, B. Li, Y. Zhao, H. Zhang, Y. Li, W. Zhao, X. Cui, L. Mao,
Composition analysis of the solid electrolyte interphase film on carbon electrode of lithium-

ion battery based on lithium difluoro(oxalate)borate and sulfolane, Journal of Power Sources. 217 (2012) 503–508. https://doi.org/10.1016/j.jpowsour.2012.05.114.

[68]   V.R. Rikka, S.R. Sahu, A. Chatterjee, P.V. Satyam, R. Prakash, M.S.R. Rao, R. Gopalan, G. Sundararajan, In Situ/ex Situ Investigations on the Formation of the Mosaic Solid Electrolyte Interface Layer on Graphite Anode for Lithium-Ion Batteries, The Journal of Physical Chemistry C. 122 (2018) 28717–28726. https://doi.org/10.1021/acs.jpcc.8b09210.

[69]   A. Léon, A. Fiedler, M. Blum, W. Yang, M. Bär, F. Scheiba, H. Ehrenberg, C. Heske, L. Weinhardt, Electrolyte Stability and Discharge Products of an Ionic-Liquid-Based Li–O2 Battery Revealed by Soft X-Ray Emission Spectroscopy, The Journal of Physical Chemistry C. 123 (2019) 30827–30832. https://doi.org/10.1021/acs.jpcc.9b08777.

[70]   J.-W. Song, C.C. Nguyen, S.-W. Song, Stabilized cycling performance of silicon oxide anode in ionic liquid electrolyte for rechargeable lithium batteries, RSC Advances. 2 (2012) 2003-2009. https://doi.org/10.1039/c2ra01183b.

[71]   M. Kawaguchi, K. Yamada, H. Ishikawa, Intercalation Chemistry and Application of B/C/N Materials to Secondary Batteries, (2017) 261–281. https://doi.org/10.1016/b978-0-12-803479-8.00011-5.

[72]   G.V. Zhuang, K. Xu, T.R. Jow, P.N. Ross, Study of SEI Layer Formed on Graphite Anodes in PC/LiBOB Electrolyte Using IR Spectroscopy, Electrochemical and Solid-State Letters. 7 (2004) A224-A227. https://doi.org/10.1149/1.1756855.

[73]   C. Wu, Y. Bai, F. Wu, Fourier-transform infrared spectroscopic studies on the solid electrolyte interphase formed on Li-doped spinel Li1.05Mn1.96O4 cathode, Journal of Power Sources. 189 (2009) 89–94. https://doi.org/10.1016/j.jpowsour.2008.11.016.

[74]   A.L. Lipson, R.S. Ginder, M.C. Hersam, Nanoscale In Situ Characterization of Li-ion Battery Electrochemistry Via Scanning Ion Conductance Microscopy, Advanced Materials. 23 (2011) 5613–5617. https://doi.org/10.1002/adma.201103094.

[75]   A. Kumatani, T. Matsue, Recent advances in scanning electrochemical microscopic analysis and visualization on lithium-ion battery electrodes, Current Opinion in Electrochemistry. 22 (2020) 228–233. https://doi.org/10.1016/j.coelec.2020.07.010.

[76]   H. Ota, Y. Sakata, A. Inoue, S. Yamaguchi, Analysis of Vinylene Carbonate Derived
SEI Layers on Graphite Anode, Journal of The Electrochemical Society. 151 (2004) A1659-
A1669. https://doi.org/10.1149/1.1785795.

[77]   S. Chattopadhyay, A.L. Lipson, H.J. Karmel, J.D. Emery, T.T. Fister, P.A. Fenter, M.C.
Hersam, M.J. Bedzyk, In Situ X-ray Study of the Solid Electrolyte Interphase (SEI)
Formation on Graphene as a Model Li-ion Battery Anode, Chem. Mater. 24 (2012) 3038–
3043. https://doi.org/10.1021/cm301584r.

[78]   A. Augustsson, M. Herstedt, J.H. Guo, K. Edström, G.V. Zhuang, J.P.N. Ross, J.E.
Rubensson, J. Nordgren, Solid electrolyte interphase on graphite Li-ion battery anodes studied
by soft X-ray spectroscopy, Phys. Chem. Chem. Phys. 6 (2004) 4185–4189.
https://doi.org/10.1039/b313434b.

[79]   W. Yang, Synchrotron-Based Soft X-Ray Spectroscopy for Battery Material Studies,
Encyclopedia of Inorganic and Bioinorganic Chemistry (2019) 1–18.
https://doi.org/10.1002/9781119951438.eibc2672.

[80]   B.L. Henke, E.M. Gullikson, J.C. Davis, X-Ray Interactions: Photoabsorption,
Scattering, Transmission, and Reflection at E = 50-30000 eV, Z = 1-92, Atomic Data and
Nuclear Data Tables. 54 (1993) 181–342. https://doi.org/10.1006/adnd.1993.1013.

[81]   A. Di Cicco, A. Giglia, R. Gunnella, S.L. Koch, F. Mueller, F. Nobili, M. Pasqualini,
S. Passerini, R. Tossici, A. Witkowska, SEI Growth and Depth Profiling on ZFO Electrodes
by Soft X-Ray Absorption Spectroscopy, Advanced Energy Materials. 5 (2015) 1500642-
1500648. https://doi.org/10.1002/aenm.201500642.

[82]   S.J. Rezvani, R. Gunnella, A. Witkowska, F. Mueller, M. Pasqualini, F. Nobili, S.
Passerini, A.D. Cicco, Is the Solid Electrolyte Interphase an Extra-Charge Reservoir in Li-Ion
Batteries?, ACS Appl. Mater. Interfaces. 9 (2017) 4570–4576.
https://doi.org/10.1021/acsami.6b12408.

[83]   D. Bleiner, Tabletop beams for short wavelength spectrochemistry, Spectrochimica
Acta Part B: Atomic Spectroscopy. (2020) 105978-105997.
https://doi.org/10.1016/J.SAB.2020.105978.

[84]   F. de Groot, A. Kotani, Core Level Spectroscopy of Solids, Taylor & Francis, New
York, 2008. http://books.google.com/books?hl=fr&lr=&id=HGHzu66i1yoC&pgis=1.

[85]   M.H. Engelhard, T.C. Droubay, Y. Du, X-Ray Photoelectron Spectroscopy Applications, in: J.C. Lindon, G.E. Tranter, D.W. Koppenaal (Eds.), Encyclopedia of Spectroscopy and Spectrometry (Third Edition), Academic Press, Oxford, 2017: pp. 716–724. https://doi.org/10.1016/B978-0-12-409547-2.12102-X.

[86]   R.W. Welker, Chapter 4 - Size Analysis and Identification of Particles, in: R. Kohli, K.L. Mittal (Eds.), Developments in Surface Contamination and Cleaning, William Andrew Publishing, Oxford, 2012: pp. 179–213. https://doi.org/10.1016/B978-1-4377-7883-0.00004-3.

[87]   W.H. Doh, V. Papaefthimiou, S. Zafeiratos, Applications of Synchrotron-Based X-Ray Photoelectron Spectroscopy in the Characterization of Nanomaterials, in: C.S.S.R. Kumar (Ed.), Surface Science Tools for Nanomaterials Characterization, Springer Berlin Heidelberg, Berlin, Heidelberg, 2015: pp. 317–366. https://doi.org/10.1007/978-3-662-44551-8_9.

[88]   A. Schild, M. Peper, C. Perry, D. Rattenbacher, H.J. Wörner, Alternative Approach for the Determination of Mean Free Paths of Electron Scattering in Liquid Water Based on Experimental Data, J. Phys. Chem. Lett. 11 (2020) 1128–1134. https://doi.org/10.1021/acs.jpclett.9b02910.

[89]   R. Seidel, B. Winter, S.E. Bradforth, Valence Electronic Structure of Aqueous Solutions: Insights from Photoelectron Spectroscopy, Annual Review of Physical Chemistry. 67 (2016) 283–305. https://doi.org/10.1146/annurev-physchem-040513-103715.

[90]   M. Wang, L. Árnadóttir, Z.J. Xu, Z. Feng, In Situ X-ray Absorption Spectroscopy Studies of Nanoscale Electrocatalysts, Nano-Micro Letters. 11 (2019) 47-64. https://doi.org/10.1007/s40820-019-0277-x.

[91]   S. Turchini, R. Delaunay, P. Lagarde, J. Vogel, M. Sacchi, Soft X-ray absorption spectroscopy in transmission mode: Ce M4,5 edges, Journal of Electron Spectroscopy and Related Phenomena. 71 (1995) 31–37. https://doi.org/10.1016/0368-2048(94)02239-9.

[92]   J. Timoshenko, B. Roldan Cuenya, In Situ/Operando Electrocatalyst Characterization by X-ray Absorption Spectroscopy, Chem. Rev. 121 (2021) 882–961. https://doi.org/10.1021/acs.chemrev.0c00396.

[93]   S.L.M. Schroeder, G.D. Moggridge, R.M. Ormerod, T. Rayment, R.M. Lambert, What determines the probing depth of electron yield XAS?, Surface Science. 324 (1995) L371–L377.

 https://doi.org/10.1016/0039-6028(94)00779-9.

[94]   A. Kotani, S. Shin, Resonant inelastic x-ray scattering spectra for electrons in solids, Reviews of Modern Physics. 73 (2001) 203–246. https://doi.org/10.1103/RevModPhys.73.203.

[95]   J. Guo, Synchrotron radiation, soft-X-ray spectroscopy and nanomaterials, International Journal of Nanotechnology. 1 (2004) 193 - 225. https://doi.org/10.1504/ijnt.2004.003729.

[96]   J. Wu, Y. Yang, W. Yang, Advances in soft X-ray RIXS for studying redox reaction states in batteries, Dalton Transactions. 49 (2020) 13519–13527. https://doi.org/10.1039/D0DT01782E.

[97]   F.M.F. de Groot, E. de Smit, M.M. van Schooneveld, L.R. Aramburo, B.M. Weckhuysen, In-situ Scanning Transmission X-Ray Microscopy of Catalytic Solids and Related Nanomaterials, ChemPhysChem. 11 (2010) 951–962. https://doi.org/10.1002/cphc.200901023.

[98]   M. Olivares-Marín, A. Sorrentino, E. Pereiro, D. Tonti, Discharge products of ionic liquid-based Li-O$_2$ batteries observed by energy dependent soft x-ray transmission microscopy, Journal of Power Sources. 359 (2017) 234–241. https://doi.org/10.1016/j.jpowsour.2017.05.039.

[99]   J. Nelson Weker, M.F. Toney, Emerging In Situ and Operando Nanoscale X-Ray Imaging Techniques for Energy Storage Materials, Advanced Functional Materials. 25 (2015) 1622–1637. https://doi.org/10.1002/adfm.201403409.

[100]   M. Wolf, B.M. May, J. Cabana, Visualization of Electrochemical Reactions in Battery Materials with X-ray Microscopy and Mapping, Chemistry of Materials. 29 (2017) 3347–3362. https://doi.org/10.1021/acs.chemmater.6b05114.

[101]   J. Wang, J. Zhou, Y. Hu, T. Regier, Chemical interaction and imaging of single Co$_3$O$_4$/graphene sheets studied by scanning transmission X-ray microscopy and X-ray

absorption spectroscopy, Energy and Environmental Science. 6 (2013) 926–934. https://doi.org/10.1039/c2ee23844f.

[102]   Y. Li, J.N. Weker, W.E. Gent, D.N. Mueller, J. Lim, D.A. Cogswell, T. Tyliszczak, W.C. Chueh, Dichotomy in the Lithiation Pathway of Ellipsoidal and Platelet LiFePO$_4$ Particles Revealed through Nanoscale Operando State-of-Charge Imaging, Advanced Functional Materials. 25 (2015) 3677–3687. https://doi.org/10.1002/adfm.201500286.

[103]   D. Nolle, M. Weigand, G. Schütz, E. Goering, High Contrast Magnetic and Nonmagnetic Sample Current Microscopy for Bulk and Transparent Samples Using Soft X-Rays, Microscopy and Microanalysis. 17 (2011) 834–842. https://doi.org/10.1017/S1431927611000560.

[104]   D.A. Shapiro, S. Babin, R.S. Celestre, W. Chao, R.P. Conley, P. Denes, B. Enders, P. Enfedaque, S. James, J.M. Joseph, H. Krishnan, S. Marchesini, K. Muriki, K. Nowrouzi, S.R. Oh, H. Padmore, T. Warwick, L. Yang, V.V. Yashchuk, Y.-S. Yu, J. Zhao, An ultrahigh-resolution soft x-ray microscope for quantitative analysis of chemically heterogeneous nanomaterials., Science Advances. 6 (2020) 4904-4912. https://doi.org/10.1126/sciadv.abc4904.

[105]   T. Sun, G. Sun, F. Yu, Y. Mao, R. Tai, X. Zhang, G. Shao, Z. Wang, J. Wang, J. Zhou, Soft X-ray Ptychography Chemical Imaging of Degradation in a Composite Surface-Reconstructed Li-Rich Cathode, ACS Nano. 15 (2021) 1475–1485. https://doi.org/10.1021/acsnano.0c08891.

[106]   Y. Yamaguchi, S. Takakusagi, Y. Sakai, M. Kato, K. Asakura, Y. Iwasawa, X-ray photoemission electron microscopy (XPEEM) as a new promising tool for the real-time chemical imaging of active surfaces, Journal of Molecular Catalysis A: Chemical. 141 (1999) 129–137. https://doi.org/10.1016/S1381-1169(98)00256-8.

[107]   S. Nemšák, E. Strelcov, H. Guo, B.D. Hoskins, T. Duchoň, D.N. Mueller, A. Yulaev, I. Vlassiouk, A. Tselev, C.M. Schneider, A. Kolmakov, In Aqua Electrochemistry Probed by XPEEM: Experimental Setup, Examples, and Challenges, Topics in Catalysis. 61 (2018) 2195–2206. https://doi.org/10.1007/s11244-018-1065-4.

[108] G.K.L. Marx, V. Gerheim, G. Schönhense, Multipole WIEN-filter for a high-resolution X-PEEM, Journal of Electron Spectroscopy and Related Phenomena. 84 (1997) 251–261. https://doi.org/10.1016/S0368-2048(97)00029-7.

[109] M. Mirolo, D. Leanza, L. Höltschi, C. Jordy, V. Pelé, P. Novák, M. El Kazzi, C.A.F. Vaz, Post Mortem and Operando XPEEM: a Surface-Sensitive Tool for Studying Single Particles in Li-Ion Battery Composite Electrodes, Anal. Chem. 92 (2020) 3023–3031. https://doi.org/10.1021/acs.analchem.9b04124.

[110] D. Leanza, C.A.F. Vaz, G. Melinte, X. Mu, P. Novak, M. El Kazzi, Revealing the Dual Surface Reactions on a HE-NCM Li-Ion Battery Cathode and Their Impact on the Surface Chemistry of the Counter Electrode, ACS Applied Materials & Interfaces. 11 (2019) 6054–6065. https://doi.org/10.1021/acsami.8b19511.

[111] D. Leanza, C.A.F. Vaz, I. Czekaj, P. Novák, M. El Kazzi, Solving the puzzle of $Li_4Ti_5O_{12}$ surface reactivity in aprotic electrolytes in Li-ion batteries by nanoscale XPEEM spectromicroscopy, Journal of Materials Chemistry A. 6 (2018) 3534–3542. https://doi.org/10.1039/c7ta09673a.

[112] X. Liu, W. Yang, Z. Liu, Recent progress on synchrotron-based in-situ soft X-ray spectroscopy for energy materials, Advanced Materials. 26 (2014) 7710–7729. https://doi.org/10.1002/adma.201304676.

[113] L. Nowack, D. Grolimund, V. Samson, F. Marone, V. Wood, Rapid Mapping of Lithiation Dynamics in Transition Metal Oxide Particles with Operando X-ray Absorption Spectroscopy, Scientific Reports. 6 (2016) 21479-201487. https://doi.org/10.1038/srep21479.

[114] J. Lim, Y. Li, D.H. Alsem, H. So, S.C. Lee, P. Bai, D.A. Cogswell, X. Liu, N. Jin, Y. Yu, N.J. Salmon, D.A. Shapiro, M.Z. Bazant, T. Tyliszczak, W.C. Chueh, Origin and hysteresis of lithium compositional spatiodynamics within battery primary particles, Science. 353 (2016) 566–571. https://doi.org/10.1126/science.aaf4914.

[115] E.J. Crumlin, Z. Liu, H. Bluhm, W. Yang, J. Guo, Z. Hussain, X-ray spectroscopy of energy materials under in situ/operando conditions, Journal of Electron Spectroscopy and Related Phenomena. 200 (2015) 264–273. https://doi.org/10.1016/j.elspec.2015.06.008.

[116] M. Nagasaka, H. Yuzawa, T. Horigome, A.P. Hitchcock, N. Kosugi, [Electrochemical Reaction of Aqueous Iron Sulfate Solutions Studied by Fe L-Edge Soft X-ray Absorption

Spectroscopy, The Journal of Physical Chemistry C. 117 (2013) 16343–16348. https://doi.org/10.1021/jp405112r.

[117]   M.I. Nandasiri, L.E. Camacho-Forero, A.M. Schwarz, V. Shutthanandan, S. Thevuthasan, P.B. Balbuena, K.T. Mueller, V. Murugesan, In Situ Chemical Imaging of Solid-Electrolyte Interphase Layer Evolution in Li–S Batteries, Chem. Mater. 29 (2017) 4728–4737. https://doi.org/10.1021/acs.chemmater.7b00374.

[118]   Y.-S. Liu, C.-H. Chuang, J. Guo, SOFT X-RAY SPECTROSCOPY ON PHOTOCATALYSIS, in: Nanomaterials for Energy Conversion and Storage, WORLD SCIENTIFIC (EUROPE), 2017: pp. 343–360. https://doi.org/10.1142/9781786343635_0008.

[119]   R.S. Weatherup, 2D Material Membranes for Operando Atmospheric Pressure Photoelectron Spectroscopy, Topics in Catalysis. 61 (2018) 2085–2102. https://doi.org/10.1007/s11244-018-1075-2

[120]   A. Yulaev, H. Guo, E. Strelcov, L. Chen, I. Vlassiouk, A. Kolmakov, Graphene Microcapsule Arrays for Combinatorial Electron Microscopy and Spectroscopy in Liquids, ACS Appl. Mater. Interfaces. 9 (2017) 26492–26502. https://doi.org/10.1021/acsami.7b02824.

[121]   R.S. Weatherup, 2D Material Membranes for Operando Atmospheric Pressure Photoelectron Spectroscopy, Topics in Catalysis. 61 (2018) 2085–2102. https://doi.org/10.1007/s11244-018-1075-2.

[122]   J. Kraus, R. Reichelt, S. Günther, L. Gregoratti, M. Amati, M. Kiskinova, A. Yulaev, I. Vlassiouk, A. Kolmakov, Photoelectron spectroscopy of wet and gaseous samples through graphene membranes, Nanoscale. 6 (2014) 14394–14403. https://doi.org/10.1039/C4NR03561E.

[123]   P. Jiang, J.-L. Chen, F. Borondics, P.-A. Glans, M.W. West, C.-L. Chang, M. Salmeron, J. Guo, In situ soft X-ray absorption spectroscopy investigation of electrochemical corrosion of copper in aqueous $NaHCO_3$ solution, Electrochemistry Communications. 12 (2010) 820–822. https://doi.org/https://doi.org/10.1016/j.elecom.2010.03.042.

[124]   X. Li, H.-Y. Wang, H. Yang, W. Cai, S. Liu, B. Liu, In Situ/Operando Characterization Techniques to Probe the Electrochemical Reactions for Energy Conversion, Small Methods. 2 (2018) 1700395-1700408. https://doi.org/10.1002/smtd.201700395.

[125]   S.K. Beaumont, Soft XAS as an in situ technique for the study of heterogeneous catalysts, Phys. Chem. Chem. Phys. 22 (2020) 18747-18756. https://doi.org/10.1039/D0CP00657B.

[126]   W. Yang, J. Guo, E. Crumlin, D. Prendergast, Z. Hussain, Experiments and Theory of In situ and Operando Soft X-ray Spectroscopy for Energy Storage, Synchrotron Radiation News. 27 (2014) 4–13. https://doi.org/10.1080/08940886.2014.952207.

[127]   B. Winter, M. Faubel, Photoemission from Liquid Aqueous Solutions, Chem. Rev. 106 (2006) 1176–1211. https://doi.org/10.1021/cr040381p.

[128]   M.A. Brown, M. Faubel, B. Winter, X-Ray photo- and resonant Auger-electron spectroscopy studies of liquid water and aqueous solutions, Annu. Rep. Prog. Chem., Sect. C: Phys. Chem. 105 (2009) 174–212. https://doi.org/10.1039/B803023P.

[129]   K.R. Wilson, B.S. Rude, T. Catalano, R.D. Schaller, J.G. Tobin, D.T. Co, R.J. Saykally, X-ray Spectroscopy of Liquid Water Microjets, The Journal of Physical Chemistry B. 105 (2001) 3346–3349. https://doi.org/10.1021/jp010132u.

[130]   R. Seidel, S. Thürmer, B. Winter, Photoelectron Spectroscopy Meets Aqueous Solution: Studies from a Vacuum Liquid Microjet, The Journal of Physical Chemistry Letters. 2 (2011) 633–641. https://doi.org/10.1021/jz101636y.

[131]   K.R. Wilson, B.S. Rude, T. Catalano, R.D. Schaller, J.G. Tobin, D.T. Co, R.J. Saykally, X-ray Spectroscopy of Liquid Water Microjets, J. Phys. Chem. B. 105 (2001) 3346–3349. https://doi.org/10.1021/jp010132u.

[132]   N. Preissler, F. Buchner, T. Schultz, A. Lübcke, Electrokinetic Charging and Evidence for Charge Evaporation in Liquid Microjets of Aqueous Salt Solution, J. Phys. Chem. B. 117 (2013) 2422–2428. https://doi.org/10.1021/jp304773n.

[133]   T. Buttersack, P.E. Mason, R.S. McMullen, T. Martinek, K. Brezina, D. Hein, H. Ali, C. Kolbeck, C. Schewe, S. Malerz, B. Winter, R. Seidel, O. Marsalek, P. Jungwirth, S.E. Bradforth, Valence and Core-Level X-ray Photoelectron Spectroscopy of a Liquid Ammonia Microjet, J. Am. Chem. Soc. 141 (2019) 1838–1841. https://doi.org/10.1021/jacs.8b10942.

[134]   T. Buttersack, P.E. Mason, R.S. McMullen, H.C. Schewe, T. Martinek, K. Brezina, M. Crhan, A. Gomez, D. Hein, G. Wartner, R. Seidel, H. Ali, S. Thürmer, O. Marsalek, B. Winter, S.E. Bradforth, P. Jungwirth, Photoelectron spectra of alkali metal–ammonia microjets: From

blue electrolyte to bronze metal, Science. 368 (2020) 1086–1091.
https://doi.org/10.1126/science.aaz7607.

[135]   J.S. Uejio, C.P. Schwartz, A.M. Duffin, W.S. Drisdell, R.C. Cohen, R.J. Saykally, Characterization of selective binding of alkali cations with carboxylate by x-ray absorption spectroscopy of liquid microjets, Proceedings of the National Academy of Sciences. 105 (2008) 6809–6812. https://doi.org/10.1073/pnas.0800181105.

[136]   K.A. Perrine, M.H.C. Van Spyk, A.M. Margarella, B. Winter, M. Faubel, H. Bluhm, J.C. Hemminger, Characterization of the Acetonitrile Aqueous Solution/Vapor Interface by Liquid-Jet X-ray Photoelectron Spectroscopy, J. Phys. Chem. C. 118 (2014) 29378–29388. https://doi.org/10.1021/jp505947h.

[137]   H. Jiang, P.S. Lee, C. Li, 3D carbon-based nanostructures for advanced supercapacitors, Energy Environ. Sci. 6 (2013) 41–53. https://doi.org/10.1039/C2EE23284G.

[138]   L.L. Zhang, X.S. Zhao, Carbon-based materials as supercapacitor electrodes, Chem. Soc. Rev. 38 (2009) 2520–2531. https://doi.org/10.1039/B813846J.

[139]   H. Wang, Z. Li, D. Mitlin, Tailoring Biomass-Derived Carbon Nanoarchitectures for High-Performance Supercapacitors, ChemElectroChem. 1 (2014) 332–337. https://doi.org/10.1002/celc.201300127.

[140]   C. Liu, Z. Yu, D. Neff, A. Zhamu, B.Z. Jang, Graphene-Based Supercapacitor with an Ultrahigh Energy Density, Nano Lett. 10 (2010) 4863–4868. https://doi.org/10.1021/nl102661q.

[141]   S. Jung, Y. Myung, B.N. Kim, I.G. Kim, I.-K. You, T. Kim, Activated Biomass-derived Graphene-based Carbons for Supercapacitors with High Energy and Power Density, Scientific Reports. 8 (2018) 1915-1922. https://doi.org/10.1038/s41598-018-20096-8.

[142]   S. Fleischmann, J.B. Mitchell, R. Wang, C. Zhan, D. Jiang, V. Presser, V. Augustyn, Pseudocapacitance: From Fundamental Understanding to High Power Energy Storage Materials, Chemical Reviews. 120 (2020) 6738–6782. https://doi.org/10.1021/acs.chemrev.0c00170.

[143]   M. Bagge-Hansen, B.C. Wood, T. Ogitsu, T.M. Willey, I.C. Tran, A. Wittstock, M.M. Biener, M.D. Merrill, M.A. Worsley, M. Otani, C.H. Chuang, D. Prendergast, J. Guo, T.F. Baumann, T. van Buuren, J. Biener, J.R. Lee, Potential-induced electronic structure changes

in supercapacitor electrodes observed by in operando soft X-ray spectroscopy, Advanced Materials. 27 (2015) 1512–1518. https://doi.org/10.1002/adma.201403680.

[144] H.W. Chang, Y.R. Lu, J.L. Chen, C.L. Chen, J.M. Chen, Y.C. Tsai, W.C. Chou, C.L. Dong, Electrochemically activated reduced graphene oxide used as solid-state symmetric supercapacitor: An X-ray absorption spectroscopic investigation, Journal of Physical Chemistry C. 120 (2016) 22134–22141. https://doi.org/10.1021/acs.jpcc.6b04936.

[145] Y.-M. Lian, M. Ni, L. Zhou, R.-J. Chen, W. Yang, Synthesis of Biomass-Derived Carbon Induced by Cellular Respiration in Yeast for Supercapacitor Applications, Chem. Eur. J. 24 (2018) 18068–18074. https://doi.org/10.1002/chem.201803836.

[146] N. Phattharasupakun, J. Wutthiprom, P. Suktha, P. Iamprasertkun, N. Chanlek, C. Shepherd, E. Hadzifejzovic, M.G. Moloney, J.S. Foord, M. Sawangphruk, High-performance supercapacitors of carboxylate-modified hollow carbon nanospheres coated on flexible carbon fibre paper: Effects of oxygen-containing group contents, electrolytes and operating temperature, Electrochimica Acta. 238 (2017) 64–73. https://doi.org/10.1016/j.electacta.2017.03.208.

[147] C.H. Yang, P.L. Huang, X.F. Luo, C.H. Wang, C. Li, Y.H. Wu, J.K. Chang, Holey graphene nanosheets with surface functional groups as high-performance supercapacitors in ionic-liquid electrolyte, ChemSusChem. 8 (2015) 1779–1786. https://doi.org/10.1002/cssc.201500030.

[148] H.W. Chang, J.X. Fu, Y.C. Huang, Y.R. Lu, C.H. Kuo, J.L. Chen, C.L. Chen, J.F. Lee, J.M. Chen, Y.C. Tsai, W. Ching Chou, C.L. Dong, NiCo2O4/graphene quantum dots (GQDs) for use in efficient electrochemical energy devices: An electrochemical and X-ray absorption spectroscopic investigation, Catalysis Today. 348 (2020) 290–298. https://doi.org/10.1016/j.cattod.2019.10.013.

[149] V. Augustyn, P. Simon, B. Dunn, Pseudocapacitive oxide materials for high-rate electrochemical energy storage, Energy & Environmental Science. 7 (2014) 1597-1614. https://doi.org/10.1039/c3ee44164d.

[150] F. Frati, M.O.J.Y. Hunault, F.M.F. de Groot, Oxygen K-edge X-ray Absorption Spectra, Chemical Reviews. 120 (2020) 4056–4110. https://doi.org/10.1021/acs.chemrev.9b00439.

[151]   X. Shan, D.S. Charles, Y. Lei, R. Qiao, G. Wang, W. Yang, M. Feygenson, D. Su, X. Teng, Bivalence Mn5O8 with hydroxylated interphase for high-voltage aqueous sodium-ion storage, Nature Communications. 7 (2016) 13370-13377. https://doi.org/10.1038/ncomms13370.

[152]   M.R. Lukatskaya, S. Kota, Z. Lin, M.-Q.Q. Zhao, N. Shpigel, M.D. Levi, J. Halim, P.-L.L. Taberna, M.W. Barsoum, P. Simon, Y. Gogotsi, Ultra-high-rate pseudocapacitive energy storage in two-dimensional transition metal carbides, Nature Energy. (2017) 17105-17110. https://doi.org/10.1038/nenergy.2017.105.

[153]   A. Al-Temimy, B. Anasori, K.A. Mazzio, F. Kronast, M. Seredych, N. Kurra, M.-A. Mawass, S. Raoux, Y. Gogotsi, T. Petit, Enhancement of Ti_3C_2 MXene Pseudocapacitance after Urea Intercalation Studied by Soft X-ray Absorption Spectroscopy, The Journal of Physical Chemistry C. 124 (2020) 5079–5086. https://doi.org/10.1021/acs.jpcc.9b11766.

[154]   A. Al-Temimy, K. Prenger, R. Golnak, M. Lounasvuori, M. Naguib, T. Petit, Impact of Cation Intercalation on the Electronic Structure of $Ti_3C_2T_x$ MXenes in Sulfuric Acid, ACS Applied Materials & Interfaces. 12 (2020) 15087–15094. https://doi.org/10.1021/acsami.9b22122.

[155]   A. Al-Temimy, F. Kronast, M.-A. Mawass, K.A. Mazzio, K. Prenger, M. Naguib, T. Petit, S. Raoux, Spatially resolved X-ray absorption spectroscopy investigation of individual cation-intercalated multi-layered $Ti_3C_2T_x$ MXene particles, Applied Surface Science. 530 (2020) 147157-147174. https://doi.org/10.1016/J.APSUSC.2020.147157.

[156]   S. Ghosh, R. Santhosh, S. Jeniffer, V. Raghavan, G. Jacob, K. Nanaji, P. Kollu, S.K. Jeong, A.N. Grace, Natural biomass derived hard carbon and activated carbons as electrochemical supercapacitor electrodes, Scientific Reports. 9 (2019) 16315-16329. https://doi.org/10.1038/s41598-019-52006-x.

[157]   S. Wenzel, T. Hara, J. Janek, P. Adelhelm, Room-temperature sodium-ion batteries: Improving the rate capability of carbon anode materials by templating strategies, Energy Environ. Sci. 4 (2011) 3342–3345. https://doi.org/10.1039/C1EE01744F.

[158]   X. Wang, L. Liu, Z. Niu, Carbon-based materials for lithium-ion capacitors, Mater. Chem. Front. 3 (2019) 1265–1279. https://doi.org/10.1039/C9QM00062C.

[159]   J. Liu, S. Wang, Q. Sun, All-carbon-based porous topological semimetal for Li-ion battery anode material, Proceedings of the National Academy of Sciences. 114 (2017) 651–656. https://doi.org/10.1073/pnas.1618051114.

[160]   J. Feng, L. Dong, X. Li, D. Li, P. Lu, F. Hou, J. Liang, S.X. Dou, Hierarchically stacked reduced graphene oxide/carbon nanotubes for as high performance anode for sodium-ion batteries, Electrochimica Acta. 302 (2019) 65–70. https://doi.org/https://doi.org/10.1016/j.electacta.2019.02.008.

[161]   K. Tasaki, Density Functional Theory Study on Structural and Energetic Characteristics of Graphite Intercalation Compounds, J. Phys. Chem. C. 118 (2014) 1443–1450. https://doi.org/10.1021/jp409700q.

[162]   J. Zou, C. Sole, N.E. Drewett, M. Velický, L.J. Hardwick, In Situ Study of Li Intercalation into Highly Crystalline Graphitic Flakes of Varying Thicknesses, J. Phys. Chem. Lett. 7 (2016) 4291–4296. https://doi.org/10.1021/acs.jpclett.6b01886.

[163]   C. Sole, N.E. Drewett, L.J. Hardwick, In situ Raman study of lithium-ion intercalation into microcrystalline graphite, Faraday Discuss. 172 (2014) 223–237. https://doi.org/10.1039/C4FD00079J.

[164]   Y. Reynier, R. Yazami, B. Fultz, The entropy and enthalpy of lithium intercalation into graphite, Journal of Power Sources. 119–121 (2003) 850–855. https://doi.org/https://doi.org/10.1016/S0378-7753(03)00285-4.

[165]   C. Wang, I. Kakwan, A.J. Appleby, F.E. Little, In situ investigation of electrochemical lithium intercalation into graphite powder, Journal of Electroanalytical Chemistry. 489 (2000) 55–67. https://doi.org/https://doi.org/10.1016/S0022-0728(00)00197-2.

[166]   C. Wang, A.J. Appleby, F.E. Little, Electrochemical impedance study of initial lithium ion intercalation into graphite powders, Electrochimica Acta. 46 (2001) 1793–1813. https://doi.org/https://doi.org/10.1016/S0013-4686(00)00782-9.

[167]   L. Zhang, X. Li, A. Augustsson, C.M. Lee, J.E. Rubensson, J. Nordgren, P.N. Ross, J.H. Guo, Revealing the electronic structure of LiC_6 by soft X-ray spectroscopy, Applied Physics Letters. 110 (2017) 104106-104110. https://doi.org/10.1063/1.4978432.

[168]   L. Zhang, Y. Ye, D. Cheng, H. Pan, J. Zhu, Intercalation of Li at the Graphene/Cu Interface, J. Phys. Chem. C. 117 (2013) 9259–9265. https://doi.org/10.1021/jp401290f.

[169]   L.L. Lapteva, Y.V. Fedoseeva, P.N. Gevko, D.A. Smirnov, A.V. Gusel'nikov, L.G. Bulusheva, A.V. Okotrub, X-ray spectroscopy study of lithiated graphite obtained by thermal deposition of lithium, Journal of Structural Chemistry. 58 (2017) 1173–1179. https://doi.org/10.1134/s0022476617060154.

[170]   C. Ma, X. Shao, D. Cao, Nitrogen-doped graphene nanosheets as anode materials for lithium ion batteries: a first-principles study, J. Mater. Chem. 22 (2012) 8911–8915. https://doi.org/10.1039/C2JM00166G.

[171]   D. Bhattacharjya, H.-Y. Park, M.-S. Kim, H.-S. Choi, S.N. Inamdar, J.-S. Yu, Nitrogen-Doped Carbon Nanoparticles by Flame Synthesis as Anode Material for Rechargeable Lithium-Ion Batteries, Langmuir. 30 (2014) 318–324. https://doi.org/10.1021/la403366e.

[172]   B. Ruan, J. Wang, D. Shi, Y. Xu, S. Chou, H. Liu, J. Wang, A phosphorus/N-doped carbon nanofiber composite as an anode material for sodium-ion batteries, J. Mater. Chem. A. 3 (2015) 19011–19017. https://doi.org/10.1039/C5TA04366B.

[173]   T. Schiros, D. Nordlund, L. Palova, D. Prezzi, L. Zhao, K.S. Kim, U. Wurstbauer, C. Gutierrez, D. Delongchamp, C. Jaye, D. Fischer, H. Ogasawara, L.G. Pettersson, D.R. Reichman, P. Kim, M.S. Hybertsen, A.N. Pasupathy, Connecting dopant bond type with electronic structure in N-doped graphene, Nano Letters. 12 (2012) 4025–4031. https://doi.org/10.1021/nl301409h.

[174]   X. Li, X. Hu, L. Zhou, R. Wen, X. Xu, S. Chou, L. Chen, A.-M. Cao, S. Dou, A S/N-doped high-capacity mesoporous carbon anode for Na-ion batteries, J. Mater. Chem. A. 7 (2019) 11976–11984. https://doi.org/10.1039/C9TA01615E.

[175]   J. Zhang, C. Li, Z. Peng, Y. Liu, J. Zhang, Z. Liu, D. Li, 3D free-standing nitrogen-doped reduced graphene oxide aerogel as anode material for sodium ion batteries with enhanced sodium storage, Scientific Reports. 7 (2017) 4886-4892. https://doi.org/10.1038/s41598-017-04958-1.

[176]   Y. Xu, C. Zhang, M. Zhou, Q. Fu, C. Zhao, M. Wu, Y. Lei, Highly nitrogen doped carbon nanofibers with superior rate capability and cyclability for potassium ion batteries, Nature Communications. 9 (2018) 1720-1730. https://doi.org/10.1038/s41467-018-04190-z.

[177]   L.G. Bulusheva, A.V. Okotrub, A.G. Kurenya, H. Zhang, H. Zhang, X. Chen, H. Song, Electrochemical properties of nitrogen-doped carbon nanotube anode in Li-ion batteries, Carbon. 49 (2011) 4013–4023. https://doi.org/https://doi.org/10.1016/j.carbon.2011.05.043.

[178]   L.G. Bulusheva, M.A. Kanygin, V.E. Arkhipov, K.M. Popov, Y.V. Fedoseeva, D.A. Smirnov, A.V. Okotrub, In Situ X-ray Photoelectron Spectroscopy Study of Lithium Interaction with Graphene and Nitrogen-Doped Graphene Films Produced by Chemical Vapor Deposition, The Journal of Physical Chemistry C. 121 (2017) 5108–5114. https://doi.org/10.1021/acs.jpcc.6b12687.

[179]   L.L. Lapteva, Y.V. Fedoseeva, E.V. Shlyakhova, A.A. Makarova, L.G. Bulusheva, A.V. Okotrub, NEXAFS spectroscopy study of lithium interaction with nitrogen incorporated in porous graphitic material, Journal of Materials Science. 54 (2019) 11168–11178. https://doi.org/10.1007/s10853-019-03586-6.

[180]   T. Hu, X. Sun, H. Sun, G. Xin, D. Shao, C. Liu, J. Lian, Rapid synthesis of nitrogen-doped graphene for a lithium ion battery anode with excellent rate performance and super-long cyclic stability, Phys. Chem. Chem. Phys. 16 (2014) 1060–1066. https://doi.org/10.1039/C3CP54494J.

[181]   Q. Xi, J. Huang, J. Li, Y. Jie, T. Wang, L. Cao, C. Wang, P. Guo, Sulfur-regulated the binding configurations of nitrogen in three-dimensional graphene to improve lithium storage kinetics, Journal of Alloys and Compounds. 786 (2019) 1013–1020. https://doi.org/10.1016/j.jallcom.2019.01.394.

[182]   Y. Li, Y.-S. Hu, X. Qi, X. Rong, H. Li, X. Huang, L. Chen, Advanced sodium-ion batteries using superior low cost pyrolyzed anthracite anode: towards practical applications, Energy Storage Materials. 5 (2016) 191–197. https://doi.org/10.1016/j.ensm.2016.07.006.

[183]   Y. Li, B. Ni, X. Li, X. Wang, D. Zhang, Q. Zhao, J. Li, T. Lu, W. Mai, L. Pan, High-Performance Na-Ion Storage of S-Doped Porous Carbon Derived from Conjugated Microporous Polymers, Nano-Micro Letters. 11 (2019) 60-72. https://doi.org/10.1007/s40820-019-0291-z.

[184]   S. Liu, J. Zhou, H. Song, Tailoring Highly N-Doped Carbon Materials from Hexamine-Based MOFs: Superior Performance and New Insight into the Roles of N

Configurations in Na-Ion Storage, Small. 14 (2018) 1703548-1703557. https://doi.org/10.1002/smll.201703548.

[185]   L.-L. Tian, S.-B. Li, M.-J. Zhang, S.-K. Li, L.-P. Lin, J.-X. Zheng, Q.-C. Zhuang, K. Amine, F. Pan, Cascading Boost Effect on the Capacity of Nitrogen-Doped Graphene Sheets for Li- and Na-Ion Batteries, ACS Appl. Mater. Interfaces. 8 (2016) 26722–26729. https://doi.org/10.1021/acsami.6b07390.

[186]   Y. Ma, Q. Guo, M. Yang, Y. Wang, T. Chen, Q. Chen, X. Zhu, Q. Xia, S. Li, H. Xia, Highly doped graphene with multi-dopants for high-capacity and ultrastable sodium-ion batteries, Energy Storage Materials. 13 (2018) 134–141. https://doi.org/10.1016/j.ensm.2018.01.005.

[187]   D. Li, L. Zhang, H. Chen, J. Wang, L.-X. Ding, S. Wang, P.J. Ashman, H. Wang, Graphene-based nitrogen-doped carbon sandwich nanosheets: a new capacitive process controlled anode material for high-performance sodium-ion batteries, J. Mater. Chem. A. 4 (2016) 8630–8635. https://doi.org/10.1039/C6TA02139E.

[188]   P. Lian, Y. Dong, Z.-S. Wu, S. Zheng, X. Wang, Sen Wang, C. Sun, J. Qin, X. Shi, X. Bao, Alkalized Ti3C2 MXene nanoribbons with expanded interlayer spacing for high-capacity sodium and potassium ion batteries, Nano Energy. 40 (2017) 1–8. https://doi.org/https://doi.org/10.1016/j.nanoen.2017.08.002.

[189]   H. Tang, Q. Hu, M. Zheng, Y. Chi, X. Qin, H. Pang, Q. Xu, MXene–2D layered electrode materials for energy storage, Progress in Natural Science: Materials International. 28 (2018) 133–147. https://doi.org/https://doi.org/10.1016/j.pnsc.2018.03.003.

[190]   Y. Li, H. Shao, Z. Lin, J. Lu, L. Liu, B. Duployer, P.O.Å. Persson, P. Eklund, L. Hultman, M. Li, K. Chen, X.-H. Zha, S. Du, P. Rozier, Z. Chai, E. Raymundo-Piñero, P.-L. Taberna, P. Simon, Q. Huang, A general Lewis acidic etching route for preparing MXenes with enhanced electrochemical performance in non-aqueous electrolyte, Nature Materials. 19 (2020) 894–899. https://doi.org/10.1038/s41563-020-0657-0.

[191]   S.-M. Bak, R. Qiao, W. Yang, S. Lee, X. Yu, B. Anasori, H. Lee, Y. Gogotsi, X.-Q. Yang, Na-Ion Intercalation and Charge Storage Mechanism in 2D Vanadium Carbide, Advanced Energy Materials. 7 (2017) 1700959-1700968. https://doi.org/10.1002/aenm.201700959.

[192]   C. Wang, S. Chen, H. Xie, S. Wei, C. Wu, L. Song, Atomic Sn^{4+} Decorated into Vanadium Carbide MXene Interlayers for Superior Lithium Storage, Advanced Energy Materials. 9 (2019) 1802977-1802984. https://doi.org/10.1002/aenm.201802977.

[193]   Q.-C. Liu, J.-J. Xu, D. Xu, X.-B. Zhang, Flexible lithium–oxygen battery based on a recoverable cathode, Nature Communications. 6 (2015) 7892-7899. https://doi.org/10.1038/ncomms8892.

[194]   K. Song, D.A. Agyeman, M. Park, J. Yang, Y.-M. Kang, High-Energy-Density Metal–Oxygen Batteries: Lithium–Oxygen Batteries vs Sodium–Oxygen Batteries, Advanced Materials. 29 (2017) 1606572-1606602. https://doi.org/10.1002/adma.201606572.

[195]   H. Yadegari, X. Sun, Sodium–Oxygen Batteries: Recent Developments and Remaining Challenges, Trends in Chemistry. 2 (2020) 241–253. https://doi.org/https://doi.org/10.1016/j.trechm.2019.12.003.

[196]   J. Lu, Y. Jung Lee, X. Luo, K. Chun Lau, M. Asadi, H.-H. Wang, S. Brombosz, J. Wen, D. Zhai, Z. Chen, D.J. Miller, Y. Sub Jeong, J.-B. Park, Z. Zak Fang, B. Kumar, A. Salehi-Khojin, Y.-K. Sun, L.A. Curtiss, K. Amine, A lithium–oxygen battery based on lithium superoxide, Nature. 529 (2016) 377–382. https://doi.org/10.1038/nature16484.

[197]   B.M. Gallant, R.R. Mitchell, D.G. Kwabi, J. Zhou, L. Zuin, C.V. Thompson, Y. Shao-Horn, Chemical and Morphological Changes of Li–O_2 Battery Electrodes upon Cycling, The Journal of Physical Chemistry C. 116 (2012) 20800–20805. https://doi.org/10.1021/jp308093b.

[198]   M. Olivares-Marin, A. Sorrentino, R.C. Lee, E. Pereiro, N.L. Wu, D. Tonti, Spatial Distributions of Discharged Products of Lithium-Oxygen Batteries Revealed by Synchrotron X-ray Transmission Microscopy, Nano Letters. 15 (2015) 6932–6938. https://doi.org/10.1021/acs.nanolett.5b02862.

[199]   A. Manthiram, Y. Fu, Y.-S. Su, Challenges and Prospects of Lithium–Sulfur Batteries, Acc. Chem. Res. 46 (2013) 1125–1134. https://doi.org/10.1021/ar300179v.

[200]   P.G. Bruce, S.A. Freunberger, L.J. Hardwick, J.-M. Tarascon, Li–O_2 and Li–S batteries with high energy storage, Nature Materials. 11 (2012) 19–29. https://doi.org/10.1038/nmat3191.

[201] D. Bresser, S. Passerini, B. Scrosati, Recent progress and remaining challenges in sulfur-based lithium secondary batteries – a review, Chem. Commun. 49 (2013) 10545–10562. https://doi.org/10.1039/C3CC46131A.

[202] S. Evers, L.F. Nazar, Graphene-enveloped sulfur in a one pot reaction: a cathode with good coulombic efficiency and high practical sulfur content, Chem. Commun. 48 (2012) 1233–1235. https://doi.org/10.1039/C2CC16726C.

[203] X. Li, X. Sun, Nitrogen-Doped Carbons in Li–S Batteries: Materials Design and Electrochemical Mechanism, Frontiers in Energy Research. 2 (2014) 49-57. https://doi.org/10.3389/fenrg.2014.00049.

[204] L. Ji, M. Rao, H. Zheng, L. Zhang, Y. Li, W. Duan, J. Guo, E.J. Cairns, Y. Zhang, Graphene Oxide as a Sulfur Immobilizer in High Performance Lithium/Sulfur Cells, J. Am. Chem. Soc. 133 (2011) 18522–18525. https://doi.org/10.1021/ja206955k.

[205] X. Li, X. Li, M.N. Banis, B. Wang, A. Lushington, X. Cui, R. Li, T.-K. Sham, X. Sun, Tailoring interactions of carbon and sulfur in Li–S battery cathodes: significant effects of carbon–heteroatom bonds, J. Mater. Chem. A. 2 (2014) 12866–12872. https://doi.org/10.1039/C4TA02007C.

[206] M.U.M. Patel, I. Arčon, G. Aquilanti, L. Stievano, G. Mali, R. Dominko, X-ray Absorption Near-Edge Structure and Nuclear Magnetic Resonance Study of the Lithium–Sulfur Battery and its Components, ChemPhysChem. 15 (2014) 894–904. https://doi.org/10.1002/cphc.201300972.

[207] X. Feng, M.-K. Song, W.C. Stolte, D. Gardenghi, D. Zhang, X. Sun, J. Zhu, E.J. Cairns, J. Guo, Understanding the degradation mechanism of rechargeable lithium/sulfur cells: a comprehensive study of the sulfur–graphene oxide cathode after discharge–charge cycling, Phys. Chem. Chem. Phys. 16 (2014) 16931–16940. https://doi.org/10.1039/C4CP01341G.

[208] J. Song, T. Xu, M.L. Gordin, P. Zhu, D. Lv, Y.-B. Jiang, Y. Chen, Y. Duan, D. Wang, Nitrogen-Doped Mesoporous Carbon Promoted Chemical Adsorption of Sulfur and Fabrication of High-Areal-Capacity Sulfur Cathode with Exceptional Cycling Stability for Lithium-Sulfur Batteries, Advanced Functional Materials. 24 (2014) 1243–1250. https://doi.org/10.1002/adfm.201302631.

[209]   Y. Qiu, W. Li, W. Zhao, G. Li, Y. Hou, M. Liu, L. Zhou, F. Ye, H. Li, Z. Wei, S. Yang, W. Duan, Y. Ye, J. Guo, Y. Zhang, High-Rate, Ultralong Cycle-Life Lithium/Sulfur Batteries Enabled by Nitrogen-Doped Graphene, Nano Lett. 14 (2014) 4821–4827. https://doi.org/10.1021/nl5020475.

[210]   K. Dai, J. Wu, Z. Zhuo, Q. Li, S. Sallis, J. Mao, G. Ai, C. Sun, Z. Li, W.E. Gent, W.C. Chueh, Y. Chuang, R. Zeng, Z. Shen, F. Pan, S. Yan, L.F.J. Piper, Z. Hussain, G. Liu, W. Yang, High Reversibility of Lattice Oxygen Redox Quantified by Direct Bulk Probes of Both Anionic and Cationic Redox Reactions, Joule. 3 (2019) 518–541. https://doi.org/10.1016/j.joule.2018.11.014.

[211]   K. Luo, M.R. Roberts, N. Guerrini, N. Tapia-Ruiz, R. Hao, F. Massel, D.M. Pickup, S. Ramos, Y.S. Liu, J. Guo, A.V. Chadwick, L.C. Duda, P.G. Bruce, Anion Redox Chemistry in the Cobalt Free 3d Transition Metal Oxide Intercalation Electrode Li[Li0.2Ni0.2Mn0.6]O2, Journal of the American Chemical Society. 138 (2016) 11211–11218. https://doi.org/10.1021/jacs.6b05111.

[212]   Z.W. Lebens-Higgins, N.V. Faenza, M.D. Radin, H. Liu, S. Sallis, J. Rana, J. Vinckeviciute, P.J. Reeves, M.J. Zuba, F. Badway, N. Pereira, K.W. Chapman, T.L. Lee, T. Wu, C.P. Grey, B.C. Melot, A. Van Der Ven, G.G. Amatucci, W. Yang, L.F.J. Piper, Revisiting the charge compensation mechanisms in LiNi0.8Co0.2-: YAlyO2 systems, Materials Horizons. 6 (2019) 2112–2123. https://doi.org/10.1039/c9mh00765b.

[213]   W.E. Gent, K. Lim, Y. Liang, Q. Li, T. Barnes, S.J. Ahn, K.H. Stone, M. McIntire, J. Hong, J.H. Song, Y. Li, A. Mehta, S. Ermon, T. Tyliszczak, D. Kilcoyne, D. Vine, J.H. Park, S.K. Doo, M.F. Toney, W. Yang, D. Prendergast, W.C. Chueh, Coupling between oxygen redox and cation migration explains unusual electrochemistry in lithium-rich layered oxides, Nature Communications. 8 (2017) 2091-2102. https://doi.org/10.1038/s41467-017-02041-x.

[214]   J. Hong, W.E. Gent, P. Xiao, K. Lim, D.H. Seo, J. Wu, P.M. Csernica, C.J. Takacs, D. Nordlund, C.J. Sun, K.H. Stone, D. Passarello, W. Yang, D. Prendergast, G. Ceder, M.F. Toney, W.C. Chueh, Metal–oxygen decoordination stabilizes anion redox in Li-rich oxides, Nature Materials. 18 (2019) 256–265. https://doi.org/10.1038/s41563-018-0276-1.

[215]   Z. Zhuo, Y.S. Liu, J. Guo, Y.D. Chuang, F. Pan, W. Yang, Full Energy Range Resonant Inelastic X-ray Scattering of O_2 and CO_2: Direct Comparison with Oxygen Redox State in

Batteries, The Journal of Physical Chemistry Letters. 11 (2020) 2618–2623. https://doi.org/10.1021/acs.jpclett.0c00423.

[216]   Q. Liu, Z. Hu, M. Chen, C. Zou, H. Jin, S. Wang, S.-L. Chou, S.-X. Dou, Recent Progress of Layered Transition Metal Oxide Cathodes for Sodium-Ion Batteries, Small. 15 (2019) 1805381-1805404. https://doi.org/10.1002/smll.201805381.

[217]   W.-S. Yoon, M. Balasubramanian, K.Y. Chung, X.-Q. Yang, J. McBreen, C.P. Grey, D.A. Fischer, Investigation of the Charge Compensation Mechanism on the Electrode System by Combination of Soft and Hard X-ray Absorption Spectroscopy, Journal of the American Chemical Society. 127 (2005) 17479–17487. https://doi.org/10.1021/ja0530568.

[218]   S. Han, Y. Xia, Z. Wei, B. Qiu, L. Pan, Q. Gu, Z. Liu, Z. Guo, A comparative study on the oxidation state of lattice oxygen among Li1.14Ni0.136Co0.136Mn0.544O2, Li2MnO3, LiNi0.5Co0.2Mn0.3O2 and LiCoO2 for the initial charge–discharge, J. Mater. Chem. A. 3 (2015) 11930–11939. https://doi.org/10.1039/C5TA02161H.

[219]   S. Bhowmick, A. Sadrzadeh, B.I. Yakobson, E.S. Penev, B.I. Yakobson, J. Gao, J. Zhao, V.V. Struzhkin, H. Mao, R.J. Hemley, C.W. Glass, L. Li, A.R. Oganov, P.B. Allen, S. Curtarolo, X. Wei, J.W. Kysar, J. Hone, Visualization of O-O peroxo-like dimers in high-capacity layered oxides for Li-ion batteries, Science. 350 (2015) 1516–1521.

[220]   D. Foix, M. Sathiya, E. McCalla, J.M. Tarascon, D. Gonbeau, X-ray Photoemission Spectroscopy Study of Cationic and Anionic Redox Processes in High-Capacity Li-Ion Battery Layered-Oxide Electrodes, Journal of Physical Chemistry C. 120 (2016) 862–874. https://doi.org/10.1021/acs.jpcc.5b10475.

[221]   N. Yabuuchi, M. Takeuchi, M. Nakayama, H. Shiiba, M. Ogawa, K. Nakayama, T. Ohta, D. Endo, T. Ozaki, T. Inamasu, K. Sato, S. Komaba, High-capacity electrode materials for rechargeable lithium batteries: Li_3NbO_4-based system with cation-disordered rocksalt structure, Proceedings of the National Academy of Sciences. 112 (2015) 7650–7655. https://doi.org/10.1073/pnas.1504901112.

[222]   K. Luo, M.R. Roberts, R. Hao, N. Guerrini, D.M. Pickup, Y.S. Liu, K. Edström, J. Guo, A.V. Chadwick, L.C. Duda, P.G. Bruce, Charge-compensation in 3d-transition-metal-oxide intercalation cathodes through the generation of localized electron holes on oxygen, Nature Chemistry. 8 (2016) 684–691. https://doi.org/10.1038/nchem.2471.

[223]   S. Roychoudhury, R. Qiao, Z. Zhuo, Q. Li, Y. Lyu, J. Kim, J. Liu, E. Lee, B.J. Polzin, J. Guo, S. Yan, Y. Hu, H. Li, D. Prendergast, W. Yang, Deciphering the oxygen absorption pre-edge: a caveat on its application for probing oxygen redox reactions in batteries, Energy Environ. Mater. 0 (2020) 1–9. https://doi.org/10.1002/eem2.12119.

[224]   M. Oishi, T. Fujimoto, Y. Takanashi, Y. Orikasa, A. Kawamura, T. Ina, H. Yamashige, D. Takamatsu, K. Sato, H. Murayama, H. Tanida, H. Arai, H. Ishii, C. Yogi, I. Watanabe, T. Ohta, A. Mineshige, Y. Uchimoto, Z. Ogumi, Charge compensation mechanisms in Li1.16Ni0.15Co0.19Mn0.50O2 positive electrode material for Li-ion batteries analyzed by a combination of hard and soft X-ray absorption near edge structure, Journal of Power Sources. 222 (2013) 45–51. https://doi.org/10.1016/j.jpowsour.2012.08.023.

[225]   T. Masese, C. Tassel, Y. Orikasa, Y. Koyama, H. Arai, N. Hayashi, J. Kim, T. Mori, K. Yamamoto, Y. Kobayashi, H. Kageyama, Z. Ogumi, Y. Uchimoto, Crystal Structural Changes and Charge Compensation Mechanism during Two Lithium Extraction/Insertion between Li2FeSiO4 and FeSiO4, The Journal of Physical Chemistry C. 119 (2015) 10206–10211. https://doi.org/10.1021/acs.jpcc.5b00362.

[226]   K. Redel, A. Kulka, K. Walczak, A. Plewa, C.N. Borca, J. Molenda, The impact of oxygen evolution and cation migration on the cycling stability of a Li-rich Li[Li0.2Mn0.6Ni0.1Co0.1]O2 positive electrode, J. Mater. Chem. A. 8 (2020) 18143–18153. https://doi.org/10.1039/D0TA05556E.

[227]   J. Wu, Z. Zhuo, X. Rong, K. Dai, Z. Lebens-Higgins, S. Sallis, F. Pan, L.F.J. Piper, G. Liu, Y. Chuang, Z. Hussain, Q. Li, R. Zeng, Z. Shen, W. Yang, Dissociate lattice oxygen redox reactions from capacity and voltage drops of battery electrodes, Science Advances. 6 (2020) 3871-3882. https://doi.org/10.1126/sciadv.aaw3871.

[228]   J. Xu, M. Sun, R. Qiao, S.E. Renfrew, L. Ma, T. Wu, S. Hwang, D. Nordlund, D. Su, K. Amine, J. Lu, B.D. McCloskey, W. Yang, W. Tong, Elucidating anionic oxygen activity in lithium-rich layered oxides, Nature Communications. 9 (2018) 1–10. https://doi.org/10.1038/s41467-018-03403-9.

[229]   R.A. House, G.J. Rees, M.A. Pérez-Osorio, J.-J. Marie, E. Boivin, A.W. Robertson, A. Nag, M. Garcia-Fernandez, K.-J. Zhou, P.G. Bruce, First-cycle voltage hysteresis in Li-rich 3d cathodes associated with molecular O2 trapped in the bulk, Nature Energy. 5 (2020) 777–785. https://doi.org/10.1038/s41560-020-00697-2.

[230] R.A. House, U. Maitra, M.A. Pérez-Osorio, J.G. Lozano, L. Jin, J.W. Somerville, L.C. Duda, A. Nag, A. Walters, K.-J. Zhou, M.R. Roberts, P.G. Bruce, Superstructure control of first-cycle voltage hysteresis in oxygen-redox cathodes, Nature. 577 (2020) 502–508. https://doi.org/10.1038/s41586-019-1854-3.

[231] W. Yang, T.P. Devereaux, Anionic and cationic redox and interfaces in batteries: Advances from soft X-ray absorption spectroscopy to resonant inelastic scattering, Journal of Power Sources. 389 (2018) 188–197. https://doi.org/10.1016/j.jpowsour.2018.04.018.

[232] Z. Zhuo, Y. Liu, J. Guo, Y. Chuang, F. Pan, W. Yang, Full Energy Range Resonant Inelastic X-ray Scattering of O_2 and CO_2 : Direct Comparison with Oxygen Redox State in Batteries, The Journal of Physical Chemistry Letters. 11 (2020) 2618–2623. https://doi.org/10.1021/acs.jpclett.0c00423.

[233] K. Yamamoto, Y. Zhou, N. Yabuuchi, K. Nakanishi, T. Yoshinari, T. Kobayashi, Y. Kobayashi, R. Yamamoto, A. Watanabe, Y. Orikasa, K. Tsuruta, J. Park, H.R. Byon, Y. Tamenori, T. Ohta, Y. Uchimoto, Charge Compensation Mechanism of Lithium-Excess Metal Oxides with Different Covalent and Ionic Characters Revealed by Operando Soft and Hard X-ray Absorption Spectroscopy, Chem. Mater. 32 (2020) 139–147. https://doi.org/10.1021/acs.chemmater.9b02838.

[234] S. Komaba, K. Shimomura, N. Yabuuchi, T. Ozeki, H. Yui, K. Konno, Study on Polymer Binders for High-Capacity SiO Negative Electrode of Li-Ion Batteries, The Journal of Physical Chemistry C. 115 (2011) 13487–13495. https://doi.org/10.1021/jp201691g.

[235] G. Liu, S. Xun, N. Vukmirovic, X. Song, P. Olalde-Velasco, H. Zheng, V.S. Battaglia, L. Wang, W. Yang, Polymers with tailored electronic structure for high capacity lithium battery electrodes, Advanced Materials. 23 (2011) 4679–4683. https://doi.org/10.1002/adma.201102421.

[236] M. Wu, X. Xiao, N. Vukmirovic, S. Xun, P.K. Das, X. Song, P. Olalde-Velasco, D. Wang, A.Z. Weber, L.-W. Wang, V.S. Battaglia, W. Yang, G. Liu, Toward an Ideal Polymer Binder Design for High-Capacity Battery Anodes, J. Am. Chem. Soc. 135 (2013) 12048–12056. https://doi.org/10.1021/ja4054465.

[237] C.C. Nguyen, T. Yoon, D.M. Seo, P. Guduru, B.L. Lucht, Systematic Investigation of Binders for Silicon Anodes: Interactions of Binder with Silicon Particles and Electrolytes and

Effects of Binders on Solid Electrolyte Interphase Formation, ACS Applied Materials & Interfaces. 8 (2016) 12211–12220. https://doi.org/10.1021/acsami.6b03357.

[238] H.Q. Pham, G. Kim, H.M. Jung, S.-W. Song, Fluorinated Polyimide as a Novel High-Voltage Binder for High-Capacity Cathode of Lithium-Ion Batteries, Advanced Functional Materials. 28 (2018) 1704690-1704698. https://doi.org/10.1002/adfm.201704690.

[239] D. Leanza, C.A.F. Vaz, P. Novák, M. El Kazzi, Instability of PVDF Binder in the LiFePO4 versus Li4Ti5O12 Li-Ion Battery Cell, Helvetica Chimica Acta. 104 (2021) e2000183-e2000192. https://doi.org/10.1002/hlca.202000183.

[240] T. Fransson, Y. Harada, N. Kosugi, N.A. Besley, B. Winter, J.J. Rehr, L.G.M. Pettersson, A. Nilsson, X-ray and Electron Spectroscopy of Water, Chemical Reviews. 116 (2016) 7551–7569. https://doi.org/10.1021/acs.chemrev.5b00672.

[241] J.W. Smith, R.J. Saykally, Soft X-ray Absorption Spectroscopy of Liquids and Solutions, Chem. Rev. 117 (2017) 13909–13934. https://doi.org/10.1021/acs.chemrev.7b00213.

[242] Ph. Wernet, D. Nordlund, U. Bergmann, M. Cavalleri, M. Odelius, H. Ogasawara, L.Å. Näslund, T.K. Hirsch, L. Ojamäe, P. Glatzel, L.G.M. Pettersson, A. Nilsson, The Structure of the First Coordination Shell in Liquid Water, Science. 304 (2004) 995 – 999.

[243] M. Cavalleri, L.-Å. Näslund, D.C. Edwards, P. Wernet, H. Ogasawara, S. Myneni, L. Ojamäe, M. Odelius, A. Nilsson, L.G.M. Pettersson, The local structure of protonated water from x-ray absorption and density functional theory, The Journal of Chemical Physics. 124 (2006) 194508-194516. https://doi.org/10.1063/1.2199828.

[244] J. Niskanen, C.J. Sahle, I. Juurinen, J. Koskelo, S. Lehtola, R. Verbeni, H. Müller, M. Hakala, S. Huotari, Protonation Dynamics and Hydrogen Bonding in Aqueous Sulfuric Acid, The Journal of Physical Chemistry B. 119 (2015) 11732–11739. https://doi.org/10.1021/acs.jpcb.5b04371.

[245] C.H. Wu, T.A. Pascal, A. Baskin, H. Wang, H.-T. Fang, Y.-S. Liu, Y.-H. Lu, J. Guo, D. Prendergast, M.B. Salmeron, Molecular-Scale Structure of Electrode–Electrolyte Interfaces: The Case of Platinum in Aqueous Sulfuric Acid, Journal of the American Chemical Society. 140 (2018) 16237–16244. https://doi.org/10.1021/jacs.8b09743.

[246]   C.D. Cappa, J.D. Smith, B.M. Messer, R.C. Cohen, R.J. Saykally, [Nature of the aqueous hydroxide ion probed by X-ray absorption spectroscopy.], The Journal of Physical Chemistry. A. 111 (2007) 4776–4785. https://doi.org/10.1021/jp070551c.

[247]   E.F. Aziz, N. Ottosson, M. Faubel, I.V. Hertel, B. Winter, Interaction between liquid water and hydroxide revealed by core-hole de-excitation, Nature. 455 (2008) 89–91. https://doi.org/10.1038/nature07252.

[248]   C. Chen, C. Huang, I. Waluyo, D. Nordlund, T.-C. Weng, D. Sokaras, T. Weiss, U. Bergmann, L.G.M. Pettersson, A. Nilsson, Solvation structures of protons and hydroxide ions in water, The Journal of Chemical Physics. 138 (2013) 154506-154513. https://doi.org/10.1063/1.4801512.

[249]   H. Ali, R. Golnak, R. Seidel, B. Winter, J. Xiao, In-Situ X-ray Spectroscopy of the Electric Double Layer around TiO_2 Nanoparticles Dispersed in Aqueous Solution: Implications for H_2 Generation, ACS Applied Nano Materials. 3 (2020) 264–273. https://doi.org/10.1021/acsanm.9b01939.

[250]   C.D. Cappa, J.D. Smith, K.R. Wilson, B.M. Messer, M.K. Gilles, R.C. Cohen, R.J. Saykally, Effects of Alkali Metal Halide Salts on the Hydrogen Bond Network of Liquid Water, The Journal of Physical Chemistry B. 109 (2005) 7046–7052. https://doi.org/10.1021/jp0445324.

[251]   I. Juurinen, T. Pylkkänen, K.O. Ruotsalainen, C.J. Sahle, G. Monaco, K. Hämäläinen, S. Huotari, M. Hakala, Saturation Behavior in X-ray Raman Scattering Spectra of Aqueous LiCl, The Journal of Physical Chemistry B. 117 (2013) 16506–16511. https://doi.org/10.1021/jp409528r.

[252]   Y.L. Jeyachandran, F. Meyer, S. Nagarajan, A. Benkert, M. Bär, M. Blum, W. Yang, F. Reinert, C. Heske, L. Weinhardt, M. Zharnikov, Ion-Solvation-Induced Molecular Reorganization in Liquid Water Probed by Resonant Inelastic Soft X-ray Scattering, The Journal of Physical Chemistry Letters. 5 (2014) 4143–4148. https://doi.org/10.1021/jz502186a.

[253]   Y.L. Jeyachandran, F. Meyer, A. Benkert, M. Bär, M. Blum, W. Yang, F. Reinert, C. Heske, L. Weinhardt, M. Zharnikov, Investigation of the Ionic Hydration in Aqueous Salt

Solutions by Soft X-ray Emission Spectroscopy, The Journal of Physical Chemistry B. 120 (2016) 7687–7695. https://doi.org/10.1021/acs.jpcb.6b03952.

[254]   Z. Yin, L. Inhester, S. Thekku Veedu, W. Quevedo, A. Pietzsch, P. Wernet, G. Groenhof, A. Föhlisch, H. Grubmüller, S. Techert, Cationic and Anionic Impact on the Electronic Structure of Liquid Water, The Journal of Physical Chemistry Letters. 8 (2017) 3759–3764. https://doi.org/10.1021/acs.jpclett.7b01392.

[255]   B. Flamme, G. Rodriguez Garcia, M. Weil, M. Haddad, P. Phansavath, V. Ratovelomanana-Vidal, A. Chagnes, Guidelines to design organic electrolytes for lithium-ion batteries: environmental impact, physicochemical and electrochemical properties, Green Chem. 19 (2017) 1828–1849. https://doi.org/10.1039/C7GC00252A.

[256]   A. Chagnes, B. Carré, P. Willmann, D. Lemordant, Modeling viscosity and conductivity of lithium salts in γ-butyrolactone, Journal of Power Sources. 109 (2002) 203–213. https://doi.org/https://doi.org/10.1016/S0378-7753(02)00073-3.

[257]   M. Morita, M. Ishikawa, Y. Matsuda, Organic Electrolytes for Rechargeable Lithium Ion Batteries, in: Lithium Ion Batteries, John Wiley & Sons, Ltd, 2007: pp. 156–180. https://doi.org/10.1002/9783527612000.ch7.

[258]   J.W. Smith, R.J. Saykally, Soft X-ray Absorption Spectroscopy of Liquids and Solutions, Chem. Rev. 117 (2017) 13909–13934. https://doi.org/10.1021/acs.chemrev.7b00213.

[259]   J.W. Smith, R.K. Lam, A.T. Sheardy, O. Shih, A.M. Rizzuto, O. Borodin, S.J. Harris, D. Prendergast, R.J. Saykally, X-Ray absorption spectroscopy of $LiBF_4$ in propylene carbonate: a model lithium ion battery electrolyte, Phys. Chem. Chem. Phys. 16 (2014) 23568–23575. https://doi.org/10.1039/C4CP03240C.

[260]   Y. Horikawa, H. Arai, T. Tokushima, S. Shin, Spectral fingerprint in X-ray absorption for hydrogen-bonded dimer formation of acetic acids in solution, Chemical Physics Letters. 522 (2012) 33–37. https://doi.org/https://doi.org/10.1016/j.cplett.2011.11.061.

[261]   M. El Kazzi, I. Czekaj, E. J. Berg, P. Novák, M.A. Brown, Investigation of Li-Ion Solvation in Carbonate Based Electrolytes Using Near Ambient Pressure Photoemission, Topics in Catalysis. 59 (2016) 628–634. https://doi.org/10.1007/s11244-015-0518-2.

[262]   J. Maibach, I. Källquist, M. Andersson, S. Urpelainen, K. Edström, H. Rensmo, H. Siegbahn, M. Hahlin, Probing a battery electrolyte drop with ambient pressure photoelectron spectroscopy, Nature Communications. 10 (2019) 3080-3087. https://doi.org/10.1038/s41467-019-10803-y.

[263]   M. Nagasaka, H. Yuzawa, N. Kosugi, Microheterogeneity in Aqueous Acetonitrile Solution Probed by Soft X-ray Absorption Spectroscopy, The Journal of Physical Chemistry B. 124 (2020) 1259–1265. https://doi.org/10.1021/acs.jpcb.0c00551.

[264]   M. Nagasaka, K. Mochizuki, V. Leloup, N. Kosugi, Local structures of methanol-water binary solutions studied by soft X-ray absorption spectroscopy., The Journal of Physical Chemistry. B. 118 (2014) 4388–96. https://doi.org/10.1021/jp4091602.

[265]   M. Olschewski, R. Gustus, O. Höfft, A. Lahiri, F. Endres, Monochromatic X-ray Photoelectron Spectroscopy Study of Three Different Ionic Liquids in Interaction with Lithium-Decorated Copper Surfaces, J. Phys. Chem. C. 121 (2017) 2675–2682. https://doi.org/10.1021/acs.jpcc.6b10139.

[266]   T. Sugimoto, M. Kikuta, E. Ishiko, M. Kono, M. Ishikawa, Ionic liquid electrolytes compatible with graphitized carbon negative without additive and their effects on interfacial properties, Journal of Power Sources. 183 (2008) 436–440. https://doi.org/10.1016/j.jpowsour.2008.05.036.

[267]   S. Men, Y. Jin, P. Licence, Probing the impact of the N3-substituted alkyl chain on the electronic environment of the cation and the anion for 1,3-dialkylimidazolium ionic liquids, Phys. Chem. Chem. Phys. 22 (2020) 17394–17400. https://doi.org/10.1039/D0CP02325F.

[268]   D. Weingarth, A. Foelske-Schmitz, A. Wokaun, R. Kötz, In situ electrochemical XPS study of the Pt/[EMIM][BF4] system, Electrochemistry Communications. 13 (2011) 619–622. https://doi.org/10.1016/j.elecom.2011.03.027.

[269]   K.R.J. Lovelock, I.J. Villar-Garcia, F. Maier, H.-P. Steinrück, P. Licence, Photoelectron Spectroscopy of Ionic Liquid-Based Interfaces, Chemical Reviews. 110 (2010) 5158–5190. https://doi.org/10.1021/cr100114t.

[270]   A.R. Santos, R.K. Blundell, P. Licence, XPS of guanidinium ionic liquids: a comparison of charge distribution in nitrogenous cations, Phys. Chem. Chem. Phys. 17 (2015) 11839–11847. https://doi.org/10.1039/C5CP01069A.

[271]   S. Men, P. Licence, H. Luo, S. Dai, Tuning the Cation–Anion Interactions by Methylation of the Pyridinium Cation: An X-ray Photoelectron Spectroscopy Study of Picolinium Ionic Liquids, J. Phys. Chem. B. 124 (2020) 6657–6663. https://doi.org/10.1021/acs.jpcb.0c05872.

[272]   Q. Ma, F. Tietz, Solid-State Electrolyte Materials for Sodium Batteries: Towards Practical Applications, ChemElectroChem. 7 (2020) 2693–2713. https://doi.org/10.1002/celc.202000164.

[273]   F. Zheng, M. Kotobuki, S. Song, M.O. Lai, L. Lu, Review on solid electrolytes for all-solid-state lithium-ion batteries, Journal of Power Sources. 389 (2018) 198–213. https://doi.org/10.1016/j.jpowsour.2018.04.022.

[274]   A. Manthiram, X. Yu, S. Wang, Lithium battery chemistries enabled by solid-state electrolytes, Nature Reviews Materials. 2 (2017) 16103-16119. https://doi.org/10.1038/natrevmats.2016.103.

[275]   F. Mizuno, A. Hayashi, K. Tadanaga, M. Tatsumisago, High lithium ion conducting glass-ceramics in the system Li2S–P2S5, Solid State Ionics. 177 (2006) 2721–2725. https://doi.org/10.1016/j.ssi.2006.04.017.

[276]   F. Mizuno, A. Hayashi, K. Tadanaga, M. Tatsumisago, New, Highly Ion-Conductive Crystals Precipitated from Li2S–P2S5 Glasses, Advanced Materials. 17 (2005) 918–921. https://doi.org/10.1002/adma.200401286.

[277]   X. Wu, C. Villevieille, P. Novák, M. El Kazzi, Monitoring the chemical and electronic properties of electrolyte–electrode interfaces in all-solid-state batteries using operando X-ray photoelectron spectroscopy, Phys. Chem. Chem. Phys. 20 (2018) 11123–11129. https://doi.org/10.1039/C8CP01213J.

[278]   M. Mirolo, X. Wu, C.A.F. Vaz, P. Novák, M. El Kazzi, Unveiling the Complex Redox Reactions of SnO2 in Li-Ion Batteries Using Operando X-ray Photoelectron Spectroscopy and In Situ X-ray Absorption Spectroscopy, ACS Appl. Mater. Interfaces. 13 (2021) 2547–2557. https://doi.org/10.1021/acsami.0c17936.

[279]   X. Wu, C. Villevieille, P. Novák, M. El Kazzi, Insights into the chemical and electronic interface evolution of Li4Ti5O12 cycled in Li2S–P2S5 enabled by operando X-ray

photoelectron spectroscopy, J. Mater. Chem. A. 8 (2020) 5138–5146. https://doi.org/10.1039/C9TA14147B.

[280] K.N. Wood, K.X. Steirer, S.E. Hafner, C. Ban, S. Santhanagopalan, S.-H. Lee, G. Teeter, Operando X-ray photoelectron spectroscopy of solid electrolyte interphase formation and evolution in Li2S-P2S5 solid-state electrolytes, Nature Communications. 9 (2018) 2490-2500. https://doi.org/10.1038/s41467-018-04762-z.

[281] M. Gauthier, T.J. Carney, A. Grimaud, L. Giordano, N. Pour, H.-H. Chang, D.P. Fenning, S.F. Lux, O. Paschos, C. Bauer, F. Maglia, S. Lupart, P. Lamp, Y. Shao-Horn, Electrode–Electrolyte Interface in Li-Ion Batteries: Current Understanding and New Insights, J. Phys. Chem. Lett. 6 (2015) 4653–4672. https://doi.org/10.1021/acs.jpclett.5b01727.

[282] M. Dahbi, N. Yabuuchi, M. Fukunishi, K. Kubota, K. Chihara, K. Tokiwa, X. Yu, H. Ushiyama, K. Yamashita, J.-Y. Son, Y.-T. Cui, H. Oji, S. Komaba, Black Phosphorus as a High-Capacity, High-Capability Negative Electrode for Sodium-Ion Batteries: Investigation of the Electrode/Electrolyte Interface, Chem. Mater. 28 (2016) 1625–1635. https://doi.org/10.1021/acs.chemmater.5b03524.

[283] X. Yu, A. Manthiram, Electrode–electrolyte interfaces in lithium-based batteries, Energy Environ. Sci. 11 (2018) 527–543. https://doi.org/10.1039/C7EE02555F.

[284] X. Yu, A. Manthiram, Electrode–Electrolyte Interfaces in Lithium–Sulfur Batteries with Liquid or Inorganic Solid Electrolytes, Acc. Chem. Res. 50 (2017) 2653–2660. https://doi.org/10.1021/acs.accounts.7b00460.

[285] A. Wang, S. Kadam, H. Li, S. Shi, Y. Qi, Review on modeling of the anode solid electrolyte interphase (SEI) for lithium-ion batteries, Npj Computational Materials. 4 (2018) 15-40. https://doi.org/10.1038/s41524-018-0064-0.

[286] F. Kong, R. Kostecki, G. Nadeau, X. Song, K. Zaghib, K. Kinoshita, F. McLarnon, In situ studies of SEI formation, Journal of Power Sources. 97–98 (2001) 58–66. https://doi.org/https://doi.org/10.1016/S0378-7753(01)00588-2.

[287] S.J. An, J. Li, C. Daniel, D. Mohanty, S. Nagpure, D.L. Wood, The state of understanding of the lithium-ion-battery graphite solid electrolyte interphase (SEI) and its relationship to formation cycling, Carbon. 105 (2016) 52–76. https://doi.org/10.1016/j.carbon.2016.04.008.

[288]   R. Qiao, I.T. Lucas, A. Karim, J. Syzdek, X. Liu, W. Chen, K. Persson, R. Kostecki, W. Yang, Distinct Solid-Electrolyte-Interphases on Sn (100) and (001) Electrodes Studied by Soft X-Ray Spectroscopy, Advanced Materials Interfaces. 1 (2014) 1300115-1300120. https://doi.org/10.1002/admi.201300115.

[289]   W. Yang, X. Liu, R. Qiao, P. Olalde-Velasco, J.D. Spear, L. Roseguo, J.X. Pepper, Y. Chuang, J.D. Denlinger, Z. Hussain, Key electronic states in lithium battery materials probed by soft X-ray spectroscopy, Journal of Electron Spectroscopy and Related Phenomena. 190 (2013) 64–74. https://doi.org/10.1016/j.elspec.2013.03.008.

[290]   B. Philippe, R. Dedryvère, J. Allouche, F. Lindgren, M. Gorgoi, H. Rensmo, D. Gonbeau, K. Edström, Nanosilicon Electrodes for Lithium-Ion Batteries: Interfacial Mechanisms Studied by Hard and Soft X-ray Photoelectron Spectroscopy, Chemistry of Materials. 24 (2012) 1107–1115. https://doi.org/10.1021/cm2034195.

[291]   Z. Zhuo, P. Lu, C. Delacourt, R. Qiao, K. Xu, F. Pan, S.J. Harris, W. Yang, Breathing and oscillating growth of solid-electrolyte-interphase upon electrochemical cycling, Chemical Communications. 54 (2018) 814–817. https://doi.org/10.1039/c7cc07082a.

[292]   C. Shen, S. Wang, Y. Jin, W.-Q. Han, In Situ AFM Imaging of Solid Electrolyte Interfaces on HOPG with Ethylene Carbonate and Fluoroethylene Carbonate-Based Electrolytes, ACS Appl. Mater. Interfaces. 7 (2015) 25441–25447. https://doi.org/10.1021/acsami.5b08238.

[293]   D.C. Bock, G.H. Waller, A.N. Mansour, A.C. Marschilok, K.J. Takeuchi, E.S. Takeuchi, Investigation of Solid Electrolyte Interphase Layer Formation and Electrochemical Reversibility of Magnetite, Fe_3O_4, Electrodes: A Combined X-ray Absorption Spectroscopy and X-ray Photoelectron Spectroscopy Study, J. Phys. Chem. C. 122 (2018) 14257–14271. https://doi.org/10.1021/acs.jpcc.8b01970.

[294]   X. Ren, S. Chen, H. Lee, D. Mei, M.H. Engelhard, S.D. Burton, W. Zhao, J. Zheng, Q. Li, M.S. Ding, M. Schroeder, J. Alvarado, K. Xu, Y.S. Meng, J. Liu, J.-G. Zhang, W. Xu, Localized High-Concentration Sulfone Electrolytes for High-Efficiency Lithium-Metal Batteries, Chem. 4 (2018) 1877–1892. https://doi.org/10.1016/j.chempr.2018.05.002.

[295] C.C. Nguyen, S.-W. Song, Characterization of SEI layer formed on high performance Si–Cu anode in ionic liquid battery electrolyte, Electrochemistry Communications. 12 (2010) 1593–1595. https://doi.org/10.1016/j.elecom.2010.09.003.

[296] G.M.A. Girard, M. Hilder, N. Dupre, D. Guyomard, D. Nucciarone, K. Whitbread, S. Zavorine, M. Moser, M. Forsyth, D.R. MacFarlane, P.C. Howlett, Spectroscopic Characterization of the SEI Layer Formed on Lithium Metal Electrodes in Phosphonium Bis(fluorosulfonyl)imide Ionic Liquid Electrolytes, ACS Appl. Mater. Interfaces. 10 (2018) 6719–6729. https://doi.org/10.1021/acsami.7b18183.

[297] J. Kruusma, A. Tõnisoo, R. Pärna, E. Nõmmiste, I. Kuusik, M. Vahtrus, I. Tallo, T. Romann, E. Lust, The Electrochemical Behavior of 1-Ethyl-3-Methyl Imidazolium Tetracyanoborate Visualized by In Situ X-ray Photoelectron Spectroscopy at the Negatively and Positively Polarized Micro-Mesoporous Carbon Electrode, Journal of The Electrochemical Society. 164 (2017) A3393–A3402. https://doi.org/10.1149/2.1861713jes.

[298] J. Xiao, J.Z. Hu, H. Chen, M. Vijayakumar, J. Zheng, H. Pan, E.D. Walter, M. Hu, X. Deng, J. Feng, B.Y. Liaw, M. Gu, Z.D. Deng, D. Lu, S. Xu, C. Wang, J. Liu, Following the Transient Reactions in Lithium–Sulfur Batteries Using an In Situ Nuclear Magnetic Resonance Technique, Nano Lett. 15 (2015) 3309–3316. https://doi.org/10.1021/acs.nanolett.5b00521.

[299] H. Kim, F. Wu, J.T. Lee, N. Nitta, H.-T. Lin, M. Oschatz, W.I. Cho, S. Kaskel, O. Borodin, G. Yushin, In Situ Formation of Protective Coatings on Sulfur Cathodes in Lithium Batteries with LiFSI-Based Organic Electrolytes, Advanced Energy Materials. 5 (2015) 1401792-1401800. https://doi.org/10.1002/aenm.201401792.

[300] Y. Wang, C.-F. Lin, J. Rao, K. Gaskell, G. Rubloff, S.B. Lee, Electrochemically Controlled Solid Electrolyte Interphase Layers Enable Superior Li–S Batteries, ACS Appl. Mater. Interfaces. 10 (2018) 24554–24563. https://doi.org/10.1021/acsami.8b07248.

[301] B. Philippe, M. Valvo, F. Lindgren, H. Rensmo, K. Edström, Investigation of the Electrode/Electrolyte Interface of Fe_2O_3 Composite Electrodes: Li vs Na Batteries, Chem. Mater. 26 (2014) 5028–5041. https://doi.org/10.1021/cm5021367.

[302] M.A. Munoz-Marquez, M. Zarrabeitia, E. Castillo-Martinez, A. Eguia-Barrio, T. Rojo, M. Casas-Cabanas, Composition and evolution of the solid-electrolyte interphase in $Na_2Ti_3O_7$

electrodes for Na-ion batteries: XPS and Auger parameter analysis, ACS Applied Materials & Interfaces. 7 (2015) 7801–7808. https://doi.org/10.1021/acsami.5b01375.

[303]   G.G. Eshetu, T. Diemant, M. Hekmatfar, S. Grugeon, R.J. Behm, S. Laruelle, M. Armand, S. Passerini, Impact of the electrolyte salt anion on the solid electrolyte interphase formation in sodium ion batteries, Nano Energy. 55 (2019) 327–340. https://doi.org/https://doi.org/10.1016/j.nanoen.2018.10.040.

[304]   L.C. Feldman, J.W. Mayer, Fundamentals of surface and thin film analysis, P T R Prentice Hall, 1986.

[305]   J.-J. Velasco-Velez, C.H. Wu, T.A. Pascal, L.F. Wan, J. Guo, D. Prendergast, M. Salmeron, The structure of interfacial water on gold electrodes studied by x-ray absorption spectroscopy, Science (New York, N.Y.). 346 (2014) 831–834. https://doi.org/10.1126/science.1259437.

[306]   J. Ren, D.S. Achilleos, R. Golnak, H. Yuzawa, J. Xiao, M. Nagasaka, E. Reisner, T. Petit, Uncovering the Charge Transfer between Carbon Dots and Water by In Situ Soft X-ray Absorption Spectroscopy, The Journal of Physical Chemistry Letters. 10 (2019) 3843–3848. https://doi.org/10.1021/acs.jpclett.9b01800.

[307]   D. Schön, R. Golnak, M.F. Tesch, B. Winter, J.-J. Velasco-Velez, E.F. Aziz, J. Xiao, Bulk-Sensitive Detection of the Total Ion Yield for X-ray Absorption Spectroscopy in Liquid Cells, The Journal of Physical Chemistry Letters. 8 (2017) 5136–5140. https://doi.org/10.1021/acs.jpclett.7b02381.

[308]   D. Schön, J. Xiao, R. Golnak, M.F. Tesch, B. Winter, J.-J. Velasco-Velez, E.F. Aziz, Introducing Ionic-Current Detection for X-ray Absorption Spectroscopy in Liquid Cells, The Journal of Physical Chemistry Letters. (2017) 2087–2092. https://doi.org/10.1021/acs.jpclett.7b00646.

[309]   S.M. Rehn, M.R. Jones, New Strategies for Probing Energy Systems with In Situ Liquid-Phase Transmission Electron Microscopy, ACS Energy Letters. 3 (2018) 1269–1278. https://doi.org/10.1021/acsenergylett.8b00527.

[310]   F. Varenne, J.P. Alper, F. Miserque, C.S. Bongu, A. Boulineau, J.-F. Martin, V. Dauvois, A. Demarque, M. Bouhier, F. Boismain, S. Franger, N. Herlin-Boime, S. Le Caër, Ex situ solid electrolyte interphase synthesis via radiolysis of Li-ion battery anode–electrolyte

system for improved coulombic efficiency, Sustainable Energy Fuels. 2 (2018) 2100–2108. https://doi.org/10.1039/C8SE00257F.

[311]   H. Steinrück, C. Cao, M.R. Lukatskaya, C.J. Takacs, G. Wan, D.G. Mackanic, Y. Tsao, J. Zhao, B.A. Helms, K. Xu, O. Borodin, J.F. Wishart, M.F. Toney, Interfacial Speciation Determines Interfacial Chemistry: X-ray-Induced Lithium Fluoride Formation from Water-in-salt Electrolytes on Solid Surfaces, Angew.Chem. Int. Ed. 2020, 59,23180–23187 https://doi.org/10.1002/anie.202007745.

[312]   Z.W. Lebens-Higgins, J. Vinckeviciute, J. Wu, N.V. Faenza, Y. Li, S. Sallis, N. Pereira, Y.S. Meng, G.G. Amatucci, A.V. Der Ven, W. Yang, L.F.J. Piper, Distinction between Intrinsic and X-ray-Induced Oxidized Oxygen States in Li-Rich 3d Layered Oxides and $LiAlO_2$, The Journal of Physical Chemistry C. 123 (2019) 13201–13207. https://doi.org/10.1021/acs.jpcc.9b01298.

[313]   E. de Smit, I. Swart, J.F. Creemer, G.H. Hoveling, M.K. Gilles, T. Tyliszczak, P.J. Kooyman, H.W. Zandbergen, C. Morin, B.M. Weckhuysen, F.M.F. de Groot, Nanoscale chemical imaging of a working catalyst by scanning transmission X-ray microscopy, Nature. 456 (2008) 222–225. https://doi.org/10.1038/nature07516.

[314]   I.K. van Ravenhorst, C. Vogt, H. Oosterbeek, K.W. Bossers, J.G. Moya-Cancino, A.P. van Bavel, A.M.J. van der Eerden, D. Vine, F.M.F. de Groot, F. Meirer, B.M. Weckhuysen, Capturing the Genesis of an Active Fischer-Tropsch Synthesis Catalyst with Operando X-ray Nanospectroscopy, Angewandte Chemie. 130 (2018) 12133–12138. https://doi.org/10.1002/ange.201806354.